KINETIC AND EQUILIBRIUM STUDIES

OF

SOME DYE-CYCLODEXTRIN INCLUSION COMPLEXES

ROBERT LINDSAY SCHILLER, B.SC.(HONS.) (ADELAIDE)

Department of Physical and Inorganic Chemistry,
The University of Adelaide,
South Australia

A thesis submitted for the degree

of

DOCTOR OF PHILOSOPHY

JULY, 1986

Awarded 5-11-1986

CONTENTS

APPENDICES

ABSTRACT

The α-, β- and γ-cyclodextrins (CD), which are, respectively, six-, seven- and eight-membered α-1,4 linked cyclic oligomers of D glucopyranose, form inclusion complexes with a variety of smaller molecules which can fit into their cavities. UV/visible absorption and temperature-jump relaxation spectrophotometry were used to study the interaction of the cyclodextrins with some selected dyes: crystal violet, pyronine Y, pyronine B and rhodamine B.

The annular radii of the cyclodextrins and the relative sizes of the dyes are important factors influencing the selectivity of the cyclo-dextrins in the formation of inclusion complexes.

No inclusion of the dyes by αCD was detected. In the presence of βCD, the dyes form the 1:1 complex, dye·βCD:

$$D + \beta CD \underset{k_{-1}}{\overset{k_1}{\rightleftharpoons}} D \cdot \beta CD \qquad (K_1)$$
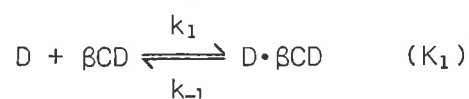
The breakdown of water structure around the dye and the release of hydrating water molecules from the cyclodextrin cavity are concluded to be the dominant rate-determining factors in the inclusion of the dyes by βCD. Pyronine Y is also able to form the 1:2 complex, dye·$(\beta CD)_2$, whose formation

$$D \cdot \beta CD + \beta CD \underset{k_{-2}}{\overset{k_2}{\rightleftharpoons}} D \cdot (\beta CD)_2 \qquad (K_2)$$
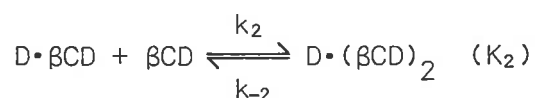
is slower than that of the corresponding 1:1 complex.

Whereas rhodamine B forms only the 1:1 complex with γCD, the other dyes are able to form the 2:1 complex, $(dye)_2 \cdot \gamma CD$:

$$D + \gamma CD \underset{k_{-1}}{\overset{k_1}{\rightleftharpoons}} D \cdot \gamma CD \qquad (K_1) \qquad fast$$

$$D + D \cdot \gamma CD \underset{k_{-2}}{\overset{k_2}{\rightleftharpoons}} D_2 \cdot \gamma CD \qquad (K_2) \qquad slow$$
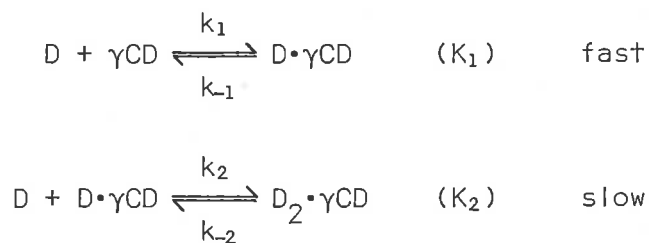
Pyronine Y may also possibly form the 2:2 complex, $(dye)_2 \cdot (\gamma CD)_2$, in which the step

$$D_2 \cdot \gamma CD + \gamma CD \underset{k_{-3}}{\overset{k_3}{\rightleftharpoons}} D_2 \cdot (\gamma CD)_2 \quad (K_3) \qquad fast$$
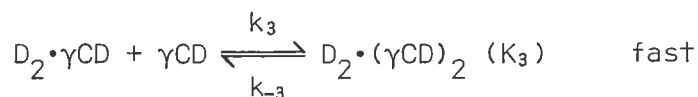
is added to the two processes shown above. Dimer formation within γCD occurs at dye concentrations at which the amount of dimer in solution is negligible in the absence of cyclodextrin. Thus, γCD effectively increases the dimerisation constant of the dyes. Kinetic parameters determined for the dimerisation of the dyes in the cavity of γCD are compared with the kinetic data for the dimerisation of the dyes in the absence of cyclo-dextrin:
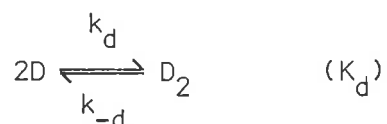
$$2D \underset{k_{-d}}{\overset{k_d}{\rightleftharpoons}} D_2 \qquad (K_d)$$

The increased stability of $(dye)_2$ included in $(dye)_2 \cdot \gamma CD$ is a consequence of a decreased dimer dissociation rate. The potential of two guest-one host complexation in the facilitation of chemical reactions is discussed.

To the best of my knowledge and belief, this thesis contains no material previously published or written by another person, nor any material previously submitted for a degree or diploma in any University, except where due reference is made in the text. I give my permission for this thesis to be photocopied.

R. L. SCHILLER

ACKNOWLEDGEMENTS

I wish to thank my supervisors, Dr. J. H. Coates and Dr. S. F. Lincoln, for their guidance throughout the course of this work.

My thanks are also due to the technical and ancillary staff of this Department, particularly Mr. J. Netting, Mr. R. Morris, Mr. T. Snigg and Mr. K. R. Shepherdson, who have assisted me in numerous ways.

I would also like to thank my colleagues, especially Ron Clarke, for their friendship.

To my mother, for her support throughout the course of this work, I would like to express my gratitude.

Special thanks must go to Etta Clark for the typing of this thesis.

CHAPTER I

Introduction

INTRODUCTION

1.1 The Cyclodextrins

Inclusion complexes are molecular compounds having the characteristic structure of an adduct, in which one of the compounds (called the host) spatially encloses another. The enclosed compound (called the guest) is situated in the cavity of the host molecule, and is held there by secondary forces alone. In view of the increasing number of publications, and in particular the review articles [1-6] and books [7-9] dealing with the cyclodextrins, perhaps they are the most important and interesting of the compounds capable of acting as host components in the formation of inclusion complexes.

The cyclodextrins (CD) are a series of homologous cyclic oligo-saccharides produced by the action of an amylase from Bacillus macerans on starch. They are composed of D glucopyranose residues that are attached by α-1,4 linkages in a macrocyclic form. The first three members of the series, α-, β- and γCD, consisting of six, seven and eight D glucopyranose units, respectively, have been studied most. Higher homologues do exist, cyclodextrins containing up to twelve residues have been identified [10]; however, they are difficult to purify and their complexing ability appears to be poor [10]. Cyclodextrins having fewer than six residues are not known to exist, probably because of steric constraints. X-ray crystallographic studies of hydrated α-, β- and γCD [11-13], which may be assumed to represent the uncomplexed or 'empty' cyclodextrin form, reveal the following common structural features (Figure 1.1). The D glucopyranose units exist in a substantially undistorted C1 chair conformation, and the lack of free rotation about the glycosidic bonds causes the cyclodextrins
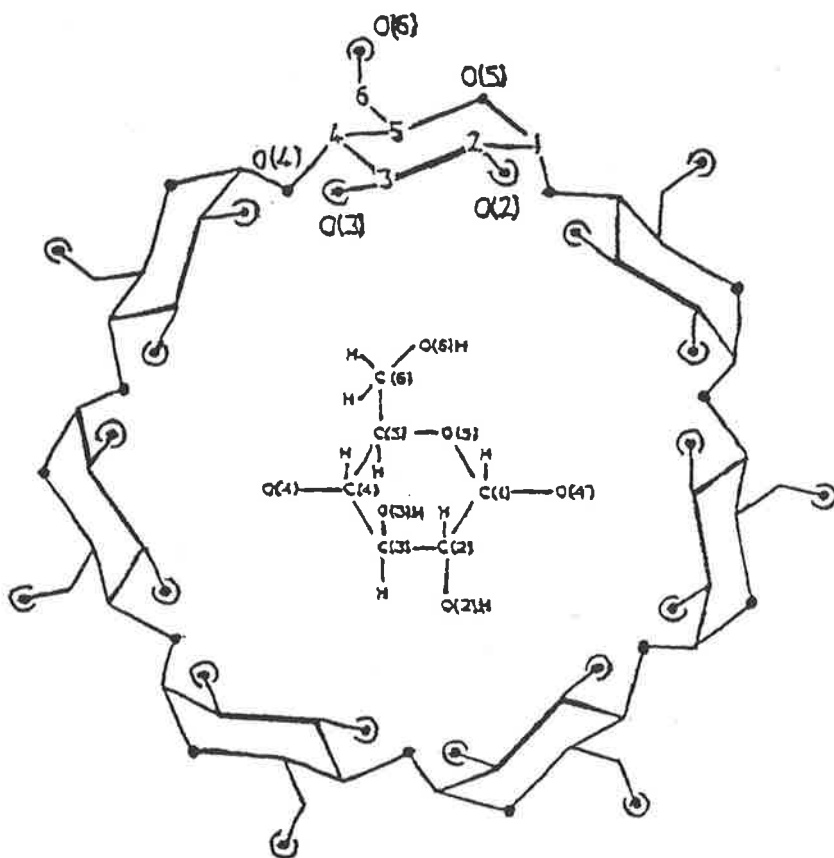
FIGURE 1.1: Chemical structure and numbering of the atoms
for β-cyclodextrin [3]

•   oxygen atoms

ℭ   hydroxyl groups

to have a round, slightly conical form. The interior of the cyclodextrin cavity is lined by a ring of hydrogen atoms (bonded to C-5), a ring of glycosidic oxygens, and another ring of hydrogen atoms (bonded to C-3) and therefore is relatively hydrophobic and apolar compared with bulk-solvent water. The cavities of the hydrated cyclodextrins are occupied by disordered water molecules. The open ends of the cyclodextrins are surrounded on one side by the primary hydroxyl groups (bonded to C-6) and on the other by the secondary hydroxyl groups (bonded to C-2 and C-3). Intramolecular hydrogen bonds exist between the secondary hydroxyl groups of adjacent D glucopyranose units, and these interactions stabilise the shape of the cyclodextrin moelcule. The cyclodextrin cavity is slightly V-shaped, the secondary hydroxyl end having a slightly wider opening than the primary hydroxyl end. Some selected physical properties of the cyclodextrins are summarised in Table 1.1. Nuclear magnetic resonance [14] and optical rotatory dispersion [15] studies have established that the features of the cyclodextrins derived for the crystalline state are retained in solution. X-ray crystallographic studies [16] of cyclodextrin inclusion complexes suggest that water molecules are expelled from the uncomplexed cyclodextrin cavity during complex formation. The structures of β- and γCD when complexed are similar to their 'empty' cyclodextrin forms. This is not the case for αCD [11]. The structure of the macrocyclic ring in 'empty' αCD is slightly distorted compared with that in β- and γCD. The αCD molecule has a somewhat collapsed form: the six D glucopyranose units are not equivalent; one unit is rotated inwards to allow the formation of a hydrogen bond between an oxygen (O-6 bonded to C-6) and a water molecule in the cavity. However, when αCD forms an inclusion complex the distortion of the macrocyclic ring vanishes. Thus, upon substrate inclusion, αCD undergoes a conformational change, and the structure of αCD in the complexed form becomes similar to that of β- and γCD. Both β- and γCD show no

Cyclodextrin	Number of Glucose Units	Molecular Weight	Water Solubility $(g/100\ cm^3)$	Cavity Dimensions (Å)*
α	6	972	14.5	4.7–5.2
β	7	1135	1.85	6.0–6.4
γ	8	1297	23.2	7.5–8.3

* As measured on Corey–Pauling–Koltun molecular models: the smaller value is for the ring of hydrogen atoms bonded to C-5 and the larger value for the ring of hydrogen atoms bonded to C-3. Depth of the cyclodextrin cavity is 7.9–8.0 Å.

TABLE 1.1: *Some physical properties of the cyclodextrins* [3]

significant deformations when they bind guest molecules [12, 13]. Recent studies of the cyclodextrins using the ultrasonic relaxation method have emphasised the dynamical nature of cyclodextrins [17, 18]. Relaxation effects were detected in aqueous α-, β- and γCD solutions and attributed to a change in solvation of the cyclodextrin cavity (ie. 'bound/free' water exchange). An additional relaxation effect was observed in the case of αCD and ascribed to a conformational change of αCD involving the rotation of a glucose structure.

Cyclodextrins form inclusion complexes with a large variety of guest molecules which are able to fit into their cavities. The fact that the guest molecule is actually contained in the cavity was first shown by the solid state studies of Hybl et al. [19]. Nuclear magnetic resonance studies provided the first direct evidence of inclusion in the cyclodextrin cavity in solution. Demarco and Thakkar [20] have shown that, in the presence of aromatic guests, the resonances of the hydrogen atoms of the cyclodextrin situated on the inside of the cavity were shifted significantly upfield due to shielding by the aromatic guests, whereas there was little effect on the resonances of the hydrogens on the exterior of the cyclodextrin torus. The ability of cyclodextrins to form inclusion complexes in aqueous solution is in contrast to the complexes formed by most other host compounds. For example, clathrates only form inclusion complexes in the solid state; the cavity in which the guest is situated is formed by the special crystal lattice of the host [21]. The inclusion complexes disintegrate once the crystal is dissolved. However, with cyclodextrins the cavity exists by virtue of the size and shape of the molecule, and hence persists in solution. In solution, the most common guest-cyclodextrin stoichiometric ratio is 1:1. In some cases, a guest may not be totally included by a single cyclo-dextrin, and a second cyclodextrin may also bind to form a 1:2 complex;

for example, the inclusion of fluorocinnamates by αCD [22]. The cavities
of β- and, in particular γCD are sufficiently large to accommodate two
guest molecules simultaneously and form complexes of the type 2:1 [23,
24] and 2:2 [24]. The included guests can be identical [24] or different
[23].

There is considerable interest in cyclodextrin inclusion complexes,
as they exhibit some of the characteristics of enzyme-substrate [25] and
drug-receptor interactions [6], and are potentially important in the de-
sign of controlled chemical synthetic pathways [3-5, 7]. Their ability
to mimic enzymes is due to the presence of a cavity of appropriate size
in the molecule and the presence of hydroxyl groups on the periphery of
the cyclodextrin, which can serve as catalytically active groups or as
points of attachment for catalytically active groups. Cyclodextrins can
facilitate chemical reactions; Bender et al. [1, 7] have described the
catalytic behaviour of 1:1 inclusion complexes. Recently, the role of
two guest-one host complexation in catalysis has been demonstrated. For
example, Breslow and Rideout [26] have found that βCD accelerates the
Diels-Alder reaction of cyclopentadiene and acrylonitrile, and Tamaki
[27] has shown that γCD enhances the photodimerisation of 2-anthracene-
sulphonate. Upon inclusion in the cyclodextrin cavity, a guest experi-
ences changes in its reactivity and physicochemical properties, and
these changes are of great practical significance. There has been
considerable research into the utilisation of cyclodextrin inclusion
complexes in the pharmaceutical, agricultural and food industries [3,
8, 9].

1.2 A Brief History of Cyclodextrin Chemistry

Cyclodextrins were first isolated in 1891 by Villiers [28] as degradation products of starch. However, Schardinger was the first to describe their preparation, isolation and properties in detail. Over the period 1903-1911, Schardinger [29-31] isolated α- and βCD, and provided evidence for their cyclic structure and their ability to form inclusion complexes. Further contributions to understanding the chemistry of the cyclodextrins did not eventuate until the 1930's and later. Freundenberg (1935) [32] developed a method of obtaining pure α- and βCD, and in the process isolated γCD. In 1938 Freundenberg [33] reported that the cyclodextrins are constructed from α-1,4 linked glucose residues, and later (1939) [34] recognised that cyclodextrins could form inclusion complexes. French [35, 36] also worked out procedures for synthesising pure cyclodextrins, and determined the molecular weights of the cyclodextrins. The formation of cyclodextrin inclusion complexes has been studied systematically by Cramer [37-39]. Cramer (1953) [40] also discovered that the cyclodextrins have a catalytic action in some reactions, and with co-workers (1967) [41] reported the first study of the kinetics of complex formation. Contemporary workers in the field of cyclodextrin chemistry include: Bender [1, 7] studies of the catalytical properties of cyclodextrins; Breslow [5] and Tabushi [4, 6], the utilisation of modified cyclodextrins as enzyme models; Saenger [3] has provided considerable X-ray structural data of cyclodextrin inclusion complexes and has highlighted the potential applications of in-clusion complexes; and Szejtli [8, 9] has applied cyclodextrin inclusion complexes to the pharmaceutical industry.

1.3 Thermodynamic Aspects of Cyclodextrin Complex Formation

The bonding in cyclodextrin inclusion complexes is nonspecific, as it does not involve strong covalent or electrostatic forces. A variety of binding forces have been suggested in the literature to explain how inclusion complexes form.

From a phenomenological point of view, inclusion complex formation is characterised by the following features. The existence of a good spatial fit between the guest and the cyclodextrin cavity is a necessary requirement for the formation of a stable complex. Complex formation is almost always associated with a negative enthalpy change ($\Delta H^\circ < 0$), whereas the entropy change can be positive or negative, though it is usually found to be negative ($\Delta S^\circ < 0$). Interestingly, if values of ΔH° are plotted against values of ΔS° for complex formation between a particular cyclodextrin but different guests spanning a wide range of structural, electrical and dipolar diversities, a linear relationship is observed [42-45]. This linear correlation implies a common interaction mechanism between the cyclodextrin and the various substrates. Such a mechanism must be divorced from the wide range of varied substrate species and so must be associated with some common attribute of these systems, the solvent water and/or the host cyclodextrin.

Several intermolecular interactions have been proposed and discussed as being responsible for the formation of cyclodextrin inclusion complexes in aqueous solution. They are:

(1) hydrogen bonding;

(2) the relief of conformational strain in the 'empty' cyclodextrin upon substrate inclusion;

(3) the release of 'high energy' water from the cyclodextrin cavity upon substrate inclusion;

(4)   hydrophobic interaction; and

(5)   van der Waals interaction.

The contribution of hydrogen bonding to the stability of inclusion complexes has been suggested by Cramer and Kampe [46], and demonstrated crystallographically in certain cases [16]. In the solid state hydrogen bonds can form between the included guest and the primary hydroxyl groups of the cyclodextrin. No decisive evidence which substantiates that hydrogen bonding also acts as a major driving force in aqueous solution has yet been presented. Indeed, hydrogen bonding between guest and cyclodextrin molecules does not seem important for the following reasons:

(1)   substrate binding is not drastically decreased when the cyclodextrin is rendered incapable of hydrogen bonding by methylation of its primary hydroxyl groups [47, 48]; and

(2)   guests incapable of hydrogen bonding to cyclodextrins, such as rare gases and alkanes, are included by cyclodextrin relatively strongly [49].

The relief of conformational strain energy in the 'empty' αCD upon substrate inclusion is regarded as the main driving force of complexation by Saenger et al. [11, 50]. The 'empty' αCD is unsymmetrically distorted and, as such, is in a 'strained' high energy conformation [11]. When a guest binds in the αCD cavity, αCD undergoes a conformational change to an unstrained 'relaxed' state. This relief of strain energy contributes to the stability of the inclusion complex. This binding force can occur only with αCD, since 'empty' β- and γCD are not strained [12, 13]. Thermo-dynamic [47, 51] and theoretical [52] considerations have suggested that this binding force is of minor importance in the case of αCD complexation. Substrate binding is not greatly reduced (rather slightly strengthened) on

methylation of the primary hydroxyl groups of αCD, which apparently

prevents the tilting of glucose units so that a conformational change

does not occur on binding a guest molecule [47].

Water plays a crucial role in the inclusion process. Inclusion

complexes tend to form most readily in aqueous solution. While cyclo-

dextrin does form inclusion complexes in such nonaqueous solvents as

dimethyl sulphoxide, the binding is very weak compared with that in

water [53]. Similarly, Gerasimowicz and Wojcik [54] have shown that

the stabilities of some inclusion complexes in aqueous solution decrease

markedly with the addition of dimethyl sulphoxide to the solution. The

linear relationship or compensation observed between ΔH° and ΔS° is in-

dicative of the participation of water in complex formation [55], and

can be attributed to changes in the solvation of guest and cyclodextrin

molecules. The slope of the straight line representing the plot of ΔH°

against ΔS° is called the compensation temperature, and values obtained

[42-45] for this slope fall in the range characteristic of processes

dominated by solvation phenomena [6, 55]. Mochida et al. [56] have also

implicated the participation of water in the inclusion process, since

changes in the activity of water caused by the presence of inorganic

salts affected the apparent association constant of a complex formed

between βCD and an azo dye. Kinetic studies [41, 57] have revealed the

importance of the breakdown of water structure around a guest and with-

in the cyclodextrin cavity to the inclusion reaction. The pre-eminence

of water in the inclusion process, and the favoured inclusion of apolar

guests by cyclodextrin [58-61] suggest the involvement of hydrophobic

interactions [62] in the formation of inclusion complexes.

The classical hydrophobic interaction essentially involves a favourable entropy change ($\Delta S° > 0$), together with a slightly positive enthalpy change ($\Delta H° \geqslant 0$) [63]. This is in contrast to the thermodynamic parameters determined for the formation of cyclodextrin complexes that show the inclusion process is mostly governed by a negative enthalpy change. Bender et al. [1, 7, 64] have explained the thermodynamic data in terms of an 'atypical' hydrophobic interaction involving the release of 'high energy' water from the cyclodextrin cavity. Water molecules enclosed within the uncomplexed cyclodextrin cavity cannot have a full complement of hydrogen bonds, owing to steric interference from the D glucopyranose ring of cyclodextrin, so that they are 'enthalpy rich.' The expulsion of the 'enthalpy rich' molecules into bulk water upon substrate inclusion results in a negative enthalpy change, together with a negative entropy change. The importance of this binding force is somewhat controversial [47, 51, 65]. The uncomplexed βCD includes a larger number of 'high energy' water molecules than uncomplexed αCD [11, 12]. If the major part of the binding energy is derived from the removal of 'high energy' water, βCD should give more negative enthalpy of complexation than αCD. In contradiction to this presumption, the values of $\Delta H°$ and $\Delta S°$ for the formation of βCD complexes with para-nitrophenol [65] and meta- and para-substituted benzenes [66] are considerably less negative than those of the corresponding αCD complexes.

Recent thermodynamic studies suggest that the classical hydrophobic interaction is involved in complex formation, but its contribution to the thermodynamic parameters is masked by contributions from other binding force(s). The hydrophobic interaction plays a primary role in the formation of βCD-1-alkanol complexes ($\Delta H° > 0$, $\Delta S° > 0$) [67]. However, as the bulkiness of the alcohol increases relative to the size of the

βCD cavity, ΔH° becomes negative and the contribution of ΔS° to the binding is less significant. Binding force(s) other than hydrophobic interaction must also be responsible for complex formation. Harrison and Eftink [68] have found that the binding of adamantanecarboxylate to βCD is hydrophobically driven. The values of ΔH° and ΔS° evaluated, however, indicated that other intrinsic binding forces were important in addition to the hydrophobic effect. The relative contribution of the hydrophobic effect and other binding forces to the overall binding were estimated. The values of ΔH° and ΔS° for the hydrophobic component were characteristic of a classical hydrophobic interaction, whereas the thermodynamic parameters for the intrinsic binding component were both negative and consistent with the involvement of van der Waals interactions resulting from the close fit of the substrate in the βCD cavity.

The van der Waals interaction generally consists of dipole-dipole and dipole-induced dipole interactions and London dispersion forces. The importance of these forces in the overall cyclodextrin-substrate binding is based on a linear relationship between the polarisability of a group of structurally similar substrates and the stability of the complexes which they form in aqueous solution [51, 64]. The importance of van der Waals interactions in inclusion complex stability has been further emphasised through thermodynamic [43, 65, 69, 70] and theoretical [52] studies. Interestingly, these forces are most likely to provide a basis for specificity in substrate binding, with cyclodextrin-substrate complexes in which the guest closely fits the cyclodextrin cavity being the most stabilised. X-ray crystallographic studies [16] have shown that guest molecules can be in close van der Waals contact with the interior of the cyclodextrin cavity.

Clearly, several binding forces contribute to the overall free energy of the inclusion process, and the respective contributions of these different forces will not necessarily be the same with different substrates and different cyclodextrins. Nevertheless, present evidence suggests that both hydrophobic interactions and van der Waals forces are major driving forces in the formation of cyclodextrin inclusion complexes [6, 52, 67, 68, 71, 72]. Cromwell et al. [72] have rationalised the different binding affinities of the cyclodextrins for adamantanecarboyxlate in terms of the relative contribution of the hydrophobic effect and van der Waals forces to the stabilities of the inclusion complexes. Tabushi et al. [6, 52] have concluded that cyclodextrin complexation involves a 'hydrophobic' interaction that is a kind of 'combined' interaction incorporating (1) van der Waals interaction between a guest molecule and the cyclodextrin cavity; (2) entropy gain due to the destruction of water assembly around the guest molecule; and (3) entropy loss due to 'freezing' motional freedom of the guest molecule in the cyclodextrin cavity.

1.4 Kinetic Aspects of Cyclodextrin Complex Formation

The majority of reported studies of cyclodextrin inclusion complex formation have been thermodynamic in nature; few kinetic studies have been reported. A possible reason for this is that cyclodextrin complexation is a very rapid process and kinetic studies require experimental techniques specialised for studying fast reactions. Cramer et al. [41] were the first to report a study of the kinetics of the inclusion reaction. They found that the rates of complex formation fall conveniently into the temperature-jump timerange. The temperature-jump method has

been the main kinetic technique used to study the inclusion reaction, although kinetic studies using ultrasonic relaxation [73], stopped-flow [74, 75] and the measurement of phosphorescence decays [57, 76] have been reported.

The most studied inclusion reaction has been 1:1 complex formation, chiefly with αCD as the host (and with azo dyes as guests) [41, 74, 75, 77-79], sometimes with βCD [57, 73, 76, 79, 80], and rarely with γCD [57]. Charge [41, 75, 78] and steric [41, 74, 75, 78, 79] effects have been shown to be important factors in influencing the kinetics. Several studies [41, 75, 78] of complex formation between azo dyes and αCD have found that the formation and dissociation rates were very sensitive to the nature of the dye and varied over several orders of magnitude, whilst the equilibrium constants exhibited a lesser variation, consistent with variations in the nature of the dye affecting the formation and dissociation rates to a similar extent. Both Cramer et al. [41] and Turro et al. [57] have discussed the role of desolvation processes in the kinetics of complex formation. The breakdown of water structure around a guest and within the cyclodextrin cavity appear to be important steps in the inclusion process. The values of activation volumes characterising the inclusion of phenolphthalein by βCD [80] indicate that desolvation from the dye and the release of hydrating water molecules from the βCD cavity occur at the transition state. Steric interactions between the guest and groups on the rim and on the inside of the cyclodextrin cavity can affect the rate of complex formation [41, 75]. Although a conformational change of cyclodextrin during the binding of a guest appears to be unimportant in the stability of the inclusion complex formed, it may affect the rate of formation of the complex. A conformational change has been proposed as being rate-determining in the complexation of inorganic anions by βCD [73]. A contact ion complex is first formed

between anion and βCD, followed by the slower rate-determining conformational change of the complex. The binding of I⁻ to αCD [77] also occurs through a similar mechanism, the conformational change resulting from the 'strained' structure of αCD. Hersey and Robinson [75] have suggested that the formation of azo dye-αCD complexes is not a simple one-step process as described by others [41, 74, 78, 79]. They have provided evidence for a reaction scheme that involves a fast pre-equilibrium step to form a binary intermediate, which then undergoes a slower isomerisation to the final stable product. Conformational change of a guest during complex formation may also occur, since deformations in the planar structure of phenolphthalein are thought to be rate-determining in its inclusion by βCD [80].

Clarke et al. [81, 82] have found that certain azo dyes can be included in the cavities of β- and γCD as dimers. The mechanism of two guest-one host complexation involved the stepwise inclusion of two dye monomers by cyclodextrin. The rate of formation of the precusor 1:1 complex was much faster than that of the 2:1 complex, and only rate constants characterising the latter step could be evaluated.

The small number of reported kinetic studies has highlighted some of the basic features of inclusion complex formation. Studies have revealed that solvation changes, steric interactions and possibly conformational change of cyclodextrin and/or guest are important in the inclusion reaction. However, a detailed description of the inclusion process and the identification of the major energetic contributions to the kinetics have as yet to be forthcoming.

1.5 The Aims of This Work

Most reported cyclodextrin studies have been limited to α- and βCD, the larger cyclodextrin, γCD, being studied relatively little [83]. The systematic variation of the annular radii of the cyclodextrins (Table 1.1) provides an opportunity to test for selectivity in the formation of inclusion complexes, and some examples have been presented in the literature [24, 45, 83, 84]. In particular, studies [24, 84] have shown that the larger cavity of γCD is readily able to accommodate two guest molecules simultaneously. This work reports kinetic and equilibrium studies of the interaction of some selected dyes: crystal violet, pyronine Y, pyronine B and rhodamine B, with the cyclodextrins. An aim of this work is to examine the manner in which the relative sizes of the dye and host cyclodextrin cavity contribute towards influencing the stoichiometry and stability of inclusion complexes formed. UV/visible absorption spectroscopy will be used to detect complex formation between dye and cyclodextrin, and to characterise the nature of the inclusion complex(es) formed. Temperature-jump relaxation spectrophotometry will be used to deduce the mechanism of inclusion complex formation and evaluate the respective kinetic parameters. A further aim of this work is to obtain some greater understanding of the kinetic aspects of the inclusion process.

Bibliography

1. GRIFFITHS, D. W. and BENDER, M. L. **Adv. Cat. 23,** 209 (1973).

2. BERGERON, R. J. **J. Chem. Ed. 54,** 204 (1977).

3. SAENGER, W. **Angew. Chem. Int. Ed. Engl. 19,** 344 (1980).

4. TABUSHI, I. **Acc. Chem. Res. 15,** 66 (1982).

5. BRESLOW, R. **Chem. Br. 1983,** 126.

6. TABUSHI, I. and KURODA, Y. **Adv. Cat. 32,** 417 (1983).

7. BENDER, M. L. and KOMIYAMA, M. **Cyclodextrin Chemistry,** Springer-Verlag, Berlin, 1978.

8. SZEJTLI, J. **Cyclodextrins and Their Inclusion Complexes,** Akademiai Kiado, Budapest, 1982.

9. SZEJTLI, J. (ed). **Proceedings of the First International Symposium on Cyclodextrins,** Akademiai Kiado, Budapest, 1982.

10. FRENCH, D., PULLEY, A. O., EFFENBERGER, J. A., ROUGUIE, M. A. and ABDULLAH, M. **Arch. Biochem. Biophys. 111,** 153 (1965).

11. MANOR, P. C. and SAENGER, W. **J. Am. Chem. Soc. 96,** 3630 (1974).

12. LINDNER, K. and SAENGER, W. **Angew. Chem. Int. Ed. Engl. 17,** 694 (1978).

13. MACLENNAN, J. H. and STEZOWSKI, J. J. **Biochem. Biophys. Res. Commun. 92,** 926 (1980).

14. CASU, B., REGGIANI, M., GALLO, G. G. and VIGERANI, A. **Carbohydr. Res. 12,** 157 (1970).

15. BEYCHOK, S. and KABAT, E. A. **Biochemistry 4,** 2565 (1965).

16. SAENGER, W. **Proc. 1st Int. Symp. on Cyclodextrins,** Budapest, 1981, 141.

17. KATO, S., NOMURA, H. and MIYAHARA, Y. **J. Phys. Chem. 89,** 5417 (1985).

18. RAUH, S. and KNOCHE, W. **J. Chem. Soc. Faraday Trans. I 81,** 255 (1985).

19. HYBL, A., RUNDLE, R. E. and WILLIAMS, D. E. **J. Am. Chem. Soc. 87,** 2779 (1965).

20. DEMARCO, P. V. and THAKKAR, A. L. **Chem. Commun. 1970,** 2.

21. CRAMER, F. **Revs. Pure Appl. Chem. 5,** 143 (1955).

22. BRERETON, I. M., SPOTSWOOD, T. M., LINCOLN, S. F. and WILLIAMS, E. H. **J. Chem. Soc. Faraday Trans. I 80,** 3147 (1984).

23. UENO, A., TOMITA, Y. and OSA, T. **J. Chem. Soc. Chem. Commun. 1983,** 976, and references cited therein.

24. CLARKE, R. J., COATES, J. H. and LINCOLN, S. F. J. Chem. Soc. Faraday Trans. I, in press.

25. CRAMER, F. Proc. 1st Int. Symp. on Cyclodextrins, Budapest, 1981, 3.

26. BRESLOW, R. and RIDEOUT, D. J. Am. Chem. Soc. 102, 7816 (1980).

27. TAMAKI, T. Chem. Letts. 1984, 53.

28. VILLIERS, A. Comptes Rendues 112, 536 (1891).

29. SCHARDINGER, F. Zeitschrift für Untersuchung der Nahrungsund Genossmittel 6, 865 (1903).

30. SCHARDINGER, F. Weinerklinischen Wochen Schrift 17, 207 (1904).

31. SCHARDINGER, F. Zentralblatt für Bakteriologie II 29, 188 (1911).

32. FREUNDENBERG, K. and JACOBI, R. Ann. 518, 102 (1935).

33. FREUNDENBERG, K. and MEYER-DELIUS, M. Ber. 71, 1596 (1938).

34. FREUNDENBERG, K. SCHAAF, E., DUMPERT, G. and PLOETZ, T. Naturwissenschaften 27, 850 (1939).

35. FRENCH, D., LEVINE, M. L., PAZUR, J. H. and NORBERG, E. J. Am. Chem. Soc. 71, 353 (1949).

36. FRENCH, D. and RUNDLE, R. E. J. Am. Chem. Soc. 64, 1651 (1942).

37. CRAMER, F. Einschlussverbindungen, Springer, Heidelberg, 1954.

38. CRAMER, F. and HETTLER, H. Naturwissenschaften 54, 625 (1967).

39. CRAMER, F. and HENGLEIN, F. H. Chem. Ber. 90, 2581 (1957).

40. CRAMER, F. Chem. Ber. 86, 1576 (1953).

41. CRAMER, F., SAENGER, W. and SPATZ, H-Ch. J. Am. Chem. Soc. 89, 14 (1967).

42. LEWIS, E. A. and HANSEN, H. D. J. Chem. Soc. Perkin Trans II 1973, 2081.

43. GELB, R. I., SCHWARTZ, L. M., CARDELINO, B. FUHRMANN, H. S., JOHNSON, R. F. and LAUFER, D. A. J. Am. Chem. Soc. 103, 1750 (1981).

44. GELB, R. I., SCHWARTZ, L. M., RADEOS, M. and LAUFER, D. A. J. Phys. Chem. 87, 3349 (1983).

45. CLARKE, R. J. Ph.D. Thesis, University of Adelaide (1985).

46. CRAMER, F. and KAMPE, W. J. Am. Chem. Soc. 87, 1115 (1965).

47. BERGERON, R. J. and MEELOY, M. P. Biorg. Chem. 5, 197 (1976).

48. CAZU, B. and REGGIANI, M. Carbohydr. Res. 76, 59 (1979).

49. CRAMER, F. and HENGLEIN, F. M. Angew. Chem. 68, 649 (1956).

50. SAENGER, W., NOLTEMEYER, M., MANOR, P. C., HINGERTY, B. and KLAR, B. Bioorg. Chem. 5, 187 (1976).

51. BERGERON, R. J., CHANNING, M. A., GIBEILY, G. J. and PILLOR, D. M. J. Am. Chem. Soc. 99, 5146 (1977).

52. TABUSHI, I., KIGUSUKE, Y-I, SUGIMOTO, T. and YAMAMURA, K. J. Am. Chem. Soc. 100, 916 (1978).

53. SIEGEL, B. and BRESLOW, R. J. Am. Chem. Soc. 97, 6869 (1975).

54. GERASIMOWICZ, W. V. and WOJCIK, J. F. Bioorg. Chem. 11, 420 (1982).

55. LUMRY, R. and RAJENDER, S. Biopolymers 9, 1125 (1970).

56. MOCHIDA, K., KAGITA, A., MATSUI, Y. and DATE, Y. Bull. Chem. Soc. Jpn. 46, 3703 (1973).

57. TURRO, N. J., OKUBO, T. and CHUNG, C-J. J. Am. Chem. Soc. 104, 1789 (1982).

58. VAN HOOIDONK, C. and BREEBAART-HANSEN, J. C. A. E. Rev. Trav. Chim. Pay-Bas. 91, 958 (1972).

59. KOMIYAMA, M. and BENDER, M. L. J. Am. Chem. Soc. 100,2259 (1978).

60. TABUSHI, I., KURODA, Y. and MIZUTANI, T. Tetrahedron 40, 545 (1984).

61. TUCKER, E. E. and CHRISTIAN, S. D. J. Am. Chem. Soc. 106, 1942 (1984).

62. NEMETHY, G. and SCHERAGA, H. A. J. Chem. Phys. 36, 3401 (1962).

63. KAUZMANN, W. Adv. Protein Chem. 14, 1 (1959).

64. VAN ETTEN, R. L., CLOWES, G. A., SEBASTIAN S. F. and BENDER, M. L. J. Am. Chem. Soc. 89, 3242 (1967).

65. HARATA, K. Bioorg. Chem. 9, 530 (1980).

66. HARATA, K. Bioorg. Chem. 10, 255 (1981).

67. MATSUI, Y. and MOCHIDA, K. Bull. Chem. Soc. Jpn. 52, 2808 (1979).

68. HARRISON, J. C. and EFTINK, M. R. Biopolymers 21, 1153 (1982).

69. HALL, E. S. and ACHE, H. J. J. Phys. Chem. 83, 1805 (1979).

70. EFTINK, M. R. and HARRISON, J. C. Bioorg. Chem. 10, 388 (1981).

71. BERGERON, R. J., PILLOR, D. M., GIBEILY, G. and ROBERTS, W. P. Bioorg. Chem. 7, 263 (1978).

72. CROMWELL, W. C., BYSTROM, K. and EFTINK, M. R. J. Phys. Chem. 89, 326 (1985).

73. ROHRBACH, R. P., RODRIGUEZ, L. J., EYRING, E. M. and WOJCIK, J. F. J. Phys. Chem. 81, 944 (1977).

74. YOSHIDA, N., SEIYAMA, A. and FUJIMOTO, M. Chem. Letts. 1984, 703.

75. HERSEY, A. and ROBINSON, B. H. J. Chem. Soc. Faraday Trans. I 80, 2039 (1984).

76. TURRO, N. J., BOLT, J. D., KURODA, Y. and TABUSHI, I. Photochem. Photobiol. 35, 69 (1982).

77. SANO, T., YAMAMOTO, M., HORI, H. and YASUNAGA, T. Bull. Chem. Soc. Jpn. 57, 678 (1984).

78. ROHRBACH, R. P. and WOJCIK, J. F. Carbohydr. Res. 92, 177 (1981).

79. YOSHIDA, N. and FUJIMOTO, M. Bull. Chem. Soc. Jpn. 55, 1039 (1982).

80. NAKATANI, H. and HIROMI, K. J. Biochem. 96, 69 (1984).

81. CLARKE, R. J., COATES, J. H. and LINCOLN, S. F. Carbohydr. Res. 127, 181 (1984).

82. CLARKE, R. J., COATES, J. H. and LINCOLN, S. F. J. Chem. Soc. Faraday Trans. I 80, 3119 (1984).

83. HIRAI, H., TOSHIMA, N. and UENOYAMA, S. Polym. J. 13, 607 (1981).

84. HIRAI, H., TOSHIMA, N. and UENOYAMA, S. Bull. Chem. Soc. Jpn. 58, 1156 (1985).

CHAPTER II

Experimental Techniques

EXPERIMENTAL TECHNIQUES

2.1 Temperature-Jump Relaxation Spectrophotometry

Chemical relaxation methods were introduced by Eigen in 1954 for the purpose of studying the rates and mechanisms of fast reactions in solution [1]. The term 'fast reaction' may be taken to mean a reaction that is fast compared with the time required for mixing and observation by conventional methods. The basic principle of relaxation methods consists of perturbing the equilibrium of a reaction mixture by rapidly changing an external parameter that influences the equilibrium (e.g. temperature, pressure, electric field intensity), followed by the direct or indirect observation of the subsequent adjustment or relaxation of the reaction mixture to its new equilibrium position, which proceeds with a finite time lag. The measurement of the rate of this adjustment to the new equilibrium position permits the kinetics of the reaction to be determined and eventually a hypothesis for the mechanism to be proposed.

The temperature-jump method is a relaxation method that utilises a rapid increase in temperature to perturb an equilibrium system; it is probably the most versatile and most widely used of the relaxation methods. The basis of the temperature-jump method is the temperature dependence of the equilibrium constant,

$$\left(\frac{\partial \ln K}{\partial T}\right)_P = \frac{\Delta H^\circ}{RT^2} \qquad (2.1)$$

Since most chemical equilibria are associated with a finite standard enthalpy of reaction, ΔH°, (or may be coupled to a reaction that is associated with a finite standard enthalpy of reaction) this facilitates the wide application of this technique in the study of the kinetics of fast reactions. Furthermore, the timerange accessible to the temperature-

jump method $(1 - 10^{-8}$ seconds) is wide, and matches the range of times over which a large number of inorganic, organic and biochemical reactions proceed. Before the temperature-jump method is discussed in detail, it is necessary to describe how kinetic and thermodynamic information can be obtained from studying chemical relaxation.

2.1.1 Principles of chemical relaxation

Consider the single step equilibrium system (Equation 2.2) that describes the dimerisation of a dye, D,

$$2D \underset{k_{-d}}{\overset{k_d}{\rightleftharpoons}} D_2 \qquad (2.2)$$

with the forward and backward rate constants, k_d and k_{-d}, respectively. The general rate equation is given by

$$-\frac{1}{2} \frac{dC_D}{dt} = \frac{dC_{D_2}}{dt} = k_d C_D^2 - k_{-d} C_{D_2} \qquad (2.3)$$

The concentrations (or strictly activities) of the species at equilibrium are fixed, and their interrelation is expressed by the thermodynamic equilibrium constant, K. Furthermore, at equilibrium,

$$-\frac{1}{2} \frac{dC_D}{dt} = 0 \qquad (2.4)$$

Consider the system initially at equilibrium, and suppose there is a sudden change in a parameter that influences the equilibrium (e.g. a rapid increase in temperature). The perturbation will momentarily result in a deviation of the concentrations from those required by the new conditions. The deviation, however, will tend to vanish. The system will adjust itself and will approach its stable equilibrium in a manner described by the rate equation. The concentrations of the species immediately after the perturbation can be expressed as

$$C_D = \bar{C}_D^f + \Delta C_D \tag{2.5}$$

and

$$C_{D_2} = \bar{C}_{D_2}^f + \Delta C_{D_2} \tag{2.6}$$

where $\bar{C}_i^f$ corresponds to the concentration of a species once the final equilibrium position has been reached, and ΔC_i is the deviation of the actual concentration from that final equilibrium value. The principle of mass conservation shows that

$$\bar{C}_D^f + 2\bar{C}_{D_2}^f = C_0 \tag{2.7}$$

where C_0 is the total dye concentration, and thus

$$\Delta C_D + 2\Delta C_{D_2} = 0 \tag{2.8}$$

or

$$\Delta C_D = -2\Delta C_{D_2} \tag{2.9}$$

If all rate constants and equilibrium concentrations refer to the final equilibrium conditions, then Equation 2.3 can be written as

$$-\tfrac{1}{2}\frac{d(\bar{C}_D + \Delta C_D)}{dt} = k_d(\bar{C}_D + \Delta C_D)^2 - k_{-d}(\bar{C}_{D_2} - \tfrac{1}{2}\Delta C_D) \tag{2.10}$$

However, from Equation 2.4 this expression reduces to

$$-\tfrac{1}{2}\frac{d\Delta C_D}{dt} = 2k_d\bar{C}_D\Delta C_D + k_d\Delta C_D^2 + \tfrac{1}{2}k_{-d}\Delta C_D \tag{2.11}$$

If only small equilibrium perturbations are considered, $\Delta C_D \ll \bar{C}_D$, then Equation 2.11 further simplifies to

$$\frac{d\Delta C_D}{dt} = -\left[4k_d\bar{C}_D + k_{-d}\right]\Delta C_D \tag{2.12}$$

This leads to the linearisation of the rate equation. Thus, the rate of disappearance of the difference between the actual and equilibrium concentrations is proportional to this difference itself. The reciprocal of the proportionality factor, $[4k_d\bar{C}_D + k_{-d}]$, has the dimensions of time,

and is called the relaxation time. Equation 2.12 can be written as

$$\frac{d\Delta C_D}{dt} = -(1/\tau)\Delta C_D \tag{2.13}$$

or, more generally,

$$\frac{d\Delta C_i}{dt} = -(1/\tau)\Delta C_i \tag{2.14}$$

The physical significance of the relaxation time can be seen by integration of Equation 2.14,

$$\int_{\Delta C_i^o}^{\Delta C_i} \frac{d\Delta C_i}{\Delta C_i} = -(1/\tau) \int_0^t dt \tag{2.15}$$

which leads to

$$\ln\left(\frac{\Delta C_i}{\Delta C_i^o}\right) = -t/\tau \tag{2.16}$$

or

$$\Delta C_i = \Delta C_i^o \exp(-t/\tau) \tag{2.17}$$

where ΔC_i^o is the difference between the initial and final equilibrium concentrations. Substituting $t = \tau$ into Equation 2.17 leads to

$$\Delta C_i = \Delta C_i^o/e$$

Thus, the relaxation time corresponds to the time taken for the initial deviation from the final equilibrium concentration to decrease by the factor e.

The experimental aspects of chemical relaxation studies involve

(1) the perturbation of the equilibrium system in a known manner; and

(2) the observation and recording of a concentration variable or related property as a function of time.

In most cases a physical property, P (e.g. absorbance, conductance), that is linearly proportional to the concentration of chemical species,

is used to observe the relaxation of the reaction mixture following perturbation, and Equation 2.17 can be written as

$$\Delta P = \Delta P^{\circ} \exp(-t/\tau) \tag{2.18}$$

where ΔP is the instantaneous deviation of P from its final equilibrium value, and ΔP° is the net change in P due to the chemical relaxation process. The output of an experiment (for a single-step reaction) is the relaxation trace from which the relaxation time can be evaluated. In general the relaxation time will have a unique dependence on the equilibrium concentrations, and the systematic study of the relaxation times as a function of concentration permits postulation of a reaction mechanism and the determination of the rate constants. For example, for a reaction given by Equation 2.2,

$$1/\tau = 4k_d\bar{C}_D + k_{-d} \tag{2.19}$$

or from Equation 2.7,

$$1/\tau^2 = 8k_d k_{-d} C_0 + k^2_{-d} \tag{2.20}$$

where C_0 is the total dye concentration. For a system in which the values of τ have been experimentally determined, a plot of $1/\tau^2$ versus C_0 must be a straight line if the reaction is to be consistent with the mechanism given by Equation 2.2. In practice, a variety of reciprocal relaxation time expressions describing different potential mechanisms are considered to explain the observed variation of $1/\tau$ with concentration. The agreement between the experimental dependence of $1/\tau$ on concentration and that predicted by the reciprocal relaxation time expression is used as a criterion for accepting or discarding a particular mechanism.

In general, reactions involving more than one chemical equilibrium step cannot be characterised by a single relaxation time. Since the individual equilibria are coupled, the relaxation times are a general function of the equilibrium concentrations of all the species present

and the associated rate constants. Thus, in a multistep reaction involving n independent concentration variables, the rate of decay of the deviation of the concentration of a component from its final equilibrium value is given by the general equation

$$\frac{d\Delta C_i}{dt} = -\sum_{i=1}^{n} (1/\tau_i)\Delta C_i \tag{2.21}$$

This equation can also be expressed as follows:

$$\frac{d\Delta C_i}{dt} = -\sum_{i,j=1}^{n} a_{ij}\Delta C_i \tag{2.22}$$

where the a_{ij} terms are functions of the rate constants and equilibrium concentrations for the particular reaction mechanism. Matrix algebra [2] may be used to derive expressions for the reciprocal relaxation times from Equation 2.22. However, if some steps equilibrate much more rapidly than the others, it is possible to simplify the equations (examples are described in Appendix D). Bernasconi [2] and Czerlinski [3] describe methods for deriving reciprocal relaxation time expressions for multistep reaction mechanisms and provide a large number of examples.

Relaxation amplitudes, the ΔP° term in Equation 2.18, are measures of equilibrium shifts, and can be used to determine thermodynamic functions (e.g. ΔH°, ΔV°) for elementary reaction steps. Thusius [4] has shown that for a one-step equilibrium system the expression for the relaxation amplitude is of the form

$$\Delta P^\circ = \Delta\phi\Gamma\Delta\ln K \tag{2.23}$$

The terms in Equation 2.23 are defined as follows:

$$\Delta\phi = \sum_{i=1}^{n} \nu_i\phi_i \quad , \quad \phi_i = \frac{\partial P_i}{\partial C_i}$$

The values of ϕ_i are proportional to the physical property that measures the changes in concentration. For example, if spectrophotometric detection is used to observe the chemical relaxation, then ϕ_i is proportional

to the molar absorbance, ε_i, for each species in the equilibrium. The ν_i are stoichiometric coefficients, defined as negative for participants on the left side of the stoichiometric equation and positive for those on the right side.

$$\Gamma = \left(\sum_{i=1}^{n} \nu_i^2 / \bar{C}_i \right)^{-1}$$

where $\bar{C}_i$ is the equilibrium concentration of species i. For example, for the equilibrium given by Equation 2.2,

$$\Gamma = \left[\frac{4}{[D]} + \frac{1}{[D_2]} \right]^{-1}$$

Finally, $\Delta \ln K$ is proportional to the relevant thermodynamic function. In the case of the temperature-jump method and finite but small changes in K, it follows from Equation 2.1 that

$$\Delta \ln K = \frac{\Delta K}{K} = \left(\frac{\Delta H^{\circ}}{RT^2} \right) \Delta T$$

where ΔT is the temperature rise obtained from the temperature jump. Thus, by measuring the relaxation amplitudes and plotting ΔP° against Γ, it is possible to evaluate the appropriate thermodynamic function. The analysis of relaxation amplitudes may also provide a way of substantiating the assignment of a mechanism to a reaction under study.

2.1.2 The temperature-jump method

The temperature-jump technique was first proposed by Eigen in 1954 [1], but it was not until 1959 that the first operational temperature-jump apparatus was described [5]. Since then, the temperature-jump method has increased in popularity.

A schematic diagram of the temperature-jump apparatus, which has been developed in this laboratory to a design similar to that described

in the literature [6], is shown in Figure 2.1. A temperature change is produced using Joule heating by discharging a high-voltage capacitor through the reaction mixture. A low-inductance capacitor is charged by a high-voltage generator, and by closing a spark gap the capacitor is discharged to ground through the sample cell containing the reaction mixture wherein the dissipated energy heats the solution by a few degrees. The Joule heating method is limited to conducting solutions, and therefore to ionising solvents. The extent of the temperature rise, as well as the time taken for the rise, are determined by the characteristics of the circuit and the applied voltage [5, 6]. The size of the temperature jump, ΔT, is given by [2, 6]

$$\Delta T = \frac{CU_0^2}{2C_p\rho V} \qquad (2.24)$$

where C is the capacitance of the condensor, U_0 is the voltage to which the capacitor is charged, C_p is the heat capacity of the solution, ρ is the density of the solution, and V is the volume occupied by the solution in the sample cell. The heating of the solution, as with chemical relaxation, proceeds exponentially with a characteristic time constant, τ_0, termed the heating time:

$$\tau_0 = \tfrac{1}{2}RC \qquad (2.25)$$

R is the total resistance of the discharge circuit but it is usually assumed to be represented only by the resistance of the sample cell. It is desirable that the temperature change should produce an equilibrium shift in the reaction mixture which is sufficient to induce measurable concentration changes. Ideally the heating time should be much shorter than the relaxation time to be measured, so that the heating process is essentially complete before chemical relaxation has made any significant progress. This is achieved by using solutions of sufficiently low resistance. If the reaction mixture is not a reasonably good electrical
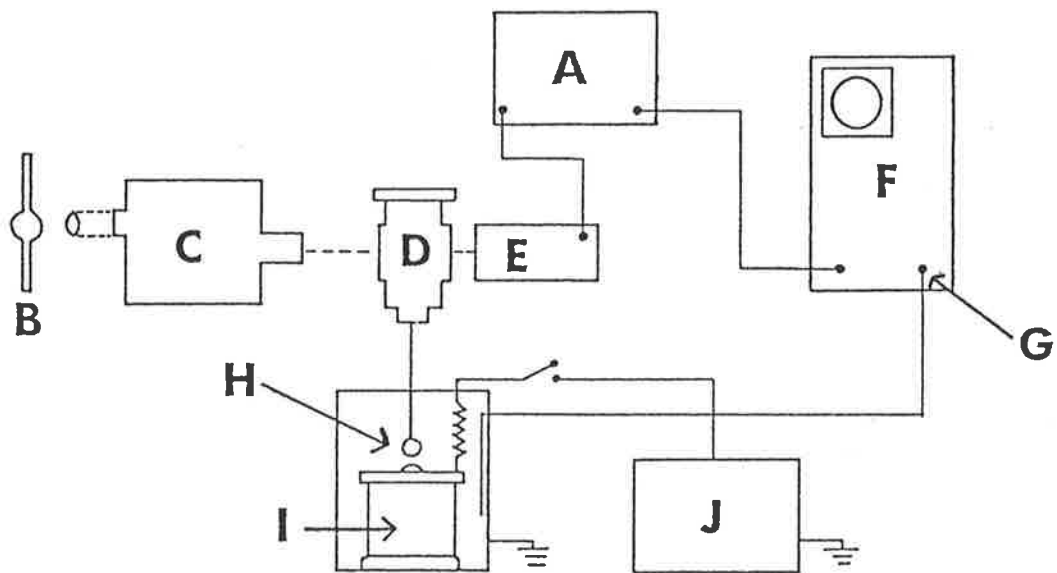
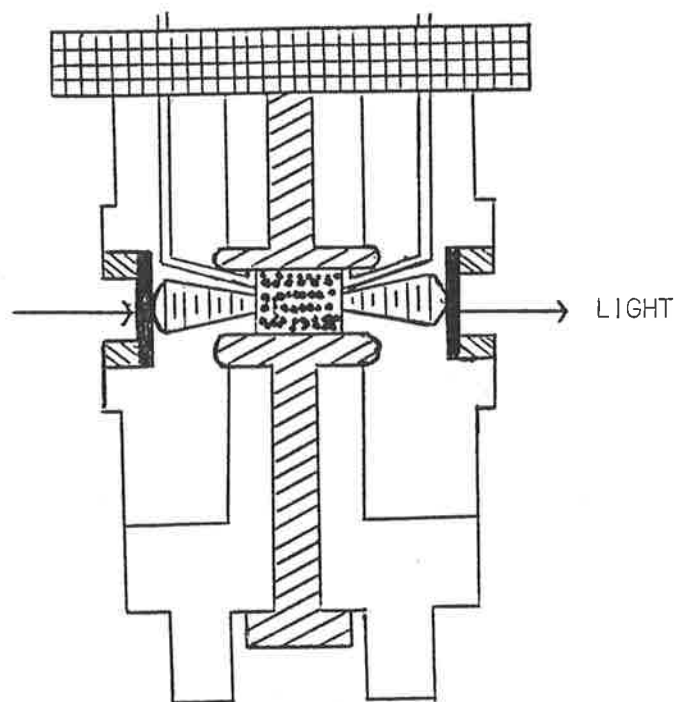*Figure 2.1: Schematic diagram of the temperature-jump apparatus* [7]

A: emitter-follower

B: lamp

C: monochromator

D: cell assembly

E: photomultiplier

F: transient recorder/oscilloscope

G: external trigger

H: moveable spark gap

I: capacitor

J: power supply

conductor, an inert salt must be added to increase the conductance and
ensure rapid heating.

A Brandenburg E.H.T. generator, which provides a stabilised voltage
output in the range 5 to 50 kilovolts, is used to charge a 0.2 microfarad
capacitor using a 25 megohm charging resistor incorporated in series with
the capacitor. The discharge of the capacitor is effected by manually
closing a spark gap, leading to a surge of current between the stainless
steel electrodes of the sample cell and an increase in temperature of
the reaction solution. Both the capacitor and the charging resistor are
shielded from other parts of the electronic equipment by means of aluminium
and iron boxes to minimise electric and magnetic disturbances caused by the
spark.

Figure 2.2 shows a schematic diagram of the temperature-jump sample
cell. The sample cell is designed to achieve uniform heating of the
solution, and it is possible to utilise appropriate optical techniques
for the detection of concentration changes. The cell body is made of
perspex, and is fitted with conical quartz windows. The windows are not
permanently fixed into the cell body but are held in place by a rubber
O-ring and a teflon screw. The joint between the cell body and window
is sealed with silicone grease. The conical lenses focus the transmitted
light at the centre of the cell, and thereby increase the intensity of
the light passing through the cell.

The course of chemical relaxation is followed spectrophotometrically.
Light from a tungsten lamp passes through a Bausch and Lomb high intensity
grating monochromator, set to a wavelength corresponding to a principle
absorption band of one of the components in the reaction mixture. The
light beam traverses the sample cell, and the resulting light intensity
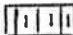
Figure 2.2: Schematic diagram of the temperature-jump cell

is measured by an EMI 5265S photomultiplier connected to an emitter-follower circuit. The photomultiplier is supplied by a stabilised high voltage supply (Nuclear Enterprises Ltd.). The emitter-follower outputs are collected using a Data Lab DL910 transient recorder. The transient recorder is triggered by the discharge of the capacitor via an unshielded wire antenna inside the capacitor discharge box. An oscilloscope is connected to the transient recorder to enable the photomultiplier output (the relaxation trace) to be displayed.

The apparatus shown in Figure 2.1 is typical of most Joule-heating temperature-jump apparatus, and is capable of producing temperature rises of ca. 5-10 K, with heating times in the order of 1-10 microseconds. If a coaxial cable is used as a capacitor, then heating times in the nanosecond timerange can be achieved. The apparatus constructed by Hoffman [8] is able to produce a temperature jump of 10 K, with a heating time as low as 50 nanoseconds. While this method still relies on Joule heating, it is more commonly called (Coaxial)-Cable temperature-jump. The main disadvantage of the methods that use Joule heating is that solutions must be of moderately high conductivity, and hence high ionic strength. This precludes studies of fast chemical systems in nonaqueous solvents (although studies may be possible if the conductance of the solution can be increased by the addition of an inert salt), and in aqueous solution when the chemical system cannot tolerate a high ionic strength (e.g. the presence of an inert salt may lead to 'salting-out'). Dielectric heating by means of microwave radiation can be used to heat a solution [9]. This method is distinctly advantageous for aqueous solutions of low ionic strength or nonaqueous solvents, provided the system has a relatively high microwave absorption coefficient and the absorption region is accessible to microwave radiation. Using this method, it is possible to obtain a temperature rise of ca. 1 K within 1 microsecond. The great

disadvantage of the Microwave temperature-jump method is that a sensitive method of detection is required to follow the small concentration changes because of the small temperature rise. Optical heating utilising laser pulses can be used to produce ultrafast temperature jumps. Turner et al. [10] have constructed a Raman-laser temperature-jump apparatus in which a temperature jump of up to 10 K with a heating time of ca. 25 nanoseconds can be achieved. The stimulated Raman effect in liquid nitrogen is used to shift the wavelength of the neodymium laser radiation from 1060 nm, where the absorbance of water is very small, to 1410 nm, where water absorbs strongly. The main disadvantage of this technique is that the absorption of light varies exponentially with pathlength, and some non-uniformity of heating occurs, requiring very small sample volumes over very short optical pathlengths (e.g. 0.01-0.1 cm).

2.1.3 Experimental procedure

The sample solution is degassed several times using the 'freeze pump thaw' method. The purpose of degassing is to minimise the formation of bubbles in the solution, which may lead to distortions of the light beam passing through the sample cell. The temperature-jump cell is then filled with the sample solution through one of the capillary inlets.

Once filled, the sample cell is placed in a thermostatted brass cell jacket, situated in the light path. Thermal equilibrium is attained after fifteen minutes. The difference method is used to detect the chemical relaxation of the reaction mixture following the temperature jump. The sample cell is rotated in the brass jacket so that the intensity of light incident on the photomultiplier is maximised, and by suitable choice of the photomultiplier load resistor and cathode

voltage, an appropriate initial photomultiplier signal is obtained.
This is then nulled using a differential preamplifier, and the relaxation of the reaction mixture following perturbation is detected as a voltage change.

Once the capacitor has been charged, it is discharged through the reaction mixture, the transient recorder is triggered by the current flow, the photomultiplier output is collected, and a relaxation trace is displayed on the oscilloscope. A time interval of at least 200 seconds is left between successive temperature jumps to allow for the complete recharging of the capacitor and for the solution to return to its initial temperature.

2.1.4 Data acquisition and analysis

A method of Computer Averaged Transients (CAT) Scanning has been developed in this laboratory [11] for the acquisition and analysis of data (relaxation traces) from temperature-jump studies. Photomultiplier voltages from each transient are collected as 4096 8-bit data points using a Data Lab DL910 transient recorder. The transient recorder is triggered by the discharge of the capacitor, and the recorder samples the photomultiplier output at a suitably selected sample time, with the choice of timescales, 0.05 microseconds per point to 2 milliseconds per point. The pretrigger facility of the transient recorder enables the synchronisation of successive transients recorded on the same timescale, and is very useful for the recording of transients for the purpose of measuring relaxation amplitudes. An oscilloscope connected to the recorder displays each digitally stored transient, and enables the user to decide on the acceptability of the relaxation trace. Acceptable relaxa-

tion traces are transferred from the transient recorder to cassette magnetic tape via an Intel SDK-8085 microcomputer and CDB-150 cassette interface system. At least four transients are collected for each solution studied.

The data stored on cassette magnetic tape is transferred to a Computer Products LSI-11 minicomputer, via the microcomputer and cassette interface system. The repetitive transients for each solution are then subjected to averaging and analysis by the appropriate software developed for the minicomputer. For the averaging process, the user is allowed the final decision of which transients are to be averaged. The reciprocal relaxation time is determined for the resultant averaged relaxation trace using a non-linear least squares fitting procedure. A different procedure is used to measure relaxation amplitudes.

To test the computer software, the following procedure was used. A simple circuit consisting of a resistor and capacitor in series was con-structed and connected to the transient recorder in such a manner that the discharge of the capacitor could be recorded. Since the discharge of a capacitor varies exponentially with time, it is a suitable model of a transient. Several discharges of the capacitor were recorded, and the relaxation time for the discharge subsequently determined using the pro-cedure outlined above. The evaluated relaxation time was identical with-in experimental error to the calculated risetime for the discharge of the capacitor using the known values of resistance and capacitance in the cir-cuit.

2.1.5 Calibration of the temperature-jump apparatus

The magnitude of the temperature jump, at a particular capacitor voltage, can be experimentally measured using a buffer-indicator system. Since the buffer proton equilibria relax very rapidly, the heating time for the apparatus can also be measured.

Phenol red in 0.05 mol dm^{-3} tris buffer (pH 8.00) made in 1.00 mol dm^{-3} NaCl was used to calibrate the temperature-jump apparatus. The pH of tris buffer shows a marked temperature dependence, and large changes in absorbance can be obtained for a small temperature change. The temperature-jump capacitor is charged at various voltages, and the absorbance change at 555 nm produced by the discharge of the capacitor through the buffer-indicator solution is measured. The absorbance change is given by the expression

$$\Delta A = \log\left(1 + \frac{\Delta V}{V_0}\right) \tag{2.26}$$

where V_0 is the photomultiplier voltage prior to the temperature jump, and ΔV is the change in photomultiplier voltage due to the temperature jump. The absorbance of the buffer-indicator solution is then determined spectrophotometrically at a range of temperatures, the resulting plot of absorbance versus temperature enabling the absorbance change for each capacitor voltage to be related to a temperature rise. A calibration curve of ΔT versus U_0^2 (Equation 2.24) can be obtained. The heating time is determined from averaged relaxation traces obtained for the relaxation detected from the temperature-jump studies of the buffer-indicator solution.

For the temperature-jump studies described herein, two temperature-jump sample cells of design similar to that shown in Figure 2.2, but differing in the optical pathlength and hence solution volume, were used. The sample cell used in the temperature-jump studies of dye/cyclodextrin solutions had an optical pathlength of 1.00 cm (sample volume ca. 1.0 cm^3),

while the cell used in the studies of dye solutions had an optical path-length of 0.23 cm (sample volume ca. 0.6 cm^3). The 1.00 cm pathlength cell gave a temperature jump of 8.8 K (20 kilovolts discharge voltage), and the heating time was ca. 2 microseconds. The 0.23 cm pathlength cell gave a temperature jump of 9.7 K (16 kilovolts discharge voltage), and the heating time was ca. 5 microseconds.

2.2 UV/Visible Absorption Spectroscopy

2.2.1 Apparatus

Absorption measurements were made using a Zeiss DMR-10 double beam recording spectrophotometer equipped with a thermostatted (±0.1 K) cell block. The spectrophotometer is interfaced [12] to an Intel SDK-8080 microcomputer, which enables some degree of automation of the recording of spectra. The microcomputer receives data from the spectrophotometer via the instrument's digital readout accessory and, when all the data has been collected for a particular solution, it is punched on to paper tape using an ASR-33 Teletype. When all spectral measurements have been completed and the data punched on to paper tape, the data are then transferred from the paper tape to a CDC Cyber 173 computer for analysis.

Quartz spectrophotometer cells were used for the spectral measure-ments. The temperature was maintained at a constant value with the aid of an MGW Lauda Thermo-boy temperature controller which circulated water through the cell block. The solution temperature was monitored using a calibrated type F53 thermistor situated in the reference cell.

2.2.2 Experimental procedure

To obtain maximum accuracy in the absorption measurements, the following procedure was used. A baseline using solvent in both the sample and reference cells was recorded prior to each set of spectral measurements to allow for the mismatching of the spectrophotometer cells. The cells were then left in position throughout the subsequent measurements, solution was removed from the sample cell by suction, and the empty cell was thoroughly rinsed and filled with the next solution to be studied.

The spectrum of each solution was recorded in duplicate with wavelength increments of 1 or 2 nm between preset wavelength limits. An integration time of 1.6 seconds was allowed at each wavelength. Once the spectral data had been transferred to the Cyber 173 computer, the appropriate program was used to average the repetitive scans, subtract the baseline spectrum, and make corrections for solution thermal expansion.

2.3 Circular Dichroism

2.3.1 Apparatus

The circular dichroism measurements were made on a Jasco J-40CS recording spectropolarimeter. The spectropolarimeter is interfaced [13] to an Intel SDK-8085 microcomputer, which enables almost complete automation of the recording of spectra. Spectra are recorded as a photomultiplier voltage by the microcomputer, and the data collected can be printed out using an ASR-33 Teletype. The data can be expressed as ellipticities by using the appropriate conversion factor derived from a calibration experiment.

2.3.2 Experimental procedure

The spectropolarimeter showed considerable baseline drift during the time taken for the recording of a spectrum. In order to eliminate the effect of this drift, measurements were made for the solution and base-line alternately at each wavelength, and the wavelength changed manually. An integration time of 48 seconds and a time constant of 0.25 seconds were used for all the spectral measurements. Each sensitivity setting of the spectropolarimeter was calibrated by using a standard solution of D-10-camphorsulphonic acid, which is known to have a molar ellipticity of 7260 deg cm^2 decimol^{-1} at 290 nm [14]. The circular dichroism results were expressed in terms of molar ellipticity, [θ], using the equation

$$[\theta] = \frac{100\Psi}{lc} \tag{2.27}$$

where Ψ is the ellipticity, l is the cell pathlength, and c is the dye concentration.

Bibliography

1. EIGEN, M. Disc. Faraday Soc. 17, 194 (1954).

2. BERNASCONI, C. F. Relaxation Kinetics, Academic Press Inc., New York, 1976.

3. CZERLINSKI, G. H. Chemical Relaxation, Dekker, New York, 1966.

4. THUSIUS, D. J. Am. Chem. Soc. 94, 356 (1972).

5. CZERLINSKI, G. H. and EIGEN, M. Z. Elektrochem. 63, 652 (1959).

6. HAMMES, G. G. (ed). Techniques of Chemistry, Vol. VI, part II, chapter IV, Wiley (Interscience), New York, 1973.

7. COLLINS, P. R. Ph.D. Thesis, University of Adelaide (1979).

8. HOFFMAN, G. W. Rev. Sci. Instrum. 42, 1643 (1971).

9. CALDIN, E. F. and BROOKS, J. E. J. Sci. Instrum. 44, 449 (1967).

10. TURNER, D. H., FLYNN, G. W., SUTIN, N. and BEITZ, J. V. J. Am. Chem. Soc. 94, 1554 (1972).

11. SCHILLER, R. L. Honours Report, University of Adelaide (1981).

12. BOEHM, G. Ph.D. Thesis, University of Adelaide (1981).

13. FORNASIERO, D. Ph.D. Thesis, University of Adelaide (1981).

14. CASSIM, J. Y. and YANG, J. T. Biochemistry 8, 1947 (1969).

CHAPTER III

A Kinetic And Equilibrium Study Of

Crystal Violet-Cyclodextrin

Inclusion Complexes

A KINETIC AND EQUILIBRIUM STUDY
OF CRYSTAL VIOLET-CYCLODEXTRIN INCLUSION COMPLEXES

3.1 Introduction

Crystal violet (CV) is a symmetrical triphenylmethane dye which has been used as a biological stain because of its metachromic properties [1]. It has also been shown to interact and form distinct complexes with a variety of macromolecules such as nucleic acids [2], synthetic polymers (eg. polyphosphate) [3] and cyclodextrins [4-7]. The studies of Cramer [4], and Broser and Lautsch [5] have shown that CV forms a 1:1 inclusion complex with βCD. Hirai et al. [6,7] have also agreed with these observations but have further demonstrated that CV forms a 2:1 inclusion complex with γCD in which CV is included as a dimer. They have presented considerable evidence from equilibrium methods to support this interpretation. Thus, the crystal violet/cyclodextrin system provides an opportunity to examine systematically the selectivity of cyclodextrins for substrates in the formation of inclusion complexes. The aim of this study is to characterise the types of crystal violet-cyclodextrin inclusion complexes that can be formed, with particular emphasis directed towards the elucidation of the inclusion mechanisms that are associated with the selectivity of the cyclodextrins.

The structure of CV is shown in Figure 3.1. The dye is not a planar molecule as represented in the diagram, since steric hindrance between the ortho hydrogen atoms of adjacent phenyl rings forces the phenyl groups out of the molecular plane by rotation about the central bonds. An X-ray diffraction study [8] of the parent compound triphenylmethane has established that in the solid state each phenyl ring is rotated in the same sense over the same angle (ca. 32°), such that triphenylmethane may be considered to have D_3 symmetry. A resonance Raman study [9]
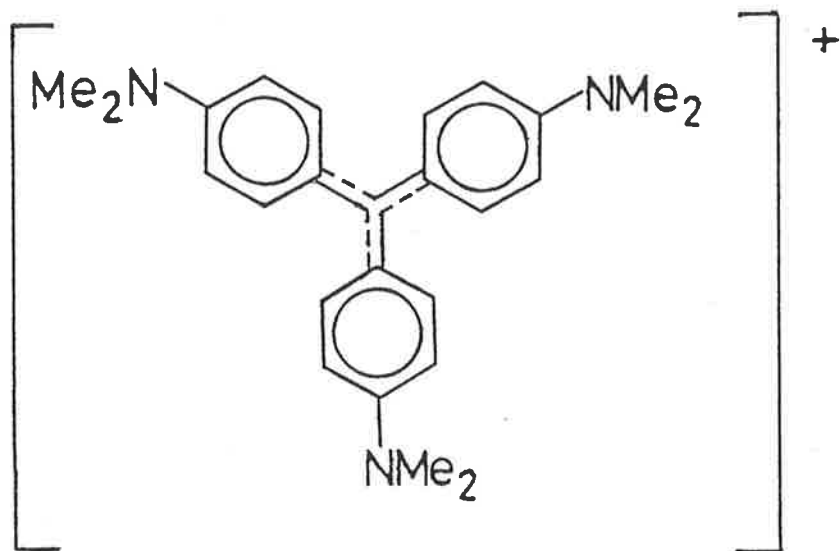
Figure 3.1: Chemical structure of crystal violet

suggests that CV exists as a single D_3 species in solution and magnetic circular dichroism studies [10] are also consistent with a single propeller-like species (either with symmetrical or asymmetrical angles of twist of the phenyl groups). Crystal violet may therefore be better represented as like a three-bladed propeller. The pH of crystal violet/ cyclodextrin solutions in aqueous 1.00 mol dm^{-3} NaCl was measured to be 6.50. Crystal violet exists as the monovalent cation [11] in the pH range 3.50-8.00, so that in this study the experimental observations pertain to the interaction of this cation with the cyclodextrins.

3.2 The Interaction of Crystal Violet with Alpha Cyclodextrin

In the presence of αCD (15 solutions were studied in which [αCD] was varied in the range 0-1.60 × 10^{-2} mol dm^{-3} and [CV] was ca. 1.4 × 10^{-5} mol dm^{-3}) CV exhibited an increase in the molar absorbance of the dye over the entire visible wavelength region. No apparent wavelength shift of the absorbance maximum of the dye was observed nor were any isosbestic points present.

The observed spectral effects were considered to be caused by some interaction between CV and the α-D glucose residues that constituted the cyclodextrin, rather than being attributed to the formation of an inclusion complex between the dye and αCD. To test this, the visible spectrum of CV in the presence of α-D glucose was determined and compared with that of CV in the presence of αCD, the concentration of which in terms of α-D glucose residues was similar (Figure 3.2). Evidently α-D glucose induces changes in the visible spectrum of CV which are similar in form and magnitude to those caused by αCD, and it must be concluded that

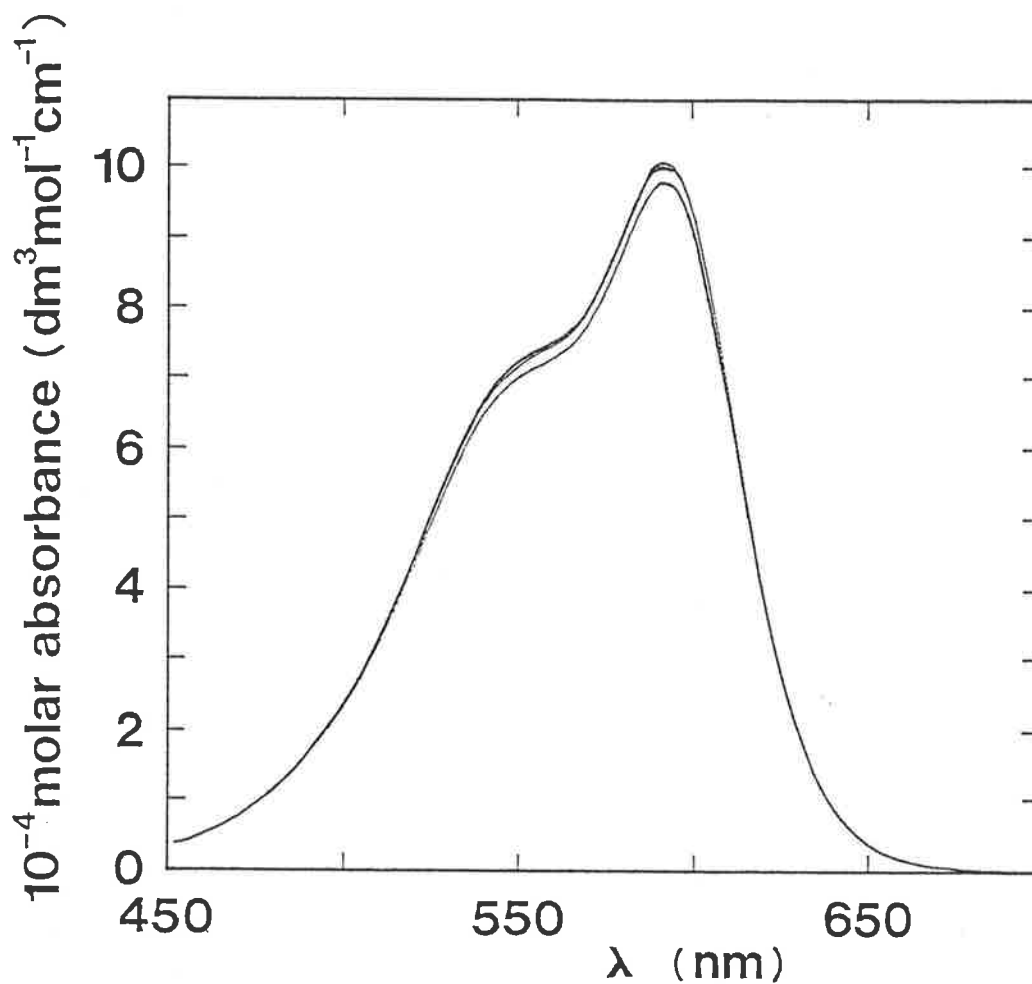*Figure 3.2:* *The spectrum of crystal violet alone, and in the presence of αCD and of α-D glucose, at pH 6.50 in aqueous 1.00 mol dm^{-3} NaCl at 298.2 K.*

The molar absorbances at 600 nm decrease in the order;
CV (1.52 × 10^{-5} mol dm^{-3}), αCD (1.59 × 10^{-3} mol dm^{-3});
CV (1.46 × 10^{-5} mol dm^{-3}), α-D glucose (1.00 × 10^{-2} mol dm^{-3});
CV (1.52 × 10^{-5} mol dm^{-3}).

there is no apparent inclusion complex formed between CV and αCD. It appears that α-D glucose, either as a single unit or incorporated in a cyclodextrin, slightly affects the spectral properties of CV. This small effect may reflect the replacement of water by the carbohydrate in the immediate solution environment of the dye. Similar variations of the ^{19}F chemical shifts of the drugs haloperidol and trifluperidol have been observed in the presence of simple saccharides such as β-D glucose and sucrose for the same reasons [12].

No significant relaxations attributable to inclusion processes were observed in temperature-jump spectrophotometric studies of CV in the presence of αCD.

3.3 The Interaction of Crystal Violet with Beta Cyclodextrin

The visible spectra of CV (ca. 1.4×10^{-5} mol dm^{-3} [CV]) alone and in the presence of βCD (20 solutions were studied and the [βCD] was varied in the range $0-7.50 \times 10^{-3}$ mol dm^{-3}) were measured, and representative spectra are shown in Figure 3.3. The isosbestic point observed was well defined only for [βCD] > 7.00×10^{-4} mol dm^{-3}. At lower [βCD] the behaviour of the spectra was quite anomalous, showing slight deviations from the formation of an isosbestic point. It was considered that, in addition to the red shift of the absorbance maximum of CV caused by complexation of the dye by βCD, there was an added spectral effect present related to the general change in the environment of the dye due to the presence of βCD, in a manner similar to that observed for αCD. This latter effect, being small in magnitude, would be observable only at low [βCD], since at greater concentrations of βCD it would be
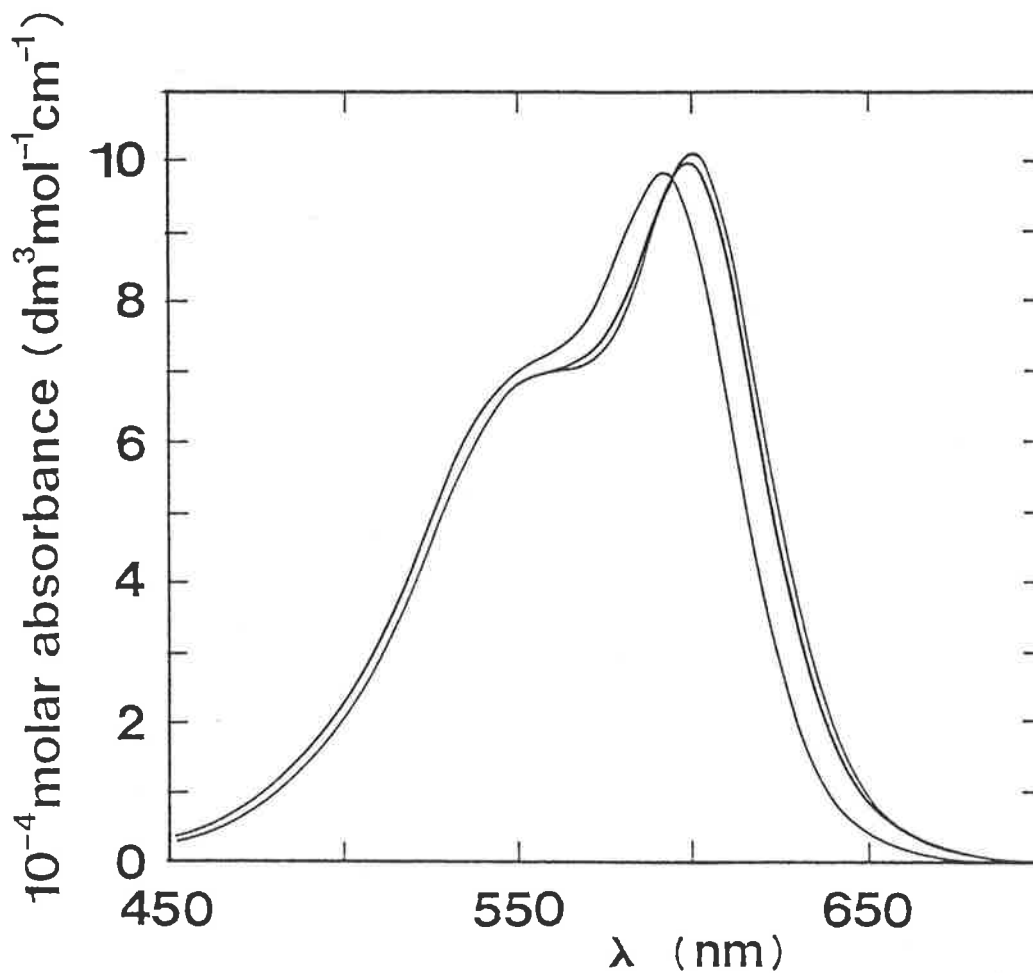
Figure 3.3: *The variation of the crystal violet spectrum in the presence of βCD, at pH 6.50 in aqueous 1.00 mol dm^{-3} NaCl at 298.2 K.*

The molar absorbance at 600 nm increases systematically as the composition of the solutions change in the order; CV (1.41 × 10^{-5} mol dm^{-3}), βCD 0; CV (1.40 × 10^{-5} mol dm^{-3}), βCD (9.05 × 10^{-4} mol dm^{-3}); CV (1.42 × 10^{-5} mol dm^{-3}), βCD (6.30 × 10^{-3} mol dm^{-3}). These three spectra exemplify the spectral variation for all twenty solutions studied.

masked by the larger spectral changes due to the inclusion complex formed between CV and βCD. A close examination of the absorbance data revealed that only the spectra relating to $[βCD] > 7.00 \times 10^{-4}$ mol dm^{-3} were consistent with the complexation of CV by βCD.

The existence of a single isosbestic point shown in Figure 3.3 is consistent with the formation of a 1:1 inclusion complex between CV and βCD according to Equilibrium 3.1:

$$CV + βCD \underset{k_{-1}}{\overset{k_1}{\rightleftharpoons}} CV \cdot βCD \qquad (K_1) \qquad\qquad (3.1)$$

For this scheme, the observed absorbance is given by

$$A = \varepsilon_{CV}[CV] + \varepsilon_{CV \cdot βCD}[CV \cdot βCD] \qquad\qquad (3.2)$$

In Equation 3.2, A is the absorbance at a given wavelength, ε is a molar absorbance, and all concentrations are equilibrium values. The absorbance data were fitted to Equation 3.2 by using the non-linear least-squares fitting routine DATAFIT. Appendix B describes the features of this program and the curve fitting procedure. In fitting the absorbance data to Equation 3.2, the values of A were weighted according to the experimental uncertainty at each wavelength, and ε_{CV} was taken from the spectrum of CV in the absence of βCD shown in Figure 3.3. Values for the equilibrium constant K_1 were derived at 2 nm intervals in the range 520–670 nm, except near the isosbestic point where the small changes in absorbance prevented DATAFIT converging to a best fit value. The K_1 values derived at each wavelength were weighted according to their estimated uncertainty and averaged to give the value $K_1 = (4.8 \pm 2.1) \times 10^3$ dm^3 mol^{-1} . The spectrum of the CV·βCD complex was computed by repeating the fitting of the absorbance data to Equation 3.2 using the averaged value of K_1 as a constant (Figure 3.4).
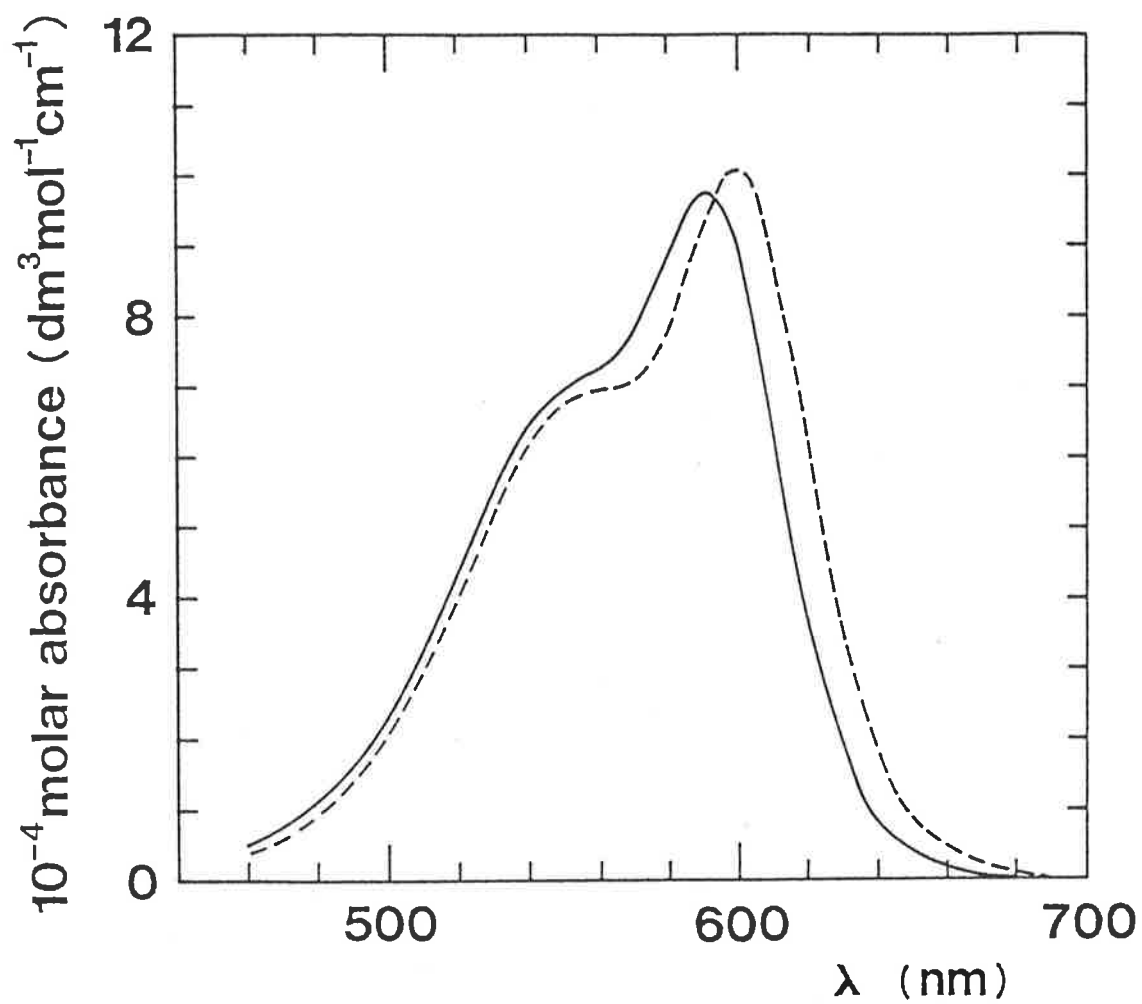
Figure 3.4: Calculated spectrum of CV·βCD (- - -) compared with the spectrum of CV alone (——)

Temperature-jump spectrophotometric studies at 550 nm of CV and βCD in aqueous 1.00 mol dm^{-3} NaCl, at pH 6.50 and 298.2 K, detected a single relaxation characterised by a decrease in absorbance. The relaxation was associated with amplitudes of small magnitude, as would be anticipated from the spectra (Figures 3.3 and 3.4). It was advantageous to perform the temperature-jump studies at 550 nm, despite the slightly greater spectral changes expected at 600 nm, because of the lower molar absorbance of dye/βCD solutions at 550 nm. Temperature-jump studies of CV alone at a concentration identical to that used in the cyclodextrin studies detected no significant relaxations.

Relaxation times were determined by fitting the averaged relaxation traces to a single exponential curve, and the variation of 1/τ with total βCD concentration is shown in Figure 3.5. The initial concentrations of dye and βCD used in the temperature-jump studies, and the respective values of 1/τ evaluated are listed in Appendix C (Table C.1). The variation of 1/τ could only be studied at total βCD concentrations up to 1.50 × 10^{-3} mol dm^{-3} , above which the relaxation time became comparable to the instrumental heating time. From Figure 3.5 there is an apparent linear relationship between 1/τ and total βCD concentration which is consistent with a relaxation arising through Equilibrium 3.1. The dependence of 1/τ on the equilibrium concentrations of the species for the formation of a 1:1 inclusion complex may be derived as outlined in Section 2.1.1:

$$1/\tau_1 = k_1([CV] + [\beta CD]) + k_{-1} \qquad (3.3)$$

The linear least-squares best fit line of the kinetic data to Equation 3.3 from **DATAFIT** is shown in Figure 3.5, and the derived values are:

$$k_1 = (1.17 \pm 0.08) \times 10^8 \text{ dm}^3 \text{ mol}^{-1} \text{ s}^{-1}$$

$$k_{-1} = (4.1 \pm 0.7) \times 10^4 \text{ s}^{-1} \qquad \text{and}$$

$$K_1 = (2.9 \pm 0.7) \times 10^3 \text{ dm}^3 \text{ mol}^{-1}$$
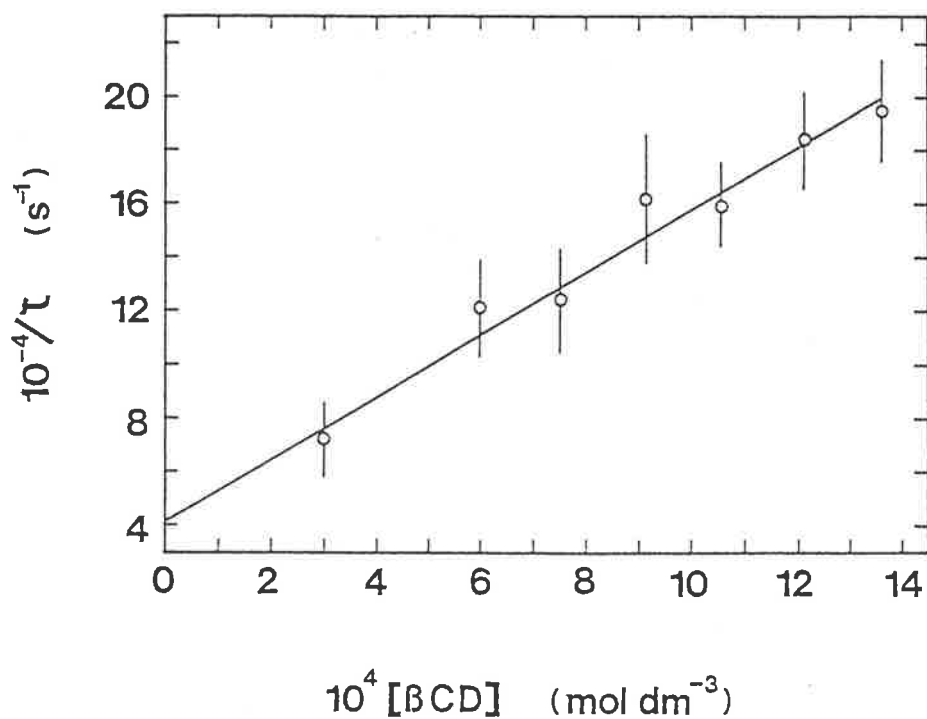
Figure 3.5: The variation of $1/\tau$ characterising the crystal violet-βCD system with total βCD concentration

The circles represent the experimental points and the solid line represents the best fit of the data to Equation 3.3. The error bars represent the standard errors in $1/\tau$ estimated from non-linear regressions of voltage against time data.

Experiments were performed at pH 6.50 in aqueous 1.00 mol dm^{-3} NaCl at 298.2 K.

The values of K_1 derived from the temperature-jump and equilibrium spectrophotometric data are the same within experimental error. The large experimental errors observed arise from the small spectral variations (changes in absorbance and magnitudes of relaxation amplitudes) of the dye in the presence of βCD.

The kinetic and equilibrium studies agree with the conclusions of others [4-7] that CV forms a 1:1 inclusion complex with βCD. An examination of space-filling (Corey-Pauling-Koltun) molecular models suggests that a $-PhNMe_2$ portion of CV is included by βCD. The two other $-PhNMe_2$ groups of CV lie over the rim of the βCD cavity, and are hindered from binding to a second βCD.

3.4 The Interaction of Crystal Violet with Gamma Cyclodextrin

The visible spectra of CV alone, and in the presence of γCD are shown in Figure 3.6, from which it is seen that there is a shift of the absorbance maximum to shorter wavelengths and a pronounced change in the shape of the spectrum as [γCD] increases (40 solutions were studied in which [γCD] was varied in the range $0-1.60 \times 10^{-2}$ mol dm^{-3} and [CV] was ca. 1.4×10^{-5} mol dm^{-3}). The systematic decrease in the molar absorbance of CV at 595 nm and the formation of a new absorbance maximum at approximately 560 nm which occur with increasing [γCD] is similar to that observed for the dimerisation of CV alone in aqueous solution [13], and indicates that the formation of the dimer $(CV)_2$ is enhanced. There was no indication of any anomalous behaviour of the spectra similar to that observed for the βCD system, as the spectral changes observed here with γCD were quite large even at low [γCD]. Furthermore, the vastly different spectral variations observed for CV in
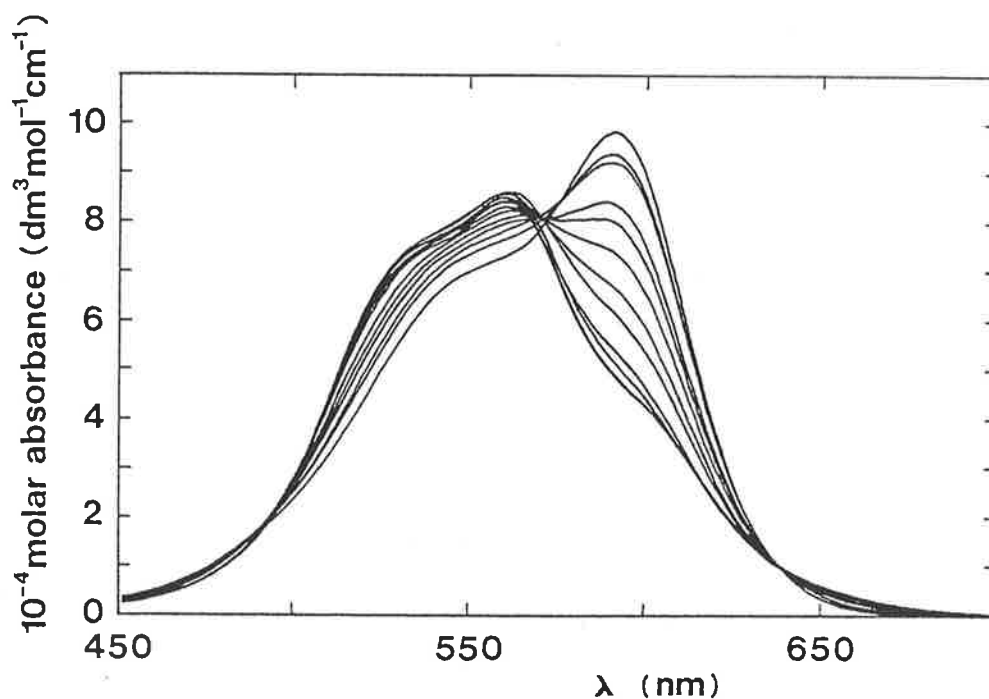
Figure 3.6: *The variation of the crystal violet spectrum in the presence of γCD, at pH 6.50 in aqueous 1.00 mol dm^{-3} NaCl at 298.2 K.*

The molar absorbance at 600 nm decreases systematically as the composition of the solutions change in the order; CV (1.34 × 10^{-5} mol dm^{-3}), γCD 0; CV (1.64 × 10^{-5} mol dm^{-3}), γCD (8.0 × 10^{-6} mol dm^{-3}); CV (1.34 × 10^{-5} mol dm^{-3}), γCD (1.57 × 10^{-5} mol dm^{-3}); CV (1.64 × 10^{-5} mol dm^{-3}), γCD (3.19 × 10^{-5} mol dm^{-3}); CV (1.62 × 10^{-5} mol dm^{-3}), γCD (4.79 × 10^{-5} mol dm^{-3}); CV (1.64 × 10^{-5} mol dm^{-3}), γCD (7.98 × 10^{-5} mol dm^{-3}); CV (1.63 × 10^{-5} mol dm^{-3}), γCD (1.60 × 10^{-4} mol dm^{-3}); CV (1.34 × 10^{-5} mol dm^{-3}), γCD (3.86 × 10^{-4} mol dm^{-3}); CV (1.46 × 10^{-5} mol dm^{-3}), γCD (7.65 × 10^{-4} mol dm^{-3}); CV (1.51 × 10^{-5} mol dm^{-3}), γCD (1.59 × 10^{-3} mol dm^{-3}); CV (1.51 × 10^{-5} mol dm^{-3}), γCD (3.99 × 10^{-3} mol dm^{-3}); CV (1.67 × 10^{-5} mol dm^{-3}), γCD (7.96 × 10^{-3} mol dm^{-3}). These twelve spectra exemplify the spectral variation observed for all forty solutions studied.

the presence of α-D glucose (Figure 3.2) compared with those observed

for γCD (Figure 3.6) indicate that the enhanced dimerisation of the dye

must be due to inclusion complex formation and not a change in the sol-

vent composition caused by the presence of cyclodextrin.

The absence of any distinct isosbestic point in the spectra shows

that CV experiences more than two environments over the γCD concentration

range studied. These spectra, which are qualitatively similar to those

of Hirai et al. [6, 7], are explicable in terms of the equilibria shown
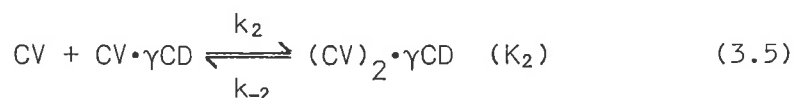
in Reactions 3.4 and 3.5:

$$CV + \gamma CD \underset{k_{-1}}{\overset{k_1}{\rightleftharpoons}} CV\cdot\gamma CD \qquad (K_1) \qquad\qquad (3.4)$$

$$CV + CV\cdot\gamma CD \underset{k_{-2}}{\overset{k_2}{\rightleftharpoons}} (CV)_2\cdot\gamma CD \quad (K_2) \qquad\qquad (3.5)$$

The values of the equilibrium constants K_1 and K_2 were derived from

absorbances determined at 2 nm intervals in the ranges 520–570 nm and

580–620 nm by fitting the data to Equation 3.6 using program DATAFIT:

$$A = \varepsilon_{CV}[CV] + \varepsilon_{CV\cdot\gamma CD}[CV\cdot\gamma CD] + 2\varepsilon_{(CV)_2\cdot\gamma CD}[(CV)_2\cdot\gamma CD] \quad (3.6)$$

The values of K_1 and K_2 derived at each wavelength were weighted

according to their estimated uncertainty, and averaged to give the

values:

$$K_1 = (5.0 \pm 1.2) \times 10^2 \text{ dm}^3 \text{ mol}^{-1} \qquad \text{and}$$

$$K_2 = (5.5 \pm 1.9) \times 10^5 \text{ dm}^3 \text{ mol}^{-1}$$

The spectra of CV$\cdot\gamma$CD and $(CV)_2\cdot\gamma$CD shown in Figure 3.7 were calculated

using the values of K_1 and K_2 derived above. The spectrum of $(CV)_2\cdot\gamma$CD

is shifted to shorter wavelengths by comparison with the spectrum of CV,

as is also the case for the spectrum of $(CV)_2$ [13].

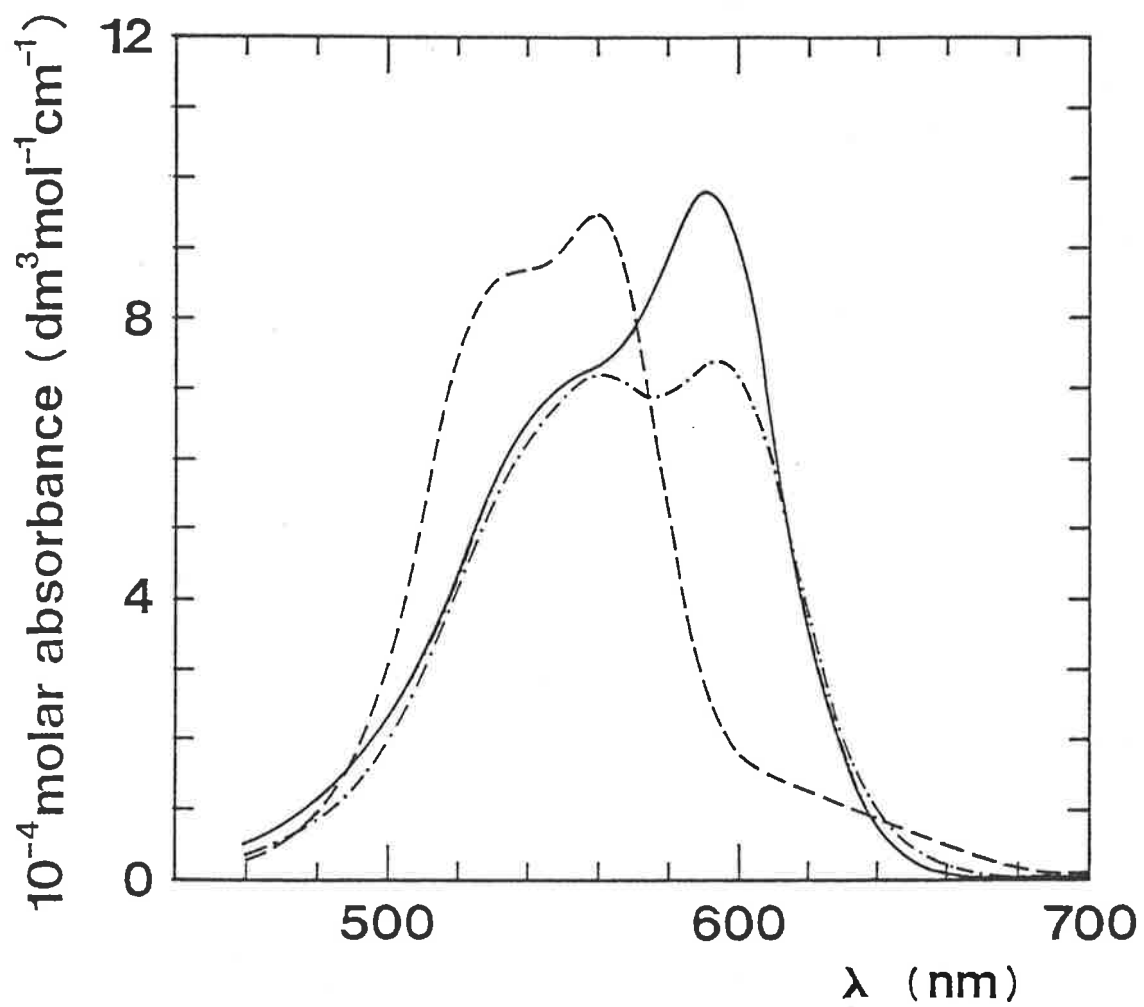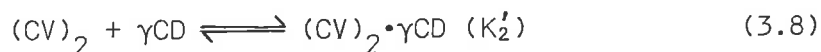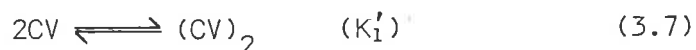*Figure 3.7:* Calculated spectra of CV·γCD (–·–·) and (CV)₂·γCD (– – –) compared with the spectrum of CV alone (——)

The formation of $(CV)_2 \cdot \gamma CD$ may also occur through the direct inclusion of $(CV)_2$ by γCD as shown in Reactions 3.7 and 3.8:

$$2CV \rightleftharpoons (CV)_2 \qquad (K_1') \qquad\qquad (3.7)$$

$$(CV)_2 + \gamma CD \rightleftharpoons (CV)_2 \cdot \gamma CD \ (K_2') \qquad\qquad (3.8)$$

In this case, the observed absorbance at a particular wavelength is given by

$$A = \varepsilon_{CV}[CV] + 2\varepsilon_{(CV)_2}[(CV)_2] + 2\varepsilon_{(CV)_2 \cdot \gamma CD}[(CV)_2 \cdot \gamma CD] \qquad (3.9)$$

This reaction scheme was considered, but was rejected because it was unable to fit the absorbance data satisfactorily. The equilibrium constants K_1' and K_2' could not be derived over a wide wavelength range, and the values of K_1' and K_2' that could be derived were characterised by relatively large standard deviations. The spectral variations shown by the spectra (Figure 3.6) were only explained adequately by the processes outlined by Equilibria 3.4 and 3.5.

Temperature-jump spectrophotometric studies at 530 and 595 nm of CV and γCD in aqueous 1.00 mol dm^{-3} NaCl, at pH 6.50 and 298.2 K, detected a single relaxation at both wavelengths. Relaxation times evaluated for this relaxation were identical within experimental error at both wavelengths, and the $1/\tau$ values together with the initial concentrations of CV and γCD used in the studies are listed in Appendix C (Table C.2). At 530 nm, the relaxation was characterised by a decrease in absorbance, whereas at 595 nm the relaxation produced an increase in absorbance consistent with the absorbance changes arising predominantly from the shift of Equilibria 3.4 and 3.5 to the left. The amplitudes characterising this relaxation were greater at 595 nm, and at both wavelengths the amplitudes were always greater than those characterising the βCD system, as anticipated from the spectra (Figures 3.3 and 3.6). The spectra in Figure 3.7 indicate that a shift to the left in the position

of the equilibria shown in Reactions 3.4 and 3.5 will produce virtually no change and a decrease in molar absorbance, respectively, at 530 nm. At 595 nm, however, the dissociations of CV·γCD and $(CV)_2$·γCD as shown in Reactions 3.4 and 3.5 both produce an increase in absorbance, but as the $1/\tau$ value determined at 530 nm is identical to that determined at 595 nm it is concluded that the absorbance changes observed at both wavelengths arise predominantly from the dissociation of $(CV)_2$·γCD. Temperature-jump studies of CV alone at a concentration identical to that used in the cyclodextrin studies detected no significant relaxations. Since CV is known to dimerise [13], the apparent absence of any relaxation attributable to this process indicates that the concentration of $(CV)_2$ is negligible at the concentration of dye used in the cyclodextrin studies, but the total dimer concentration is increased in the presence of γCD, and this explains the greater relaxation amplitudes observed.

The dependence of $1/\tau$ on the total γCD concentration (Figure 3.8) indicates that the observed relaxation is coupled to other faster processes occurring within the instrumental heating time, and which are characterised by small absorbance changes at the monitored wavelengths. If the equilibrium in which CV·γCD is formed (Reaction 3.4) is considered to be a fast pre-equilibrium step for the formation of $(CV)_2$·γCD as shown in Reaction 3.5, an expression for the variation of $1/\tau$ with [γCD] may be derived (see Appendix D):

$$1/\tau_2 = k_2[CV]\frac{[CV]+[CV \cdot \gamma CD]+4[\gamma CD]}{[CV]+[\gamma CD]+1/K_1} + k_{-2} \qquad (3.10)$$

where all concentrations are equilibrium values. A non-linear least-squares fit of the $1/\tau$ data to Equation 3.10 using program DATAFIT produces the best fit curve shown in Figure 3.8, and the values of k_2, k_{-2}, K_1. and K_2 derived are:
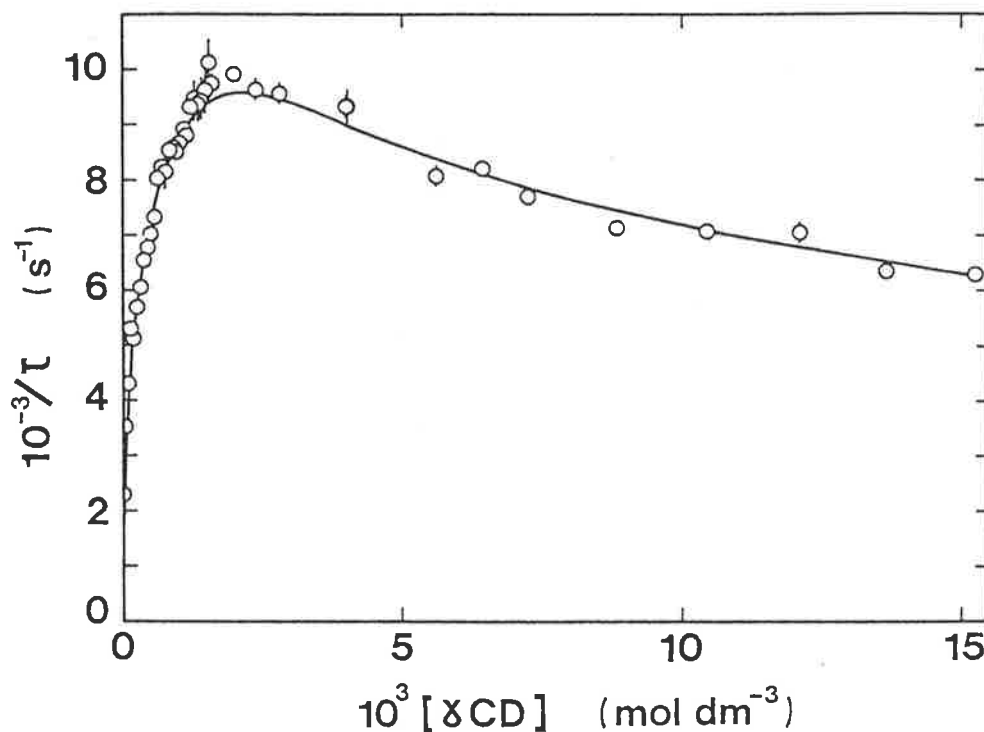
Figure 3.8: The variation of $1/\tau$ characterising the crystal violet-γCD system with total γCD concentration

The circles represent the averaged experimental data points obtained at 530 and 595 nm and the solid curve represents the best fit of these data to Equation 3.10. The error bars represent the mean errors of $1/\tau$ obtained at 530 and 595 nm.

Experiments were performed at pH 6.50 in aqueous 1.00 mol dm^{-3} NaCl at 298.2 K.

$$k_2 = (1.73 \pm 0.08) \times 10^9 \ dm^3 \ mol^{-1} \ s^{-1}$$

$$k_{-2} = (1.68 \pm 0.07) \times 10^3 \ s^{-1}$$

$$K_1 = (4.63 \pm 0.07) \times 10^2 \ dm^3 \ mol^{-1} \qquad and$$

$$K_2 = (1.03 \pm 0.09) \times 10^6 \ dm^3 \ mol^{-1}$$

The scheme outlined by Reactions 3.7 and 3.8 was also considered as an explanation of the temperature-jump data. Two variations of this general scheme are possible: either the formation of $(CV)_2$ (Reaction 3.7) is a fast pre-equilibrium step for the formation of $(CV)_2 \cdot \gamma CD$ (Reaction 3.8), or the formation of $(CV)_2 \cdot \gamma CD$ is sufficiently fast to be considered in equilibrium throughout the relaxation of the preceding step (Reaction 3.7). Both these kinetic mechanisms were rejected. It was clear from the function and residuals plots obtained from the DATAFIT analysis that both mechanisms were unable to explain the experimental observations (ie. Figure 3.8).

A similar variation of $1/\tau$ shown in Figure 3.8 has been observed for the formation of γCD inclusion complexes of the type $(dye)_2 \cdot (\gamma CD)_2$ with the azo dyes methyl orange [14] and tropaeolin [15]. Th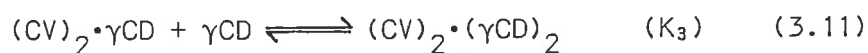e $1/\tau$ data were fitted to a reaction scheme in which the fast third step shown in Reaction 3.11 was added to the processes shown in Reactions 3.4 and 3.5:

$$(CV)_2 \cdot \gamma CD + \gamma CD \rightleftharpoons (CV)_2 \cdot (\gamma CD)_2 \qquad (K_3) \qquad (3.11)$$

While this scheme fitted the $1/\tau$ data satisfactorily, this treatment increased the standard deviation in K_1 and K_2, and produced $K_3 = 2 \pm 3$ $dm^3 \ mol^{-1}$. This constitutes insufficient evidence for the occurrence of the third step. In view of the structure of CV, it appears that $(CV)_2 \cdot \gamma CD$ is unable to bind another γCD in the manner possible for the linear azo dyes.

The similarity of K_1 and K_2 derived from the equilibrium and temperature-jump spectrophotometric studies is reasonable, and indicates satisfactory internal consistency. The enhanced dimerisation of CV in the presence of γCD arises from the formation of $(CV)_2 \cdot \gamma CD$ through the stepwise inclusion of two CV monomers by γCD. Space-filling molecular models suggest that the structure of $(CV)_2$ consists of a planar superimposition of the CV phenyl rings, and that the γCD cavity is large enough to include a $(-PhNMe_2)_2$ portion of the dimer.

While the value of K_2 derived from the equilibrium spectrophotometric study is within an acceptable order of magnitude of that derived from the temperature-jump spectrophotometric study, the slight discrepancy observed does require some comment. The values of K_1 and K_2 derived from the $1/\tau$ data are characterised by smaller errors than those derived from the absorbance data, despite the fact that the magnitude of relaxation amplitudes and changes in absorbance, respectively, are relatively large in both cases, and that the measurement of absorbances is more precise than that of relaxation times. The analysis of the absorbance data is certainly able to discern the appropriate reaction scheme that best explains the spectral variations observed, but it is unable to derive values of the equilibrium constants with reasonable precision.

Prediction analysis, which is discussed in Appendix B, was used to determine the optimum conditions that were necessary to derive from the absorbance data equilibrium constants of comparable certainty to those derived from the $1/\tau$ data. Prediction analysis specified that to achieve this aim an enormously large number of spectra (approximately 60 CV/γCD solutions) must be studied, and that about two-thirds of these should be distributed at high $[\gamma CD]$ ($> 6.00 \times 10^{-3}$ mol dm^{-3} $[\gamma CD]$). It was considered unwarranted to study such a large number of spectra, given that

reasonable values of the equilibrium constants could be derived from a slightly lesser number. The equilibrium spectrophotometric study, however, did incorporate the study of a substantial number of spectra at high $[\gamma CD]$. The fact that studying spectra at high $[\gamma CD]$ should be emphasised may seem surprising, given that the largest changes in absorbance occur at low $[\gamma CD]$, but can be explained by considering Figure 3.9. Although the spectra (Figure 3.6) exhibit small variations in absorbance at $[\gamma CD] > 4.00 \times 10^{-3}$ mol dm^{-3} (eg. consider the last two spectra in Figure 3.6), substantial variations in species concentrations occur. It appears that the species CV·γCD is crucial to the fitting of the absorbance data, as the term $\varepsilon_{CV \cdot \gamma CD}[CV \cdot \gamma CD]$ in Equation 3.6 only exerts a significant influence in the fitting at high $[\gamma CD]$. The neglect of studying a large number of spectra overall, and at high $[\gamma CD]$, can lead to incorrect assumptions in the interpretation of the absorbance data. For instance, the fitting of the absorbance data may indicate that the species CV·γCD is unimportant because its concentration is apparently negligible, and thus the equilibria shown in Reactions 3.4 and 3.5 may be better represented as a single process in which these separate reactions are combined, although this may be incorrect as shown by kinetic evidence. Since only small changes in absorbance are observed at high $[\gamma CD]$, a relatively large number of spectra must be studied to obtain reasonable precision in the equilibrium constants. The equilibrium spectrophotometric method appears to be limited in its ability to characterise complex equilibria, such as those involved in two guest-one host inclusion complex formation.

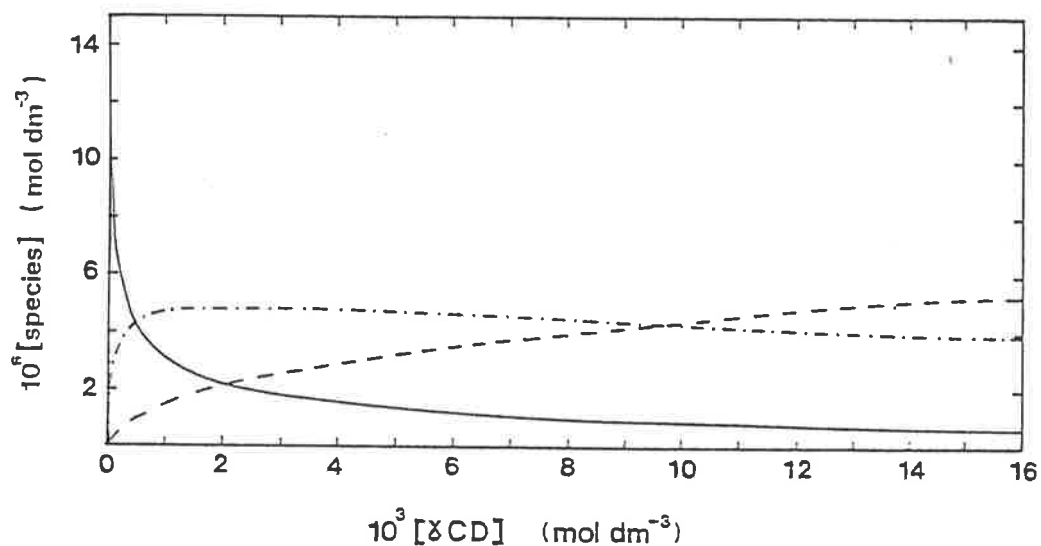Figure 3.9: The variation of $[CV]$ (——), $[CV \cdot \gamma CD]$ (– – –) and $[(CV)_2 \cdot \gamma CD]$ (–·–·) with total γCD concentration at constant total $[CV] = 1.4 \times 10^{-5}$ mol dm^{-3}.

The species concentrations were calculated using $K_1 = 4.63 \times 10^2$ dm^3 mol^{-1} and $K_2 = 1.03 \times 10^6$ dm^3 mol^{-1} derived from the temperature-jump spectrophotometric study.

3.5 Summary and Discussion

The interaction of crystal violet with the cyclodextrins is summarised
in Table 3.1. The observation that αCD forms no inclusion complex with
CV, βCD forms only CV·βCD, and γCD can include a CV dimer (the complexing
ability of the cyclodextrins for CV decreases in the order γCD > βCD > αCD),
indicates that the annular radii of the cyclodextrins exert a substantial
degree of selectivity for a given included species. Furthermore, for a
given annular radius a substantial degree of selectivity for different
included species is indicated by the ca. 10^3-fold difference between K_1
and K_2 characterising the inclusion of CV and $(CV)_2$, respectively, by
γCD. This selectivity of the cyclodextrins can be explained by the
compatibility of the size of the guest with the cavity of the host
cyclodextrin. An examination of space-filling molecular models suggests
that CV is too large to be accommodated by the αCD annulus. The βCD
annulus, however, is of sufficient size to allow the inclusion of a
single CV molecule only, the $(CV)_2$ species is too large to be included,
and the CV·βCD complex formed can be described as a 'tight' fit of the
dye in the βCD cavity. In contrast, the larger γCD annulus can accom-
modate relatively easily a single CV molecule, and the CV·γCD complex
can be described as a 'loose' fit of the dye in the γCD cavity. There
is sufficient space in the γCD cavity after the formation of the CV·γCD
complex, however, to allow the inclusion of another CV molecule to form
the $(CV)_2$·γCD species, in which there is a 'tight' fit of $(CV)_2$ in the
γCD cavity. The trends of cyclodextrin selectivity shown in Table 3.1
and demonstrated by molecular models indicate clearly that an optimum
matching between the size of the included species and the size of the
cyclodextrin cavity leads to optimum binding. This concept of larger
stability constants being associated with guests which fit most closely
into the cyclodextrin cavity is consistent with the importance of dis-
persion forces in inclusion complex stability.

Alpha Cyclodextrin	Beta Cyclodextrin	Gamma Cyclodextrin
No Inclusion Complex Formed	$CV + \beta CD \underset{k_{-1}}{\overset{k_1}{\rightleftharpoons}} CV \cdot \beta CD \ (K_1)$ $K_1^{equil} \ (4.8 \pm 2.1) \times 10^3 \ dm^3 \ mol^{-1}$ $K_1^{kin} \ (2.9 \pm 0.7) \times 10^3 \ dm^3 \ mol^{-1}$ $k_1 \ (1.17 \pm 0.08) \times 10^8 \ dm^3 \ mol^{-1} \ s^{-1}$ $k_{-1} \ (4.1 \pm 0.7) \times 10^4 \ s^{-1}$	$CV + \gamma CD \rightleftharpoons CV \cdot \gamma CD \ (K_1) \ fast$ $CV + CV \cdot \gamma CD \underset{k_{-2}}{\overset{k_2}{\rightleftharpoons}} (CV)_2 \cdot \gamma CD \ (K_2) \ slow$ $K_1^{equil} \ (5.0 \pm 1.2) \times 10^2 \ dm^3 \ mol^{-1}$ $K_2^{equil} \ (5.5 \pm 1.9) \times 10^5 \ dm^3 \ mol^{-1}$ $K_1^{kin} \ (4.63 \pm 0.07) \times 10^2 \ dm^3 \ mol^{-1}$ $K_2^{kin} \ (1.03 \pm 0.09) \times 10^6 \ dm^3 \ mol^{-1}$ $k_2 \ (1.73 \pm 0.08) \times 10^9 \ dm^3 \ mol^{-1} \ s^{-1}$ $k_2 \ (1.68 \pm 0.07) \times 10^3 \ s^{-1}$

Table 3.1:   Summary of the interaction of crystal violet with the cyclodextrins

The broad visible absorption band observed in the spectrum of the CV monomer appears to consist of two overlapping bands. The D_3 symmetry of CV gives rise to a doubly degenerate lowest excited state, but Korppi-Tommola and Yip [16] have concluded that in aqueous solution this 'free' cation degeneracy undergoes a slight splitting due to solvent-cation interactions. Wakelin et al. [2] have attributed the spectral changes that arise from the binding of CV to nucleic acids to be the result of changes in the propeller-like conformation of the dye due to rotations which affect the relative disposition of the phenyl rings and/or their dimethylamino groups. The two bands that constitute the CV spectrum appear to be more resolved in the spectrum of CV·βCD (Figure 3.4) due presumably to changes in the conformation of CV as a result of its inclusion by βCD. The greater magnitude of the spectral effects observed for the formation of CV·βCD (Figure 3.4) compared with those for CV·γCD (Figure 3.7) can be attributed to the greater changes in the environment and conformation of CV because of its 'tighter' fit in the βCD cavity. For a given dye, there appears to be a correlation between the magnitude of the observed spectral changes that arise with 1:1 complex formation and the fit of the dye in the cavity of cyclodextrins of differing annular radii. The markedly different spectrum observed for $(CV)_2 \cdot \gamma CD$ (Figure 3.7) compared with the spectra of CV or the 1:1 inclusion complexes can be ascribed to the existence of the $(CV)_2$ species in which exciton interactions [17] between the monomer units take place. The structure of the dimer may be assumed to consist of a planar superimposition of the CV phenyl rings for which exciton theory [17] predicts a blue shift in the spectrum of $(CV)_2 \cdot \gamma CD$ relative to the spectrum of CV.
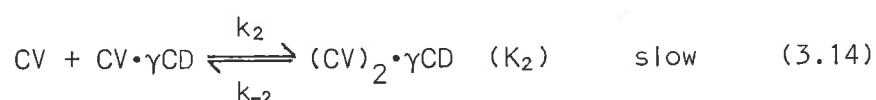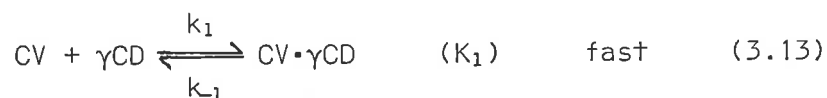
The equilibrium and temperature-jump spectrophotometric studies have revealed the existence of a range of inclusion mechanisms which

increase in complexity as the size of the cyclodextrin annulus increases. The inclusion of CV by βCD was observed to be a rapid bimolecular process:

$$CV + \beta CD \underset{k_{-1}}{\overset{k_1}{\rightleftharpoons}} CV \cdot \beta CD \qquad (K_1) \qquad (3.12)$$

The variation of $1/\tau$ for this kinetic process could not be studied over an extensive βCD concentration range. The variation of $1/\tau$ with total βCD or γCD cyclodextrin concentration (Figures 3.5 and 3.8) are both linear in the region up to 1.50×10^{-3} mol dm^{-3}, and it is by considering the $1/\tau$ data in conjunction with the equilibrium spectrophotometric data (Figures 3.3 and 3.6) that Reaction 3.12 is seen to best explain the $1/\tau$ data for the βCD system.

At concentrations of CV in which the dimer concentration is negligible, there is observed, in the presence of γCD, increased concentrations of the CV dimer due to the formation of $(CV)_2 \cdot \gamma CD$ arising through Equilibria (3.13) and (3.14):

$$CV + \gamma CD \underset{k_{-1}}{\overset{k_1}{\rightleftharpoons}} CV \cdot \gamma CD \qquad (K_1) \qquad fast \qquad (3.13)$$

$$CV + CV \cdot \gamma CD \underset{k_{-2}}{\overset{k_2}{\rightleftharpoons}} (CV)_2 \cdot \gamma CD \quad (K_2) \qquad slow \qquad (3.14)$$

Hirai et al. [7] have presented detailed evidence from equilibrium measurements to support the existence of the $(CV)_2 \cdot \gamma CD$ species, but have concluded that it is formed by the direct inclusion of $(CV)_2$ by γCD. The temperature-jump study presented here, however, provides the unambiguous determination of the likely inclusion mechanism. A variety of reaction schemes were considered to explain the $1/\tau$ data, but only the scheme given by Reactions 3.13 and 3.14 could fit the kinetic data satisfactorily. Schemes similar to that given by Reactions 3.13 and 3.14 have also been deduced from kinetic and equilibrium studies of the enhanced dimerisation of methyl orange [14] and tropaeolin [15] in the

presence of cyclodextrins, and this increases the plausibility of the reaction scheme proposed here.

It has not been possible to determine directly kinetic parameters for the formation of CV•γCD (Reaction 3.13) because it was found to be a rapid pre-equilibrium in the treatment of the kinetics pertaining to the formation of $(CV)_2$•γCD (Reaction 3.14). The more facile formation of CV•γCD is presumably a consequence of the 'loose' fit of the dye in the γCD cavity, whereas the entrance of the second dye monomer into the cavity to form the 'tightly' fitting $(CV)_2$ in $(CV)_2$•γCD is relatively hindered. The high lability and low stability of CV•γCD is in marked contrast to the low lability and high stability of $(CV)_2$•γCD.

The equilibrium and temperature-jump spectrophotometric techniques used in the present study have revealed some interesting features about each method's ability to characterise different inclusion processes. The study of the CV/βCD system was distinguished by the detection of small changes in absorbance (either the magnitude of spectral changes or relaxation amplitudes), and the measurement of a rapid relaxation (measured relaxation times were close to the instrumental heating time), but the values of K_1 derived from both experimental methods were indistinguishable, given the large experimental error. The study of the CV/γCD system, conversely, was characterised by the detection of large changes in absorbance, and the measurement of a slow relaxation (measured relaxation times were considerably less than the instrumental heating time), but the values of K_1 and K_2 derived from the experimental methods showed only reasonable agreement. In this latter system, the complex nature of the inclusion process lends itself to precise measurements by the temperature-jump technique only. Prediction analysis has emphasised the requirements necessary in the design of the equilibrium spectrophoto-

metric study to achieve a meaningful interpretation of the absorbance data and suitable precision of the equilibrium constants derived.

This kinetic and equilibrium study of the interaction of crystal violet with the cyclodextrins has highlighted how the annular radii of the cyclodextrins are important in the various facets of inclusion complex formation.

Bibliography

1. MICHAELIS, L. and GRANICK, S. J. Am. Chem. Soc. 67, 1212 (1945).

2. WAKELIN, L. P. G., ADAMS, A., HUNTER C. and WARING M. J. Biochemistry 20, 5779 (1981).

3. TAKATSUKI, M. Bull. Chem. Soc. Jpn. 53, 1922 (1980).

4. CRAMER, F. Chem. Ber. 84, 851 (1951).

5. BROSER, W. and LAUTSCH, W. Naturwissenschaften 40, 220 (1953).

6. HIRAI, H., TOSHIMA, N. and UENOYAMA, S. Polymer J. 13, 607 (1981).

7. HIRAI, H., TOSHIMA, N. and UENOYAMA, S. Bull. Chem. Soc. Jpn. 58, 1156 (1985).

8. GOMES DE MESQUITA, A. H., MacGILLAVRY, C. H. and ERIKS, K. Acta Crystallogr. 18, 437 (1965).

9. ANGELONI, L., SMULEVICH, G. and MARZOCCHI, M. P. J. Raman Spectroscopy 8, 305 (1979).

10. DEKKERS, H. P. J. M. and KIELMAN-VAN LUYT, E. C. M. Mol. Phys. 31, 1001 (1976).

11. STORK, W. H. J., DE HASSETH, P. L., SCHIPPERS, W. B., KORMELING, C. M. and MANDEL, M. J. Phys. Chem. 77, 1772 (1973).

12. PISANIELLO, D. L., LINCOLN, S. F. and COATES, J. H. J. Chem. Soc. Faraday Trans. I 81, 1247 (1985).

13. STORK, W. H. J., LIPPITS, G. J. M. and MANDEL, M. J. Phys. Chem. 76, 1772 (1972).

14. CLARKE, R. J., COATES, J. H. and LINCOLN, S. F. Carbohydr. Res. 127, 181 (1984).

15. CLARKE, R. J., COATES, J. H. and LINCOLN, S. F. J. Chem. Soc. Faraday Trans. I 80, 3119 (1984).

16. KORPPI-TOMMOLA, J. and YIP, R. W. Can. J. Chem. 59, 191 (1981).

17. KASHA, M., RAWLS, H. R. and ASHRAF EL-BAYOUMI, M. Pure Appl. Chem. 11, 371 (1965).

CHAPTER IV

A Kinetic And Equilibrium Study Of

Some Xanthene Dye-Cyclodextrin

Inclusion Complexes

A KINETIC AND EQUILIBRIUM STUDY
OF SOME XANTHENE DYE-CYCLODEXTRIN INCLUSION COMPLEXES

4.1 Introduction

The dyes pyronine Y (PY), pyronine B (PB), and rhodamine B (RB) (Figure 4.1) belong to the class of dyes based on the dibenzo 1,4 pyran nucleus known as the xanthene series. While PY and PB are planar molecules, space-filling molecular models suggest that for RB the ortho-carboxyphenyl group lies out of the plane of the xanthene moiety due to steric inter-actions caused by the carboxyl functional group.

In the literature there have been few reports about the interaction of xanthene dyes with the cyclodextrins. The only detailed studies that have been reported have involved the interaction of RB [1] and fluorescein [2] (the structure of which is similar to RB) with βCD, for which both dyes have been shown to form 1:1 inclusion complexes. The examination of space-filling molecular models reveals that PY, PB and RB interact with the cyclodextrins in a manner similar to that observed for the crystal violet/cyclodextrin system. Thus, this series of dyes provides a basis for a comparative study of inclusion complex formation in terms of the variation of the annular radii of the cyclodextrins to the size of the guest. The aim of this study is to determine the types of in-clusion complexes that may be formed between these xanthene dyes and the cyclodextrins, to elucidate the inclusion mechanisms and evaluate the equilibrium and kinetic parameters.
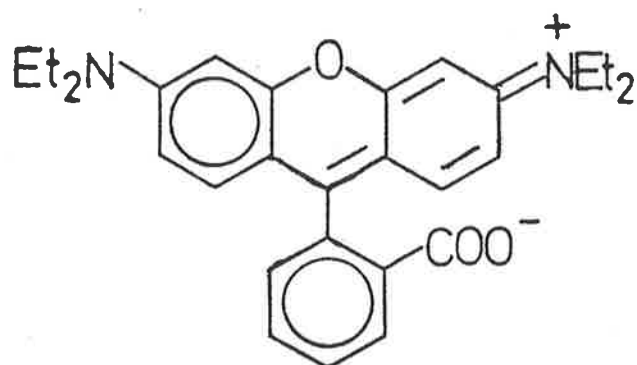
The pH of dye/cyclodextrin solutions in aqueous 1.00 mol dm^{-3} NaCl was measured to be 6.10, 5.70 and 6.40 for PY, PB, and RB, respectively. In aqueous solution RB exists as several species in equilibrium, depend-ing on the pH, and each species has a characteristic visible spectrum
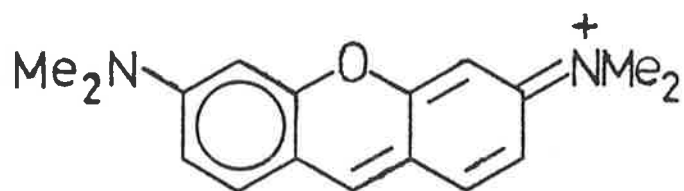
pyronine Y
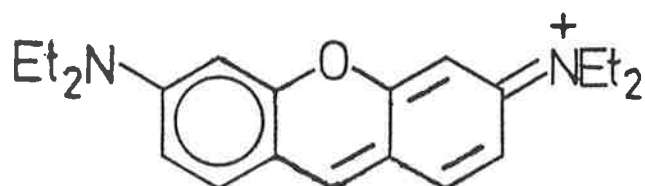
pyronine B

rhodamine B

Figure 4.1: Chemical structures of the xanthene dyes studied

[3]. In the pH range 4.00-13.00, RB exists as the zwitterion (Figure 4.1). At pH <4.00, the carboxyl functional group of RB is protonated and the visible spectrum of this species is identical to that of the zwitterion, except it is slightly shifted to longer wavelengths. At pH <0, protonation of the $-NEt_2$ groups of RB occurs, and this causes marked changes in the visible spectrum. There have been no similar pH studies of PY and PB, so that the visible spectrum of these dyes was studied in pH range 0-13.00 (Figure 4.2). The visible spectrum of both dyes is invariant with pH in the range 2.00-7.00, and by comparison with RB can be attributed to the existence of the monovalent cationic species. At pH <2.00, the dyes begin to undergo protonation of their dialkylamino groups, which causes the visible spectrum of the cation to be shifted to shorter wavelengths. The change in the visible spectrum of PY and PB, but not RB, at pH >7.00 arises from the formation of the carbinol species [4], as a result of attack by hydroxyl ion on the carbon of the pyran ring. This process is complete at pH 13.00. The carbinol is a colourless species due to the loss of conjugation in the dye. Rhodamine B does not form the carbinol because the ortho-carboxyphenyl group sterically hinders the attack by hydroxyl ion.

4.2 The Interaction of Some Xanthene Dyes with Alpha Cyclodextrin

In the presence of αCD (1.00×10^{-4} - 1.00×10^{-2} mol dm^{-3} [αCD]) the visible spectrum of each of the xanthene dyes (ca. 10^{-5} mol dm^{-3} [dye]) showed no significant changes to suggest the possibility of the formation of an inclusion complex. No significant changes in the visible spectrum of the xanthene dyes were observed in the presence of α-D glucose.

Figure 4.2: The variation of the pyronine Y and pyronine B spectra in the pH range 0-13.00 at 298.2 K

(A)   Pyronine Y

The total pyronine Y concentration was constant at 1.37×10^{-5} mol dm^{-3}.   The spectra shown refer to pyronine Y solutions at:
(a) pH 1.90, 3.86 and 6.98 (spectra are coinicident);
(b) pH 8.07;
(c) pH 9.75;
(d) pH 0.01.

(B)   Pyronine B

The total pyronine B concentration was constant at 8.9×10^{-6} mol dm^{-3}.   The spectra shown refer to pyronine B solutions at:
(a) pH 2.00, 3.89 and 6.98 (spectra are coincident);
(b) pH 8.00;
(c) pH 9.35;
(d) pH 1.00;
(e) pH 0.05.
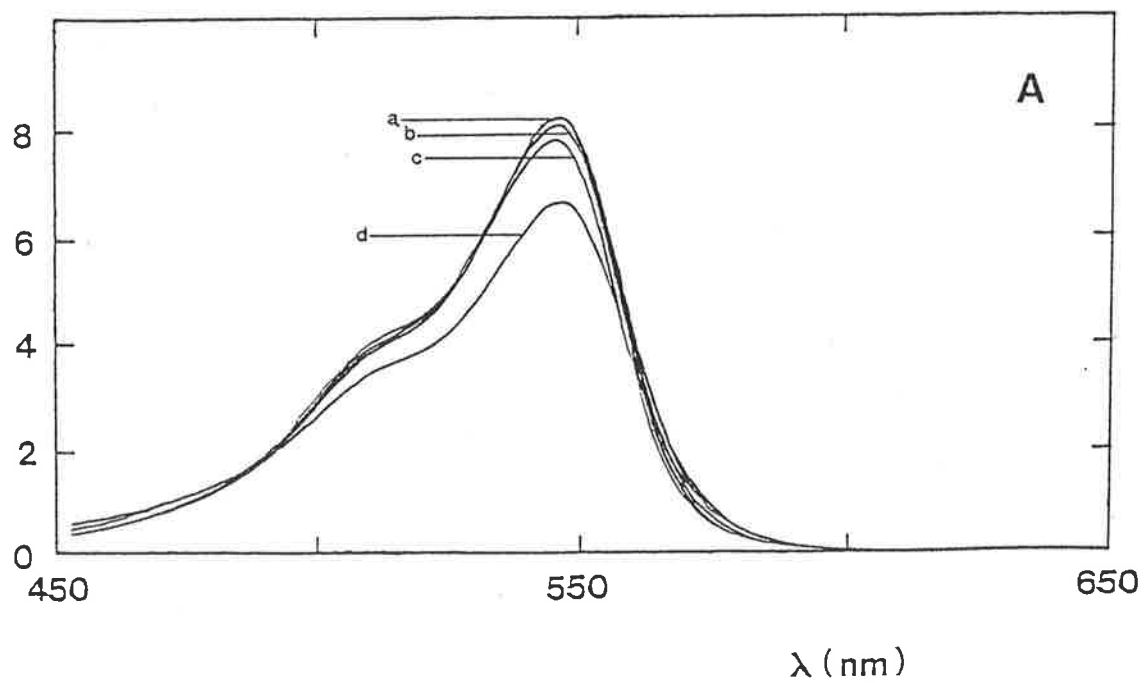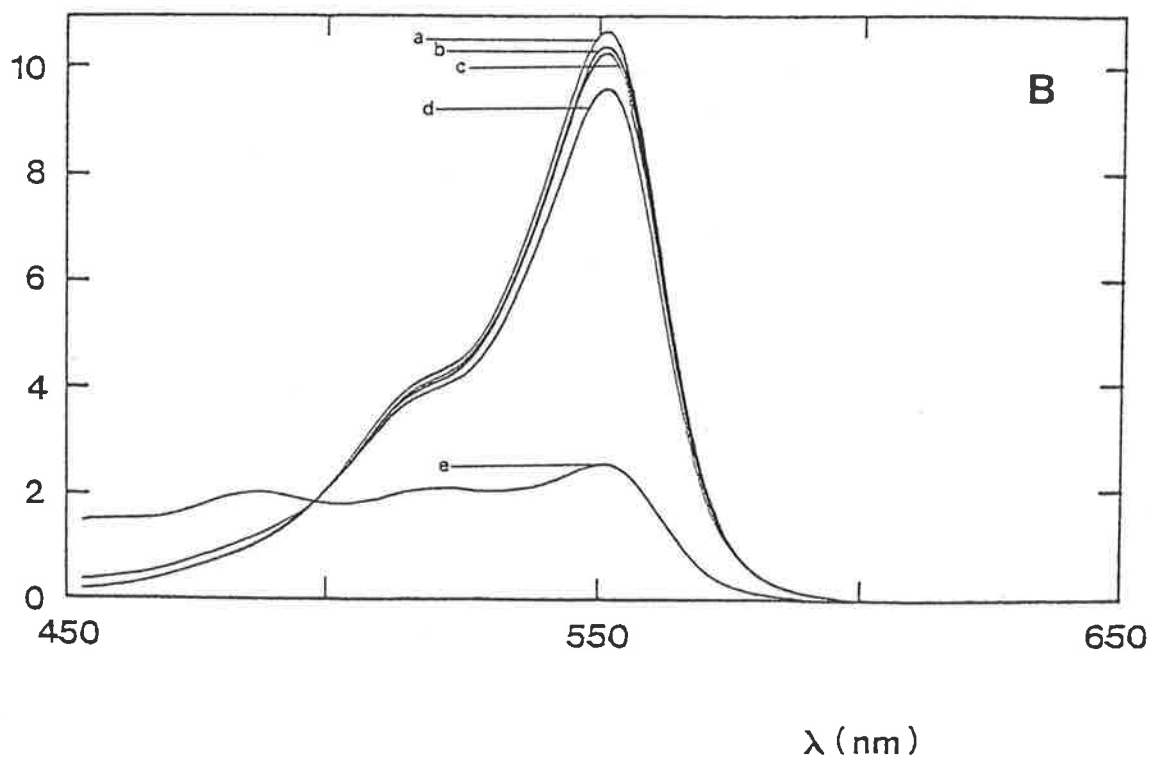
No significant relaxations attributable to inclusion processes were observed in temperature-jump spectrophotometric studies of the xanthene dyes in the presence of αCD.

There is no apparent complexation of the xanthene dyes by αCD, a conclusion supported by examination of space-filling molecular models, which shows these dyes to be too large to fit into the αCD cavity.

4.3 The Interaction of Some Xanthene Dyes with Beta Cyclodextrin

4.3.1 Pyronine Y

The visible spectra of PY (ca. 1.2×10^{-5} mol dm^{-3} [PY]) alone and in the presence of βCD (25 solutions were studied in which the [βCD] was varied in the range $0-1.00 \times 10^{-2}$ mol dm^{-3}) were measured, and representative spectra are shown in Figure 4.3 It appears that for [βCD] $< 8.00 \times 10^{-4}$ mol dm^{-3} there is a very slight red shift of the absorbance maximum of PY and the formation of an isosbestic point at ca. 511 nm. At greater [βCD] there is a further red shift of the absorbance maximum and the shifting of this isosbestic point, until at [βCD] $> 7.00 \times 10^{-3}$ mol dm^{-3} a second apparent isosbestic point at ca. 547 nm is formed. The appearance of two unrelated isosbestic points indicates that PY can also form inclusion complexes with βCD with higher stoichiometric ratios than 1:1. These observations are potentially explicable in terms of the equilibria shown in Reactions 4.1 and 4.2:

$$PY + \beta CD \underset{k_{-1}}{\overset{k_1}{\rightleftharpoons}} PY \cdot \beta CD \qquad (K_1) \qquad\qquad (4.1)$$

$$PY \cdot \beta CD + \beta CD \underset{k_{-2}}{\overset{k_2}{\rightleftharpoons}} PY \cdot (\beta CD)_2 \qquad (K_2) \qquad (4.2)$$
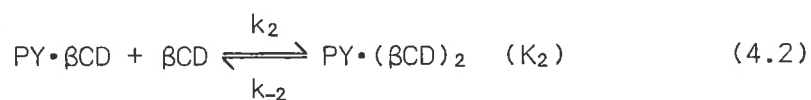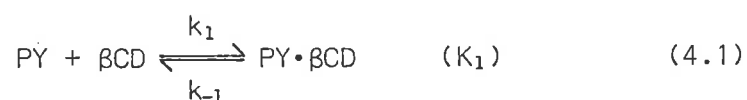
Figure 4.3:   *The variation of the pyronine Y spectrum in the presence of of βCD, at pH 6.10 in aqueous 1.00 mol dm^{-3} NaCl at 298.2 K*

(A)   *The molar absorbance at 550 nm increases systematically as the composition of the solutions changes in the order:*
PY (1.20×10^{-5} mol dm^{-3}), βCD 0; PY (1.19×10^{-5} mol dm^{-3}),
βCD (9.9×10^{-5} mol dm^{-3}); PY (1.19×10^{-5} mol dm^{-3}),
βCD (2.02×10^{-4} mol dm^{-3}); PY (1.19×10^{-5} mol dm^{-3}),
βCD (5.02×10^{-4} mol dm^{-3}).
These four spectra exemplify the spectral variation for all eight solutions studied at [βCD] $< 8.00 \times 10^{-4}$ mol dm^{-3}.

(B)   *The molar absorbance at 550 nm decreases systematically as the composition of the solutions changes in the order:*
PY (1.20×10^{-5} mol dm^{-3}), βCD (1.00×10^{-3} mol dm^{-3});
PY (1.20×10^{-5} mol dm^{-3}), βCD (2.00×10^{-3} mol dm^{-3});
PY (1.19×10^{-5} mol dm^{-3}), βCD (5.00×10^{-3} mol dm^{-3});
PY (1.20×10^{-5} mol dm^{-3}), βCD 0.
These four spectra exemplify the spectral variation for all sixteen solutions studied at [βCD] $> 8.00 \times 10^{-4}$ mol dm^{-3}.
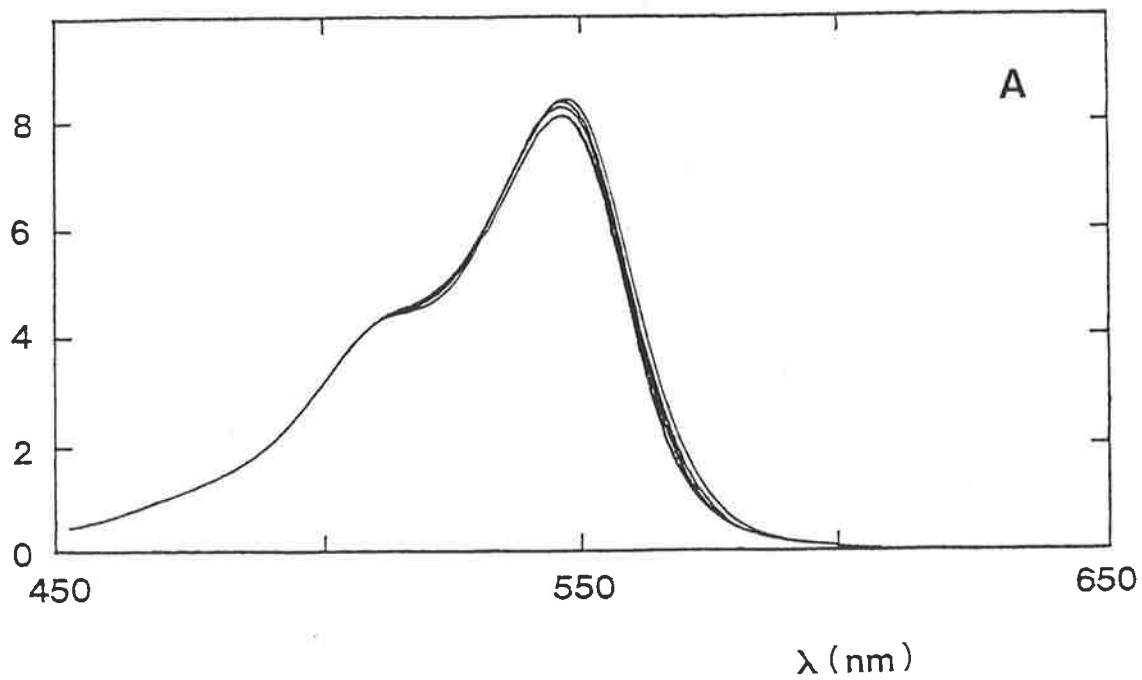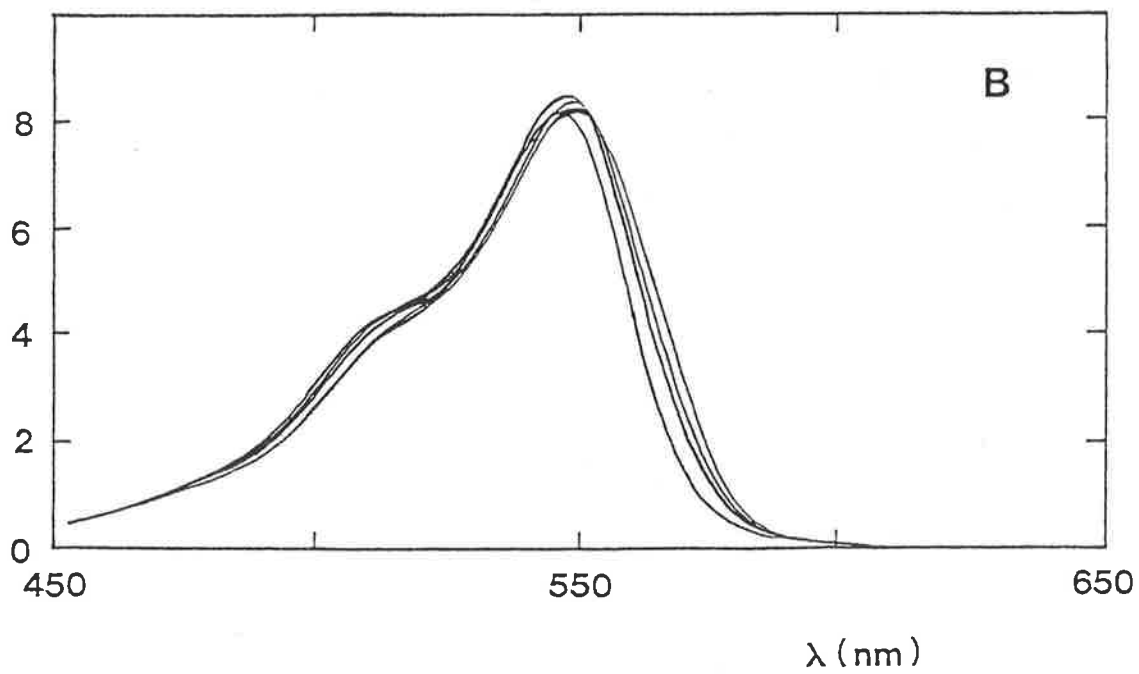
For this scheme, the observed absorbance is given by

$$A = \varepsilon_{PY}[PY] + \varepsilon_{PY \cdot \beta CD}[PY \cdot \beta CD] + \varepsilon_{PY \cdot (\beta CD)_2}[PY \cdot (\beta CD)_2] \qquad (4.3)$$

In Equation 4.3, A is the absorbance at a given wavelength, ε is a molar absorbance, and all concentrations are equilibrium values. The values of the equilibrium constants K_1 and K_2 were derived from absorbances determined at 1 nm intervals in the range 515–560 nm by fitting the data to Equation (4.3) using program **DATAFIT**. In fitting the data to Equation 4.3, the values of A were weighted according to the experimental uncertainty at each wavelength and ε_{PY} was taken from the spectrum of PY in the absence of βCD shown in Figure 4.3. The values of K_1 and K_2 derived at each wavelength were weighted according to their estimated uncertainty and averaged to give the values:

$$K_1 = (5.2 \pm 1.2) \times 10^3 \ dm^3 \ mol^{-1} \qquad and$$

$$K_2 = (1.7 \pm 0.4) \times 10^2 \ dm^3 \ mol^{-1}$$

These values of K_1 and K_2 were used to calculate the spectra of the PY·βCD and PY·$(\beta CD)_2$ species shown in Figure 4.4. The spectral changes induced in PY by the formation of the complexes with βCD are consistent with a change in the local environment of the chromophore such as would be experienced on inclusion. The larger spectral changes observed for PY·$(\beta CD)_2$ arise from the almost total encapsulation of the dye by the two βCD cavities.

Temperature-jump spectrophotometric studies at 547 nm of PY and βCD in aqueous 1.00 mol dm^{-3} NaCl, at pH 6.10 and 298.2 K, detected a relaxation characterised by an increase in absorbance. However, an analysis of this relaxation revealed that it consisted of two components, a fast phase and a slow phase, both characterised by an increase in absorbance (the amplitude of the fast phase was <10% amplitude of the slow phase). Relaxation times were best evaluated by fitting the averaged relaxation
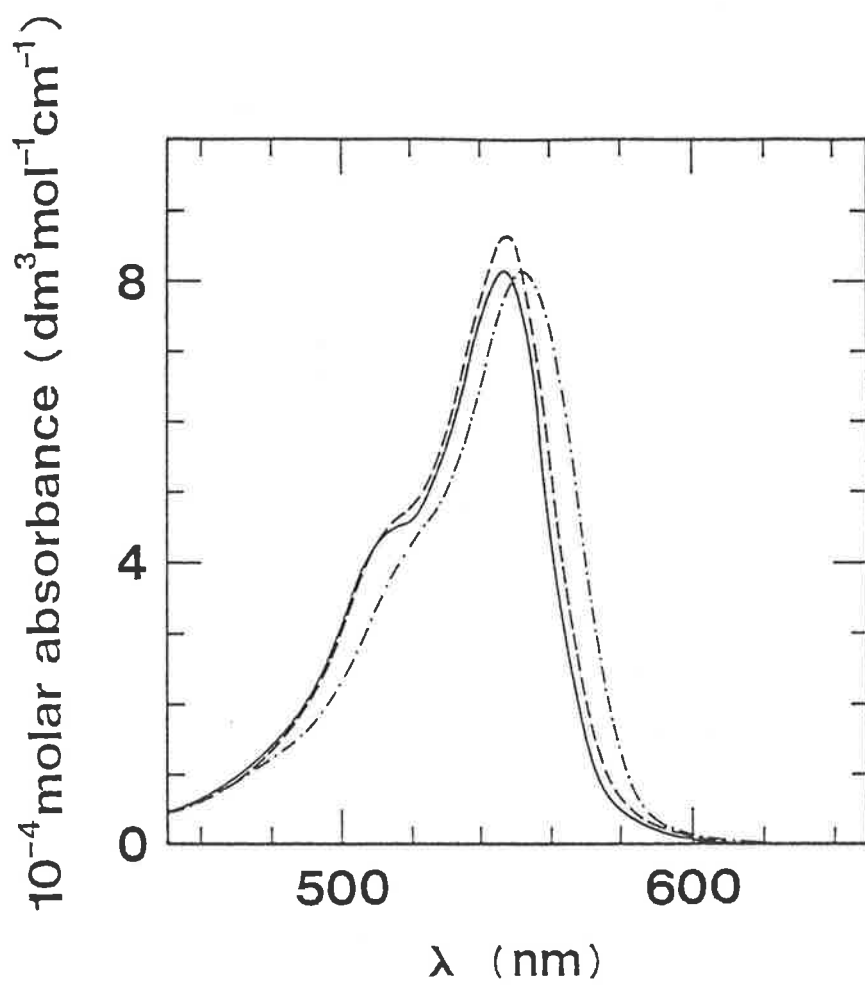
Figure 4.4: Calculated spectra of PY·βCD (– – –) and PY·(βCD)$_2$ (–·–·) compared with the spectrum of PY alone (——)

traces to a double exponential curve. The fast phase was characterised by relaxation times which were always comparable to the instrumental heating time, whereas the slow phase was characterised by relaxation times which exhibited considerable variation with the total βCD concentration (Figure 4.5). The values of $1/\tau$ for this slow process and initial concentrations of dye and βCD used in the temperature-jump studies are listed in Appendix C (Table C.3). Temperature-jump studies of PY alone at a concentration identical to that used in the cyclodextrin studies detected a single relaxation characterised by an increase in absorbance. Averaged relaxation traces were fitted to a single exponential curve, and the relaxation times evaluated were comparable to the instrumental heating time. Thus, the fast phase detected from the temperature-jump studies of PY/βCD solutions is related to a property of the dye itself.

The variation of $1/\tau$ shows two distinct types of behaviour over the [βCD] range studied (Figure 4.5). On the basis of the equilibrium spectrophotometric study, the $1/\tau$ data may be interpreted in the following manner. For [βCD] $< 5.00 \times 10^{-4}$ mol dm^{-3}, the value of $1/\tau$ increases rapidly with βCD such that it may be assumed to characterise the relaxation arising through Equilibrium 4.1. The nature of this relaxation is similar to that observed from the temperature-jump study of the CV/βCD system (Section 3.3). For [βCD] $> 5.00 \times 10^{-3}$ mol dm^{-3}, there is only a slight variation of $1/\tau$ with [βCD]. Assumably, this characterises the relaxation arising through Equilibrium 4.2. It appears likely that at high [βCD] the relaxation arising through Equilibrium 4.1 would occur within the instrumental heating time and there would be sufficient concentration of species for a relaxation arising through Equilibrium 4.2 to be observed. Averaged relaxation traces obtained from temperature-jump studies in the [βCD] range 5.00×10^{-4}–5.00×10^{-3} mol dm^{-3} could not be fitted to either
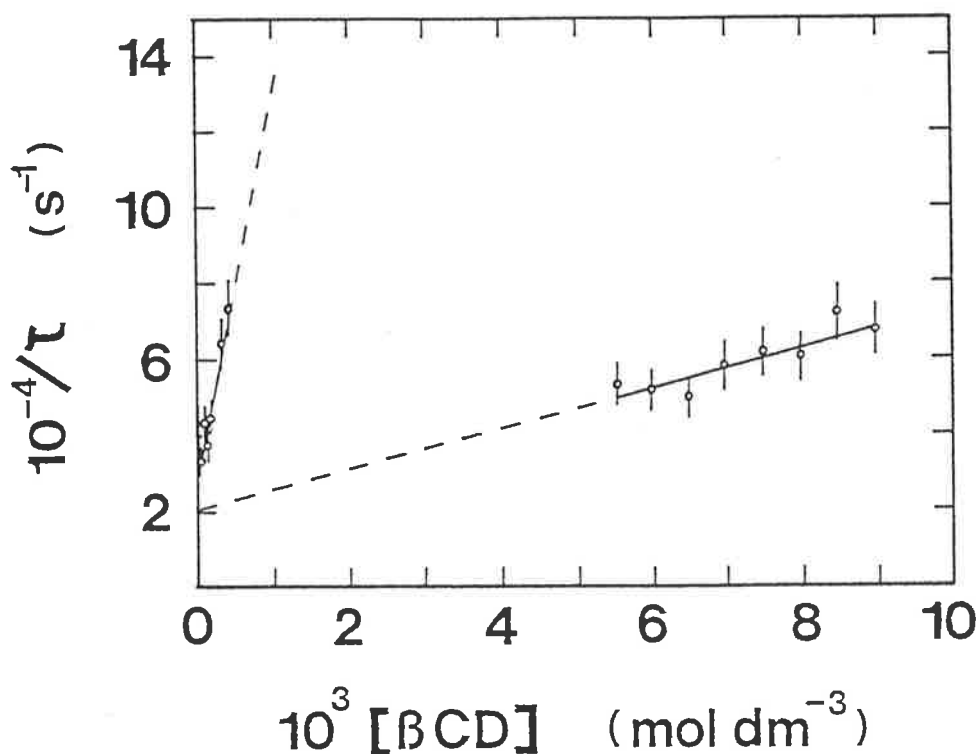
Figure 4.5: The variation of 1/τ characterising the pyronine Y-βCD system with total βCD concentration

The circles represent the experimental points and the the error bars represent the standard errors in 1/τ estimated from non-linear regressions of voltage against time data. The solid line for [βCD] < 1.00 × 10⁻³ mol dm⁻³ represents the best fit of the data to Equation 4.4, and the solid line for [βCD] > 5.00 × 10⁻³ mol dm⁻³ represents the best fit of the data to Equation 4.6. The broken lines represent extrapolations of the best fit lines.

Experiments were performed at pH 6.10 in aqueous 1.00 mol dm⁻³ NaCl at 298.2 K.

single or double exponential curves, due presumably to the presence of too many relaxations, ie. relaxations arising from PY itself and from the equilibria given by Reactions 4.1 and 4.2. The inability to determine reliable relaxation times over this $[\beta CD]$ region prevents any direct evidence that two distinct kinetic processes are present, and gives rise to the variation of $1/\tau$ observed in Figure 4.5. In view of the spectral data, however, the kinetic data may be qualitatively explained by Reactions 4.1 and 4.2.

The variation of $1/\tau$ for a relaxation arising through Equilibrium 4.1 may be expressed through Equation 4.4:

$$1/\tau_1 = k_1([PY] + [\beta CD]) + k_{-1} \qquad (4.4)$$

The linear least-squares best fit line of the data (values of $1/\tau$ for which $[\beta CD] < 5.00 \times 10^{-4}$ mol dm^{-3}) to Equation 4.4 using program DATAFIT is shown in Figure 4.5, and the derived values are:

$$k_1 = (1.1 \pm 0.2) \times 10^8 \text{ dm}^3 \text{ mol}^{-1} \text{ s}^{-1}$$

$$k_{-1} = (2.6 \pm 0.4) \times 10^4 \text{ s}^{-1} \qquad \text{and}$$

$$K_1 = (4.2 \pm 1.4) \times 10^3 \text{ dm}^3 \text{ mol}^{-1}$$

If, at those $[\beta CD]$ in which the relaxation arising through Equilibrium 4.2 is observed, the Reaction 4.1 is sufficiently fast to be considered in equilibrium throughout the relaxation of the second reaction, an expression for the variation of $1/\tau$ with $[\beta CD]$ may be derived (Appendix D):

$$1/\tau_2 = k_2[\beta CD]\frac{[\beta CD] + [PY\cdot\beta CD] + 4[PY]}{[\beta CD] + [PY] + 1/K_1} + k_{-2} \qquad (4.5)$$

where all concentrations are equilibrium values. It was not possible to obtain a unique fit of the $1/\tau$ data to Equation 4.5 using program DATAFIT, as the fitting was found to be independent of the initial estimate of K_1. It was considered that this was caused by the $1/\tau$ data used arising from

high $[\beta CD]$ in which the following approximations are valid:

$$[\beta CD] \simeq [\beta CD]_0$$

where $[\beta CD]_0$ is the total βCD concentration and

$$[\beta CD]_0 \gg [PY], [PY \cdot \beta CD], 1/K_1$$

since the total PY concentration is ca. 10^{-5} mol dm^{-3}, such that Equation 4.5 reduces to the form

$$1/\tau_2 \simeq k_2[\beta CD]_0 + k_{-2} \qquad\qquad (4.6)$$

The linear least-squares best fit line of the data (values of $1/\tau$ for which $[\beta CD] > 5.00 \times 10^{-3}$ mol dm^{-3}) to Equation 4.6 using program DATAFIT is shown in Figure 4.5, and the derived values are:

$$k_2 = (5.4 \pm 1.2) \times 10^6 \; dm^3 \; mol^{-1} \; s^{-1}$$

$$k_{-2} = (2.0 \pm 0.9) \times 10^4 \; s^{-1} \qquad \text{and}$$

$$K_2 = (2.7 \pm 1.8) \times 10^2 \; dm^3 \; mol^{-1}$$

The kinetic observations may be summarised by Figure 4.6, which shows the variation of the concentrations of species in solution with $[\beta CD]$. The values of K_1 and K_2 derived from the temperature-jump and equilibrium spectrophotometric studies are essentially the same, given the large experimental errors. The small changes in absorbance and the small relaxation amplitudes observed for the dye in the presence of βCD contribute to the large experimental errors.

4.3.2 Pyronine B

The visible spectra of PB alone and in the presence of βCD are shown in Figure 4.7, from which it is seen that there is both a slight red shift and a decrease in the molar absorbance of the absorbance maximum of the dye (16 solutions were studied, in which $[\beta CD]$ was varied in the range $0 - 1.00 \times 10^{-2}$ mol dm^{-3} and $[PB]$ was constant at 1.02×10^{-5} mol dm^{-3}).
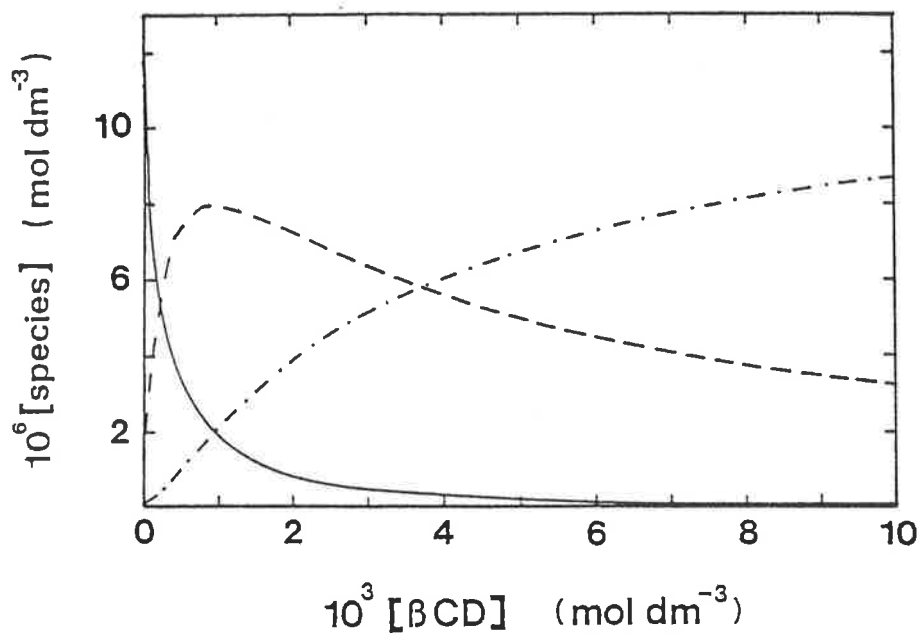
Figure 4.6: The variation of $[PY]$ (———), $[PY \cdot \beta CD]$ (— — —) and $[PY \cdot (\beta CD)_2]$ (—·—·) with total βCD concentration at constant total $[PY] = 1.20 \times 10^{-5}$ mol dm^{-3}

The species concentrations were calculated using $K_1 = 4.2 \times 10^3$ dm^3 mol^{-1} and $K_2 = 2.7 \times 10^2$ dm^3 mol^{-1} derived from the temperature-jump spectrophotometric study.
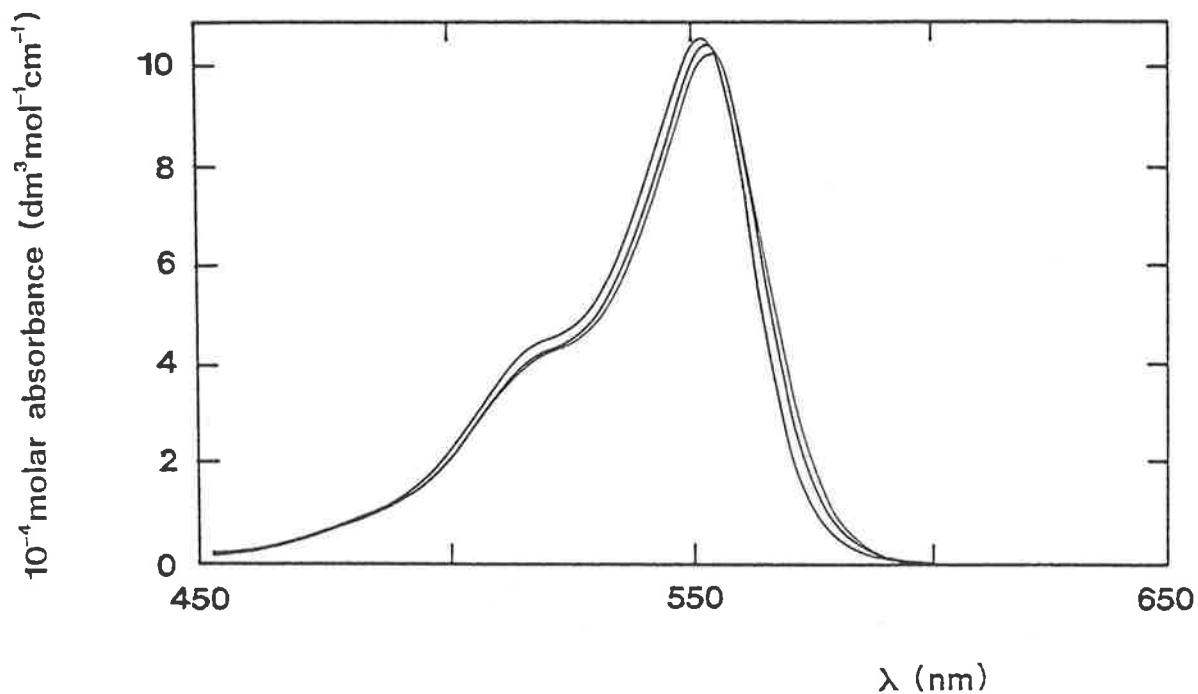
Figure 4.7: The variation of the pyronine B spectrum in the presence of βCD, at pH 5.70 in aqueous 1.00 mol dm^{-3} NaCl at 298.2 K

The molar absorbance at 550 nm decreases systematically as the total βCD concentration increases sequentially in the range 0, 4.00 × 10^{-4} and 4.02 × 10^{-3} mol dm^{-3} with the total pyronine B concentration constant at 1.02 × 10^{-5} mol dm^{-3}. These three spectra exemplify the spectral variation observed for all sixteen solutions studied.

These spectral changes are consistent with the formation of the 1:1 inclusion complex PB·βCD as the greatly predominant complex, according to Equilibrium 4.7:

$$PB + \beta CD \underset{k_{-1}}{\overset{k_1}{\rightleftharpoons}} PB \cdot \beta CD \qquad (K_1) \qquad\qquad (4.7)$$

The value of the equilibrium constant K_1 was derived from absorbances determined at 1 nm intervals in the ranges 500–556 nm and 559–576 nm by fitting the data to Equation 4.8 using the non-linear least-squares program DATAFIT:

$$A = \varepsilon_{PB}[PB] + \varepsilon_{PB \cdot \beta CD}[PB \cdot \beta CD] \qquad\qquad (4.8)$$

The K_1 values derived at each wavelength were weighted according to their estimated uncertainty, and averaged to give the value $K_1 = (4.0 \pm 2.4) \times 10^3$ dm^3 mol^{-1}. The spectrum of PB·βCD shown in Figure 4.8 was calculated using this value of K_1.

Temperature-jump spectrophotometric studies at 555 nm of PB and βCD in aqueous 1.00 mol dm^{-3} NaCl, at pH 5.70 and 298.2 K, detected a single relaxation characterised by a decrease in absorbance. Temperature-jump studies of PB alone at a concentration identical to that used in the cyclodextrin studies detected no significant relaxations.

Relaxation times were determined by fitting the averaged relaxation traces to a single exponential curve, and the variation of $1/\tau$ with total βCD concentration is shown in Figure 4.9. The initial concentrations of dye and βCD used in the temperature-jump studies and the respective values of $1/\tau$ evaluated are listed in Appendix C (Table C.4). The variation of $1/\tau$ could only be studied at total βCD concentrations up to 1.00×10^{-3} mol dm^{-3}, above which the relaxation time became comparable to the instrumental heating time. Figure 4.9 shows that $1/\tau$ increases with [βCD], and is consistent with a relaxation arising through Equilibrium 4.7. The
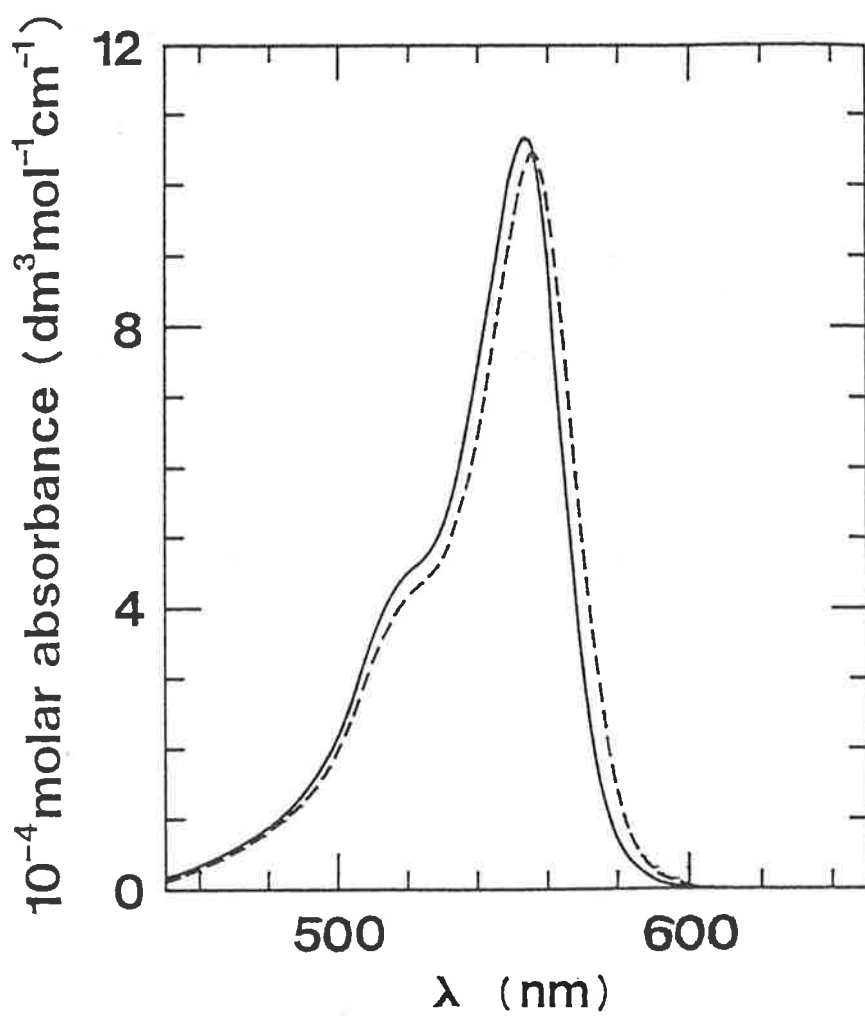
Figure 4.8: Calculated spectrum of PB·βCD (– – –) compared with the spectrum of PB alone (——)

variation of $1/\tau$ with $[\beta CD]$ may be expressed through Equation 4.9:

$$1/\tau_1 = k_1([PB] + [\beta CD]) + k_{-1} \qquad (4.9)$$

The linear least-squares best fit line of the $1/\tau$ data to Equation 4.9 using program DATAFIT is shown in Figure 4.9, and the derived values are:

$$k_1 = (1.1 \pm 0.1) \times 10^8 \ dm^3 \ mol^{-1} \ s^{-1}$$

$$k_{-1} = (1.5 \pm 0.5) \times 10^4 \ s^{-1} \qquad and$$

$$K_1 = (7.3 \pm 3.1) \times 10^3 \ dm^3 \ mol^{-1}$$

Pyronine Y and pyronine B both form 1:1 inclusion complexes with βCD of similar stability, but PB does not appear to form the $PB \cdot (\beta CD)_2$ species observed for PY. The examination of space-filling molecular models does suggest a possible explanation for this observed difference. Clearly, both dyes are included axially by βCD, ie. the long axis of the xanthene moiety is approximately parallel to the principal symmetry axis of the cyclodextrin. However, there does appear to be a subtle difference between the two dyes in the actual mode of this inclusion. It is proposed that for PY to achieve a 'tight' fit in the βCD cavity the dye be aligned along the C_7-rotational symmetry axis of the cavity, such that one $-NMe_2$ group is located in the βCD cavity and the other protrudes from the cavity to the extent that it may be included by a second βCD. With PB, on the other hand, for the larger $-NEt_2$ group to achieve a 'tight' fit in the βCD cavity the dye is aligned slightly askew from the symmetry axis, the unincluded $-NEt_2$ group lies over the rim of the βCD cavity such that it is hindered from being bound to a second βCD.

Figure 4.9: *The variation of 1/τ characterising the pyronine B-βCD system with total βCD concentration*

The circles represent the experimental points, and the solid line represents the best fit of the data to Equation 4.9. The error bars represent the standard errors in 1/τ estimated from non-linear regressions of voltage against time data.

Experiments were performed at pH 5.70 in aqueous 1.00 mol dm^{-3} NaCl at 298.2 K.

4.3.3 Rhodamine B

The variation of the visible spectrum of RB in the presence of βCD may

be seen from Figure 4.10, and is consistent with the formation of the

1:1 complex RB·βCD according to Equilibrium 4.10 (16 solutions were

studied in which [βCD] was varied in the range 0-1.00 × 10^{-2} mol dm^{-3}

and [RB] was constant at 9.3 × 10^{-6} mol dm^{-3}):

$$RB + \beta CD \underset{k_{-1}}{\overset{k_1}{\rightleftharpoons}} RB \cdot \beta CD \qquad (K_1) \qquad\qquad (4.10)$$

Fitting the absorbance data to this equilibrium in the ranges 500-535 nm

and 549-599 nm at 1 nm intervals using program DATAFIT yields K_1 = (6.9 ± 0.7)

× 10^3 dm^3 mol^{-1} and the spectrum of RB·βCD in Figure 4.11.

Temperature-jump spectrophotometric studies at 555 nm of RB and βCD

in aqueous 1.00 mol dm^{-3} NaCl, at pH 6.40 and 298.2 K, detected a single

relaxation characterised by an increase in absorbance. Temperature-jump

studies of RB alone at a concentration identical to that used in the

cyclodextrin studies detected no significant relaxations.

The values of 1/τ measured and the initial concentrations of RB and

βCD used are listed in Appendix C (Table C.5), and the variation of 1/τ

with total βCD concentration is shown in Figure 4.12. The variation of

1/τ could only be studied at total βCD concentrations up to 6.00 × 10^{-4}

mol dm^{-3} because the relaxation only had observable amplitudes over this

concentration range. At greater [βCD] it was difficult to detect the

presence of a relaxation and measure reliable relaxation times. This

is in contrast to the temperature-jump studies of PB and CV with βCD,

where the study of the variation of 1/τ was limited by the concentration

range over which the observed relaxation was slower than the instrumental

heating time. Nevertheless, the variation of 1/τ seen in Figure 4.12 is

consistent with relaxation arising through Equilibrium 4.10, such that

Figure 4.10: *The variation of the rhodamine B spectrum in the presence*
of βCD, at pH 6.40 in aqueous 1.00 mol dm^{-3} NaCl at 298.2 K

The molar absorbance at 550 nm decreases systematically as
the total βCD concentration increases sequentially in the
range 0, 1.01 × 10^{-4}, 2.02 × 10^{-4}, 4.97 × 10^{-4}, 1.01 × 10^{-3}
and 5.01 × 10^{-3} mol dm^{-3} with total rhodamine B concentration
constant at 9.3 × 10^{-6} mol dm^{-3}. These six spectra exemplify
the spectral variation for all sixteen solutions studied.
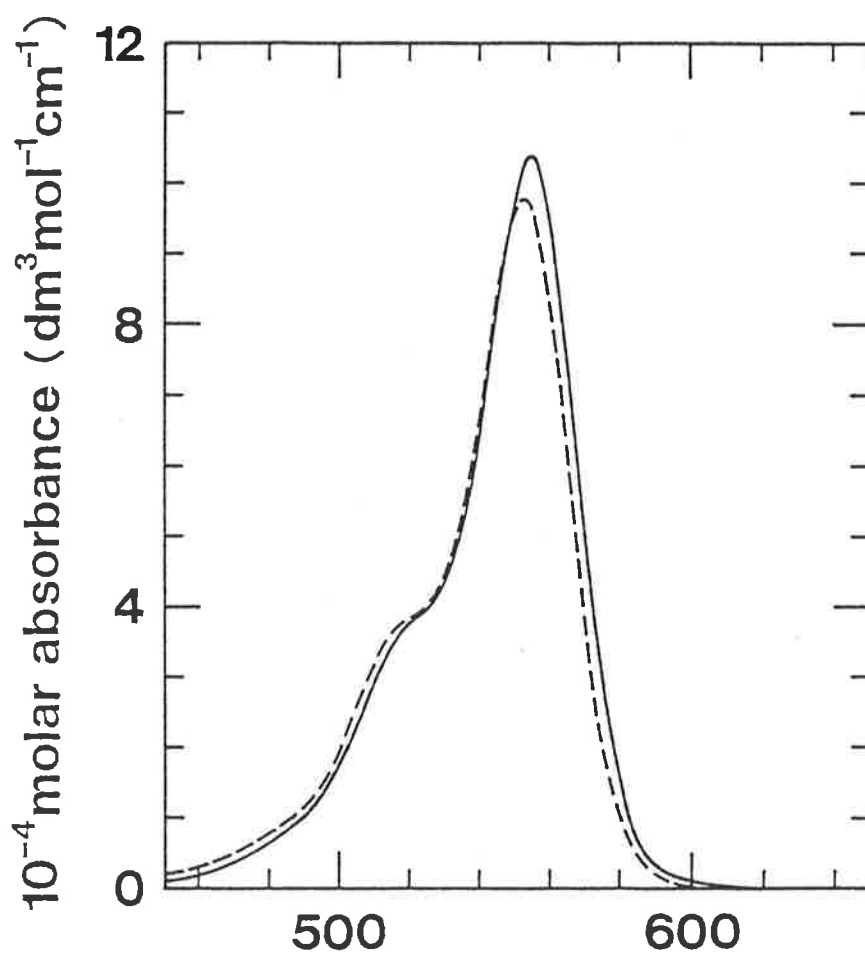
Figure 4.11: Calculated spectrum of RB·βCD (- - -)
compared with the spectrum of RB alone (——)

the variation of $1/\tau$ may be expressed through Equation 4.11:

$$1/\tau_1 = k_1([RB] + [\beta CD]) + k_{-1} \qquad (4.11)$$

The linear least-squares best fit line of the $1/\tau$ data to Equation 4.11 using program DATAFIT is shown in Figure 4.12, and the derived values are:

$$k_1 = (1.3 \pm 0.2) \times 10^8 \ dm^3 \ mol^{-1} \ s^{-1}$$

$$k_{-1} = (2.2 \pm 0.5) \times 10^4 \ s^{-1} \qquad and$$

$$K_1 = (5.9 \pm 2.3) \times 10^3 \ dm^3 \ mol^{-1}$$

Space-filling molecular models suggest that either a $-NEt_2$ group or the ortho-carboxyphenyl moiety of RB may be included by βCD. Since only a single relaxation was observed from the temperature-jump studies, assumably only one of the above orientations of the dye in the βCD cavity is possible. Circular dichroism (c.d.) can be used to determine experimentally the preferred orientation of RB in the RB·βCD complex. The inherently asymmetrical cyclodextrin molecule can induce chirality in an included achiral guest molecule [5]. Furthermore, for a 1:1 inclusion complex, the sign of the observed induced circular dichroism is related to the orientation of the guest in the cyclodextrin cavity [6]. For instance, a positive c.d. signal indicates that the transition moment corresponding to the electronic transition giving rise to the spectrum lies within a 30° cone centred on the principal rotational axis of symmetry of the cyclodextrin. A negative c.d. signal implies that the transition moment lies outside this cone. The induced circular dichroic spectrum of RB in the presence of βCD is shown in Figure 4.13. The concentrations of dye and βCD were chosen such that RB exists predominantly as the RB·βCD complex. A positive c.d. signal is observed, and its general form is similar to that observed for the visible absorption spectrum of RB. The $\pi \rightarrow \pi^*$
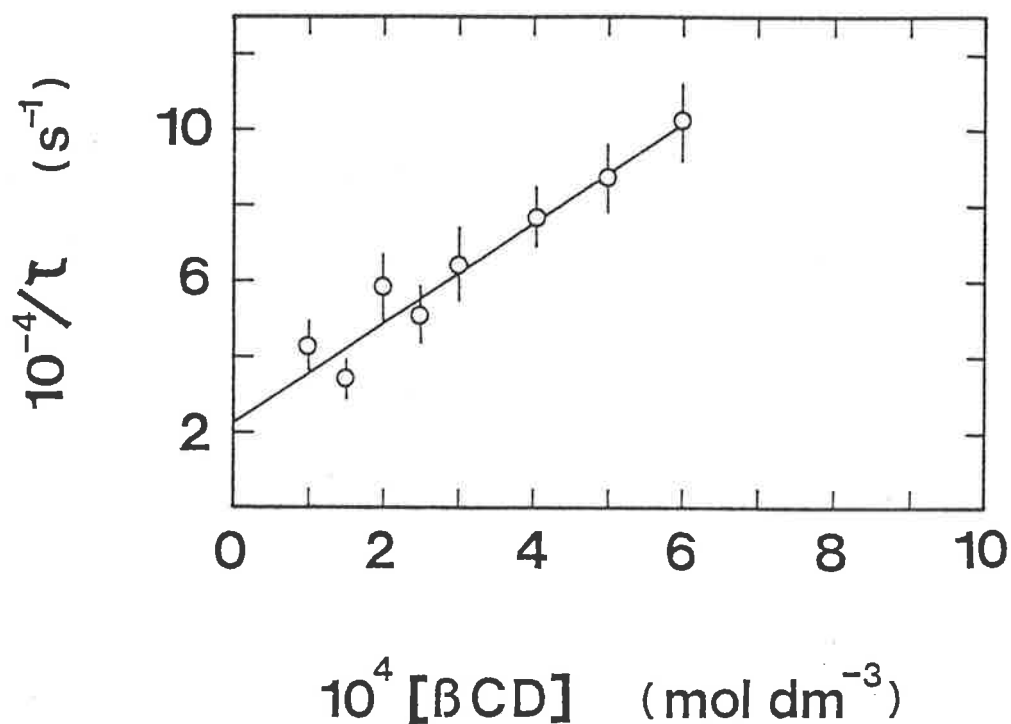
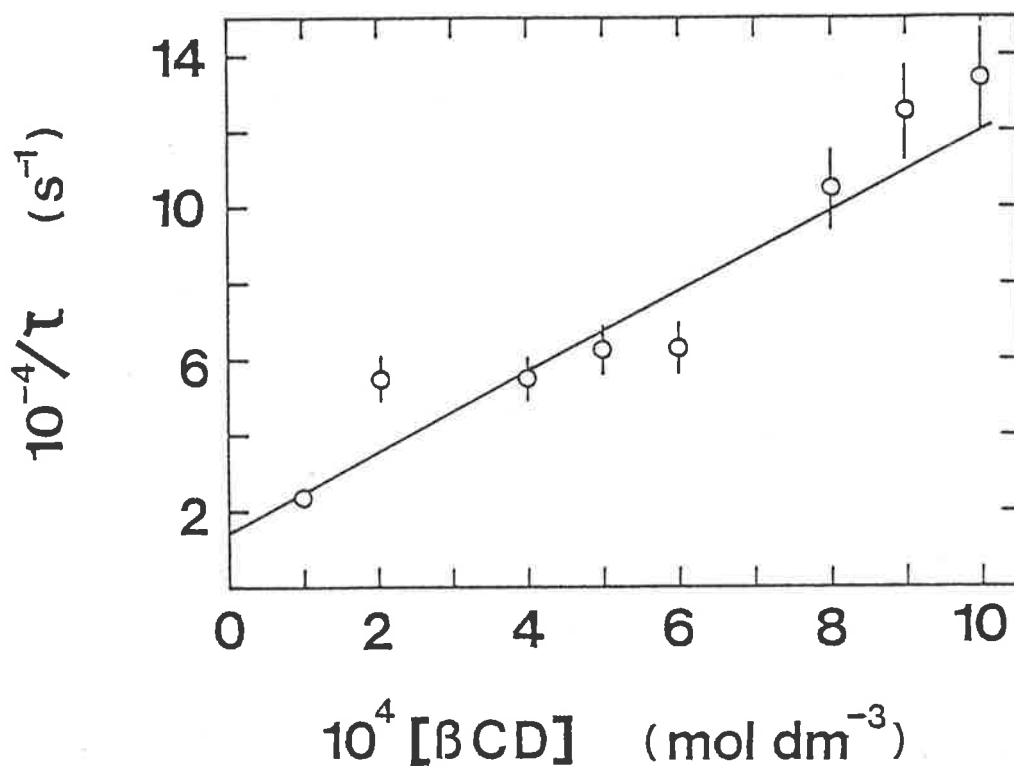*Figure 4.12:* The variation of 1/τ characterising the rhodamine B-βCD
system with total βCD concentration

The circles represent the experimental points, and the
solid line represents the best fit of the data to Equation
4.11. The error bars represent the standard errors in 1/τ
estimated from non-linear regressions of voltage against
time data.

Experiments were performed at pH 6.40 in aqueous 1.00 mol
dm^{-3} NaCl at 298.2 K.
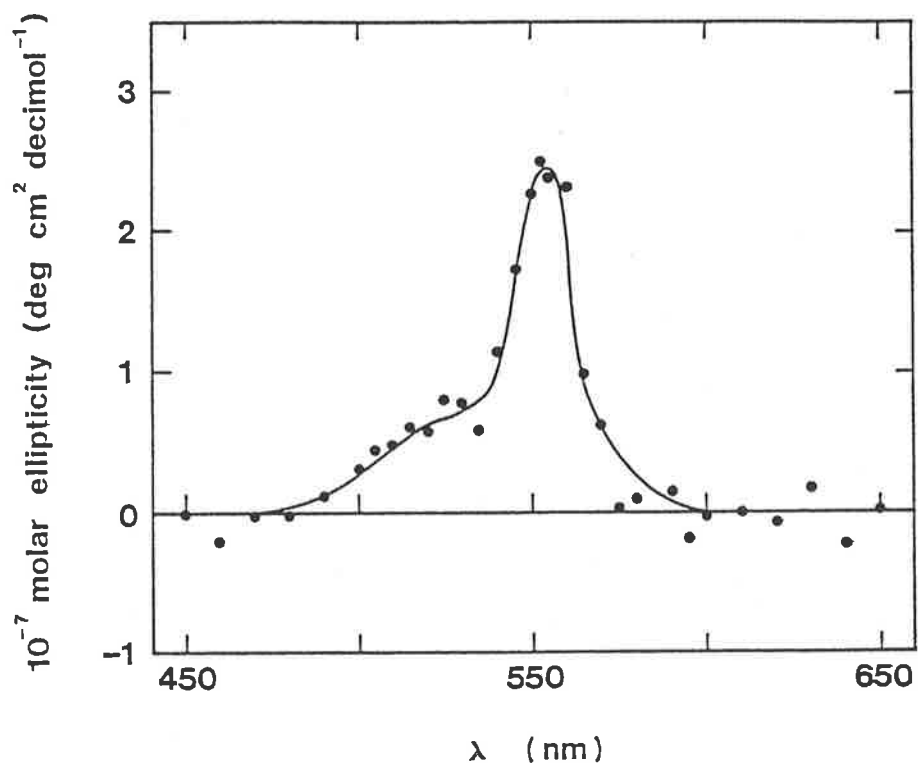
Figure 4.13: *The induced circular dichroic spectrum of rhodamine B in the presence of βCD, at pH 6.40 in aqueous 1.00 mol dm^{-3} NaCl at 298.2 K*

$$[\overline{RB}] = 1.50 \times 10^{-5} \ mol \ dm^{-3}$$
$$[\overline{\beta CD}] = 9.71 \times 10^{-3} \ mol \ dm^{-3}$$

transition that gives rise to the spectrum of RB is polarised along the long axis of the xanthene moiety [7], thus a $-NEt_2$ group of RB is preferentially included by βCD.

4.4 The Interaction of Some Xanthene Dyes with Gamma Cyclodextrin

4.4.1 Pyronine Y

The visible spectra of PY (ca. 8.8×10^{-6} mol dm^{-3} [PY]) alone and in the presence of γCD (36 solutions were studied in which the [γCD] was varied in the range $0-1.00 \times 10^{-2}$ mol dm^{-3}) were measured, and representative spectra are shown in Figure 4.14. There is a systematic decrease in the molar absorbance of PY at 545 nm, and the formation of a new absorbance maximum at approximately 517 nm which occur with increasing [γCD]. This is similar to that observed for the dimerisation of PY alone in aqueous solution [8], and indicates enhanced dimerisation of PY arising from the formation of γCD inclusion complexes.

The near approach to an isosbestic point indicates that, whilst two species dominate the observed spectral variations, a third species is also present, consistent with Equilibria 4.12 and 4.13:

$$PY + \gamma CD \underset{k_{-1}}{\overset{k_1}{\rightleftharpoons}} PY \cdot \gamma CD \qquad (K_1) \qquad\qquad (4.12)$$

$$PY + PY \cdot \gamma CD \underset{k_{-2}}{\overset{k_2}{\rightleftharpoons}} (PY)_2 \cdot \gamma CD \quad (K_2) \qquad\qquad (4.13)$$
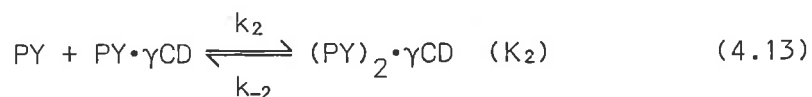
For this scheme, the observed absorbance is given by

$$A = \varepsilon_{PY}[PY] + \varepsilon_{PY \cdot \gamma CD}[PY \cdot \gamma CD] + 2\varepsilon_{(PY)_2 \cdot \gamma CD}[(PY)_2 \cdot \gamma CD] \qquad (4.14)$$

The values of the equilibrium constants K_1 and K_2 were derived from
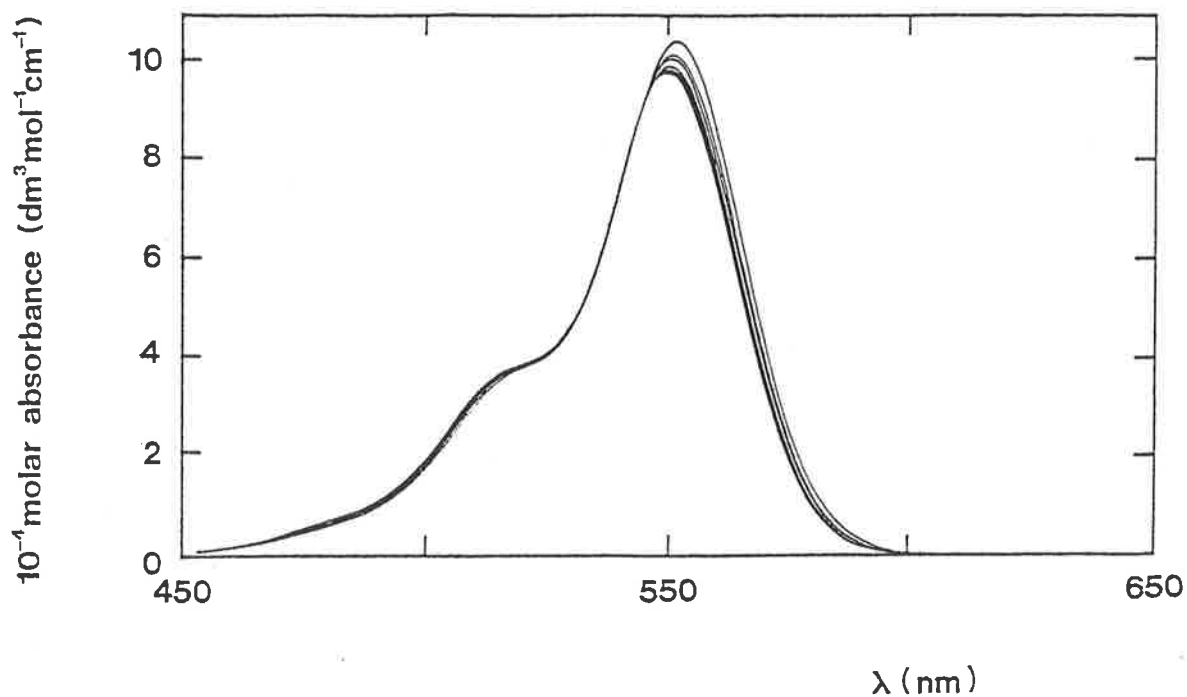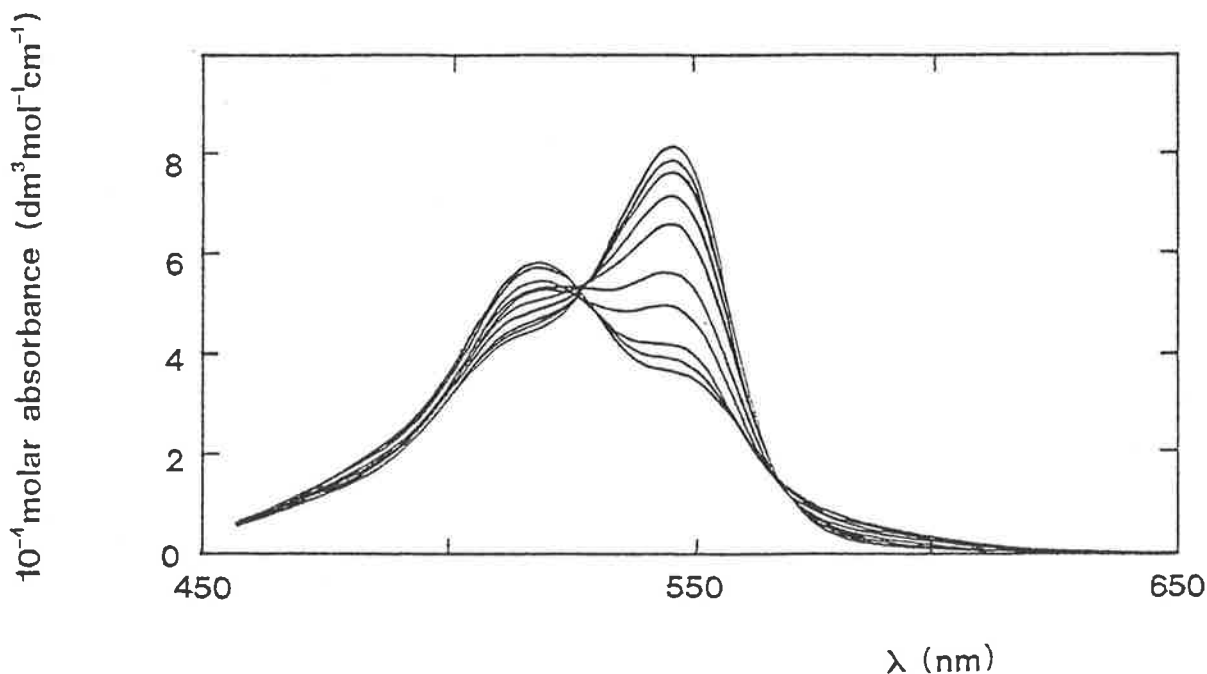
Figure 4.14: The variation of the pyronine Y spectrum in the presence of γCD, at pH 6.10 in aqueous 1.00 mol dm^{-3} NaCl at 298.2 K

The molar absorbance at 550 nm decreases systematically as the composition of the solutions changes in the order; PY (1.04 × 10^{-5} mol dm^{-3}), γCD 0; PY (1.03 × 10^{-5} mol dm^{-3}), γCD (2.10 × 10^{-5} mol dm^{-3}); PY (1.04 × 10^{-5} mol dm^{-3}), γCD (3.99 × 10^{-5} mol dm^{-3}); PY (1.03 × 10^{-5} mol dm^{-3}), γCD (1.00 × 10^{-4} mol dm^{-3}); PY (1.03 × 10^{-5} mol dm^{-3}), γCD (2.00 × 10^{-4} mol dm^{-3}); PY (1.04 × 10^{-5} mol dm^{-3}), γCD (5.02 × 10^{-4} mol dm^{-3}); PY (8.7 × 10^{-6} mol dm^{-3}), γCD (1.00 × 10^{-3} mol dm^{-3}); PY (8.7 × 10^{-6} mol dm^{-3}), γCD (2.50 × 10^{-3} mol dm^{-3}); PY (8.4 × 10^{-6} mol dm^{-3}), γCD (5.02 × 10^{-3} mol dm^{-3}); PY (8.4 × 10^{-6} mol dm^{-3}), γCD (9.51 × 10^{-3} mol dm^{-3}). These ten spectra exemplify the spectral variation for all thirty-six solutions studied.

absorbances determined at 1 nm intervals in the ranges 505-525 nm and 535-565 nm by fitting the absorbance data to Equation 4.14 using program DATAFIT. In fitting the absorbance data to Equation 4.14, the values of A were weighted according to their experimental uncertainty at each wavelength, and ε_{PY} was taken from the spectrum of PY in the absence of γCD shown in Figure 4.14. However, it proved difficult to obtain a unique fit of the spectral data to these two equilibria if at each wavelength the molar absorbances of PY in both inclusion complexes were allowed to vary during the fitting procedure. The values of K_1 and K_2 derived showed a considerable systematic variation over the fitted wavelength region. Accordingly, the approximation was made that the spectrum of PY·γCD was identical to the known spectrum of free PY. For a 1:1 inclusion complex, the magnitude of the observed spectral changes that arise with inclusion of a dye by cyclodextrin are determined by the degree of fit of the dye in the cavity of the cyclodextrin. If it is presumed that the PY·γCD complex formed involves a 'loose' fit of PY in the γCD cavity, in which the local environment of PY in PY·γCD is not much different from that of free PY (eg. the first hydration sphere of the dye molecule in PY·γCD is similar to that in free solution) then, in contrast to the spectrum of PY·βCD for which there is a 'tight' fit of the dye in the βCD cavity, it would be expected that the spectra of PY and PY·γCD would be similar to each other. When this assumption was incorporated into Equation 4.14, it was possible to obtain a satisfactory fit of the absorbance data. The values of K_1 and K_2 derived at each wavelength were weighted according to their estimated uncertainty and averaged to give the values:

$$K_1 = (1.1 \pm 0.5) \times 10^2 \ dm^3 \ mol^{-1} \qquad and$$

$$K_2 = (5.3 \pm 2.5) \times 10^5 \ dm^3 \ mol^{-1}$$

If the spectrum of PY·γCD is assumed to have the same shape as the spectrum of PY but, for example, is allowed to differ by 10% in the magnitude of the molar absorbances, then there is no change in the

values of K_1 and K_2 derived from the fitting procedure. This further supports the assumption that the spectrum of PY·γCD is very similar to that of free PY.

Within the approximation employed in the fitting of the spectral variations shown in Figure 4.14 to Equilibria 4.12 and 4.13, the spectrum of $(PY)_2$·γCD was calculated from the values of K_1 and K_2 derived, and is shown in Figure 4.15.

Temperature-jump spectrophotometric studies at 517 and 547 nm of PY and γCD in aqueous 1.00 mol dm^{-3} NaCl, at pH 6.10 and 298.2 K, detected a single relaxation at both wavelengths. At 517 nm the relaxation was characterised by a decrease in absorbance, whereas at 547 nm the relaxation produced an increase in absorbance. The amplitudes characterising this relaxation were always greater at 547 nm. By comparison with the CV/γCD temperature-jump study, the absorbance changes observed at both wavelengths are consistent with those expected to arise predominantly from the dissociation of the $(PY)_2$·γCD species. The amplitudes observed for this relaxation at both wavelengths were always greater than those characterising the βCD system, as anticipated from the spectra (Figures 4.3 and 4.14). Averaged relaxation traces were fitted to a single exponential curve, and the relaxation times evaluated were identical within experimental error at both wavelengths. The $1/\tau$ values together with the initial concentrations of PY and γCD used are listed in Appendix C (Table C.6). Temperature-jump studies of PY alone at a concentration identical to that used in the cyclodextrin studies detected a single relaxation characterised by a decrease and an increase in absorbance at 517 and 547 nm, respectively. Relaxation times determined for this process were comparable to the instrumental heating time, and the amplitude of this relaxation contributed <1% amplitude to that observed in
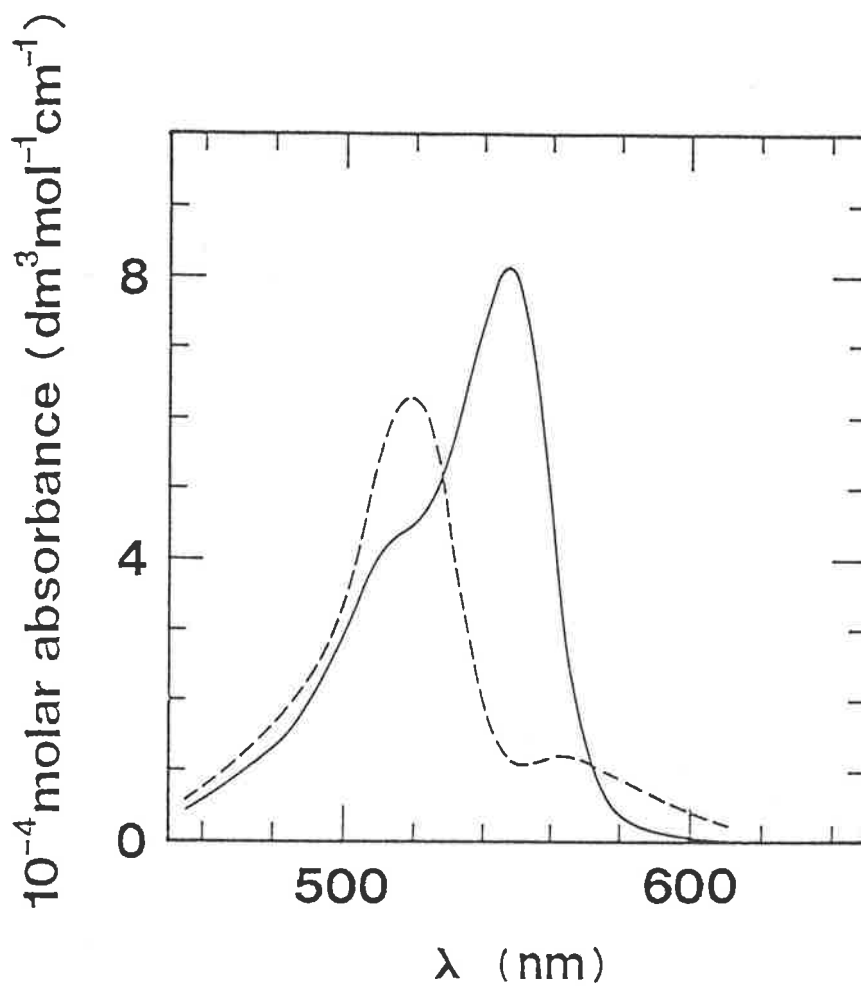
Figure 4.15: Calculated spectrum of (PY)$_2 \cdot \gamma$CD (- - -) compared with the spectrum of PY alone (——)

the presence of γCD. This relaxation may be assumed to arise from a property of the dye itself, presumably the dimerisation reaction of PY, and the greater relaxation amplitudes observed in the presence of γCD are caused by the increased total dimer concentration.

The dependence of $1/\tau$ on the total γCD concentration is shown in Figure 4.16, and is similar to that observed for the CV/γCD system (Figure 3.8). The $1/\tau$ data were found to be consistent with a reaction scheme in which a fast third step arising from the formation of the $(PY)_2 \cdot (\gamma CD)_2$ species (Reaction 4.15) was added to the processes shown in Reactions 4.12 and 4.13.

$$(PY)_2 \cdot \gamma CD + \gamma CD \underset{k_{-3}}{\overset{k_3}{\rightleftharpoons}} (PY)_2 \cdot (\gamma CD)_2 \qquad (K_3) \qquad (4.15)$$
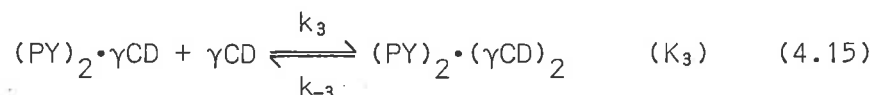
Provided that the first and last steps (Reactions 4.12 and 4.15) are sufficiently fast to be considered in equilibrium throughout the relaxation of the second step (Reaction 4.13), an expression for the variation of $1/\tau$ with $[\gamma CD]$ may be derived (Appendix D):

$$1/\tau = k_2[PY]\frac{[PY] + [PY \cdot \gamma CD] + 4[\gamma CD]}{[PY] + [\gamma CD] + 1/K_1} + k_{-2}\frac{[(PY)_2 \cdot \gamma CD] + 1/K_3}{[(PY)_2 \cdot \gamma CD] + [\gamma CD] + 1/K_3}$$

$$(4.16)$$

A non-linear least-squares fit of the $1/\tau$ data to Equation 4.16 using program DATAFIT produced the best fit curve shown in Figure 4.16, and the values of k_2, k_{-2}, K_1, K_2 and K_3 derived are:

$$k_2 = (1.7 \pm 1.0) \times 10^9 \text{ dm}^3 \text{ mol}^{-1} \text{ s}^{-1}$$

$$k_{-2} = (1.4 \pm 0.5) \times 10^4 \text{ s}^{-1}$$

$$K_1 = (1.0 \pm 0.1) \times 10^3 \text{ dm}^3 \text{ mol}^{-1}$$

$$K_2 = (1.2 \pm 1.1) \times 10^5 \text{ dm}^3 \text{ mol}^{-1} \qquad \text{and}$$

$$K_3 = (5.2 \pm 2.2) \times 10^1 \text{ dm}^3 \text{ mol}^{-1}$$

The $1/\tau$ data were also fitted to a reaction scheme given by Reactions
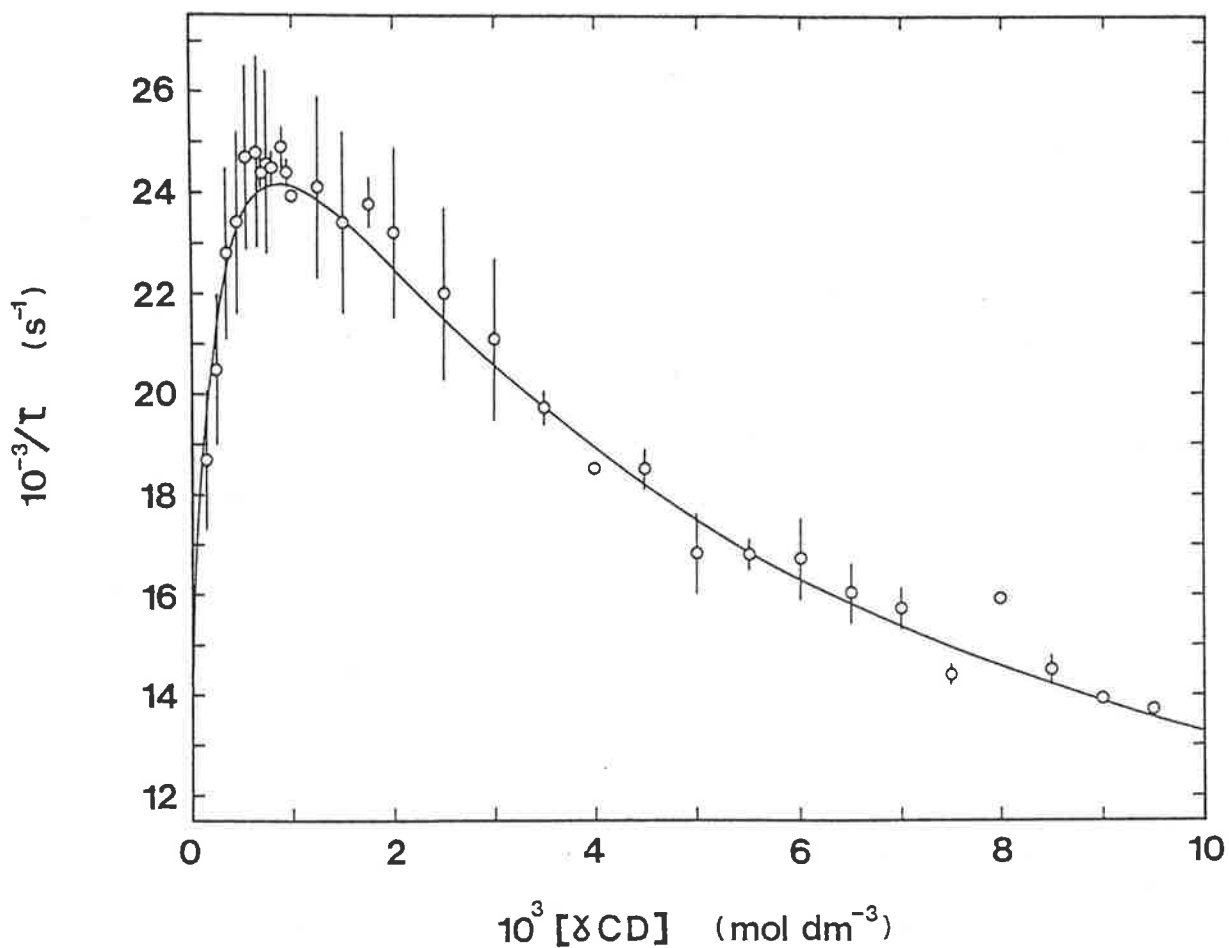
Figure 4.16: *The variation of 1/τ characterising the pyronine Y-γCD system with total γCD concentration*

The circles represent the averaged experimental data points obtained at 517 and 547 nm, and the solid curve represents the best fit of these data to Equation 4.16. The error bars represent the mean errors of 1/τ obtained at 517 and 547 nm.

Experiments were performed at pH 6.10 in aqueous 1.00 mol dm⁻³ NaCl at 298.2 K.

4.12 and 4.13 only, but this treatment increased the standard deviation in the parameters derived:

$$k_2 = (1.0 \pm 0.7) \times 10^{10} \ dm^3 \ mol^{-1} \ s^{-1}$$

$$k_{-2} = (3.3 \pm 2.2) \times 10^3 \ s^{-1}$$

$$K_1 = (1.13 \pm 0.07) \times 10^3 \ dm^3 \ mol^{-1} \qquad and$$

$$K_2 = (3.0 \pm 4.1) \times 10^6 \ dm^3 \ mol^{-1}$$

although the best fit curve characterising this model differed little from that shown in Figure 4.16. The sum of the squares of the residuals for the two-step equilibrium model (2.17×10^8) was marginally smaller than that for the three-step equilibrium model (3.3×10^8).

Although the values of K_1 and K_2 determined from the $1/\tau$ data and from the equilibrium spectrophotometric study using the two-step equilibrium model differ substantially, this may be a consequence of a combination of experimental error and the approximation made in the derivation of K_1 and K_2 from the spectrophotometric data. On the other hand, the equilibrium spectrophotometric study was unable to deduce the existence of the $(PY)_2 \cdot (\gamma CD)_2$ species proposed from the fitting of the $1/\tau$ data to the three-step equilibrium model, the formation of which is possible on stereochemical grounds from examining space-filling molecular models. Figure 4.17 shows that $[(PY)_2 \cdot (\gamma CD)_2]$ is always small compared with $[PY \cdot \gamma CD]$ and $[(PY)_2 \cdot \gamma CD]$ over the γCD concentration range studied. This, in combination with the observation that the dominant spectral change in the PY/γCD system arises from the enhanced dimerisation of PY, and the likelihood that the spectrum of $(PY)_2 \cdot (\gamma CD)_2$ will not differ greatly from that of $(PY)_2 \cdot \gamma CD$, renders the fitting of the observed equilibrium spectra insensitive to the presence of $(PY)_2 \cdot (\gamma CD)_2$. Thus, a definitive choice between the two-step and three-step equilibrium models cannot be made on the basis of the spectrophotometric and
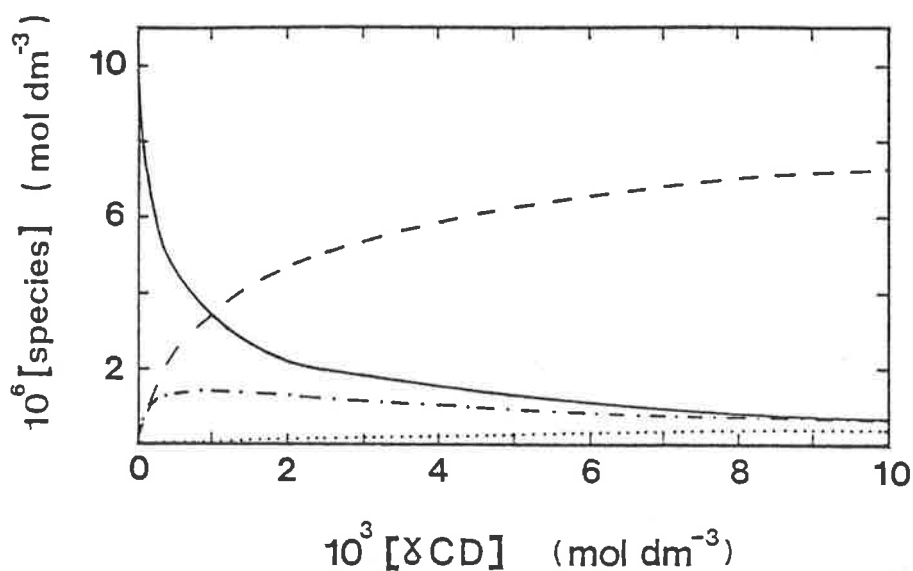
Figure 4.17: The variation of $[PY]$ (——), $[PY \cdot \gamma CD]$ (---), $[(PY)_2 \cdot \gamma CD]$ (-·-·) and $[(PY)_2 \cdot (\gamma CD)_2]$ (···) with total γCD concentration at constant total $[PY] = 1.00 \times 10^{-5}$ mol dm^{-3}. The species concentrations were calculated using $K_1 = 1.0 \times 10^3$ dm^3 mol^{-1}, $K_2 = 1.2 \times 10^5$ dm^3 mol^{-1} and $K_3 = 5.2 \times 10^1$ dm^3 mol^{-1} derived from the temperature-jump spectrophotometric study.

and temperature-jump data. Nevertheless, the formation of $(PY)_2 \cdot \gamma CD$ through Equilibria 4.12 and 4.13 is firmly established, and only the existence of this third equilibrium (Equilibrium 4.15) is conjectural.

4.4.2 Pyronine B

The visible spectra of PB alone, and in the presence of γCD are shown in Figure 4.18, from which it is seen that there is a shift of the absorbance maximum to shorter wavelengths and a pronounced change in the shape of the spectrum as $[\gamma CD]$ increases (35 solutions were studied in which $[\gamma CD]$ was varied in the range $0-1.00 \times 10^{-2}$ mol dm^{-3} and $[PB]$ was constant at 9.7×10^{-6} mol dm^{-3}).

The observed spectral changes are consistent with the formation of the 2:1 inclusion complex $(PB)_2 \cdot \gamma CD$ according to Equilibria 4.17 and 4.18:
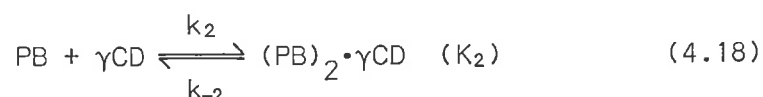
$$PB + \gamma CD \underset{k_{-1}}{\overset{k_1}{\rightleftharpoons}} PB \cdot \gamma CD \qquad (K_1) \qquad\qquad (4.17)$$

$$PB + \gamma CD \underset{k_{-2}}{\overset{k_2}{\rightleftharpoons}} (PB)_2 \cdot \gamma CD \quad (K_2) \qquad\qquad (4.18)$$

The values of the equilibrium constants K_1 and K_2 were derived from absorbances determined at 1 nm intervals in the ranges 520–537 nm and 540–567 nm by fitting the data to Equation 4.19 using program DATAFIT:

$$A = \varepsilon_{PB}[PB] + \varepsilon_{PB \cdot \gamma CD}[PB \cdot \gamma CD] + 2\varepsilon_{(PB)_2 \cdot \gamma CD}[(PB)_2 \cdot \gamma CD] \quad (4.19)$$

To obtain a unique fit of the spectral data to Equation 4.19, it was necessary to use the approximation that the spectrum of $PB \cdot \gamma CD$ was identical to the known spectrum of free PB. The values of K_1 and K_2 derived at each wavelength were weighted according to their estimated uncertainty and averaged to give the values:

Figure 4.18: The variation of the pyronine B spectrum in the presence of γCD, at pH 5.70 in aqueous 1.00 mol dm^{-3} NaCl at 298.2 K

The molar absorbance at 550 nm decreases systematically as the total γCD concentration increases sequentially in the range 0, 2.03 × 10^{-5}, 5.10 × 10^{-5}, 1.01 × 10^{-4}, 2.04 × 10^{-4}, 5.12 × 10^{-4}, 1.03 × 10^{-4}, 2.04 × 10^{-3} and 4.09 × 10^{-3} mol dm^{-3} with the total pyronine B concentration constant at 9.7 × 10^{-6} mol dm^{-3}. These nine spectra exemplify the spectral variation observed for all thirty-five solutions studied.

$$K_1 = (2.6 \pm 0.7) \times 10^2 \ dm^3 \ mol^{-1} \qquad and$$

$$K_2 = (2.5 \pm 1.4) \times 10^5 \ dm^3 \ mol^{-1}$$

The values of K_1 and K_2 were used to compute the spectrum of the (PB)$_2 \cdot \gamma$CD species shown in Figure 4.19.

Temperature-jump spectrophotometric studies at 533 and 553 nm of PB and γCD in aqueous 1.00 mol dm^{-3} NaCl, at pH 5.70 and 298.2 K, detected a single relaxation at both wavelengths. At 533 nm the relaxation was characterised by a decrease in absorbance, whereas at 553 nm the relaxation produced an increased absorbance, consistent with the absorbance changes arising predominantly from the shift of Equilibria 4.17 and 4.18 to the left. At both wavelengths the relaxation was characterised by relaxation times identical within experimental error, and the $1/\tau$ values and initial concentrations of PB and γCD used are listed in Appendix C (Table C.7).

The variation of $1/\tau$ with total γCD concentration is shown in Figure 4.20, and is consistent with the observed relaxation arising from the coupled fast formation of PB$\cdot\gamma$CD in Equilibrium 4.17 and the slower formation of (PB)$_2 \cdot \gamma$CD in Equilibrium 4.18. It may be expressed through Equation 4.20:

$$1/\tau_2 = k_2[PB]\frac{[PB] + [PB \cdot \gamma CD] + 4[\gamma CD]}{[PB] + [\gamma CD] + 1/K_1} + k_{-2} \qquad (4.20)$$

A non-linear least-squares fit of the $1/\tau$ data to Equation 4.20 using program DATAFIT produced the best fit curve shown in Figure 4.20, and the values of k_2, k_{-2}, K_1 and K_2 derived are:

$$k_2 = (8.2 \pm 0.2) \times 10^8 \ dm^3 \ mol^{-1} \ s^{-1}$$

$$k_{-2} = (6.40 \pm 0.05) \times 10^3 \ s^{-1}$$

$$K_1 = (4.3 \pm 0.1) \times 10^2 \ dm^3 \ mol^{-1} \qquad and$$
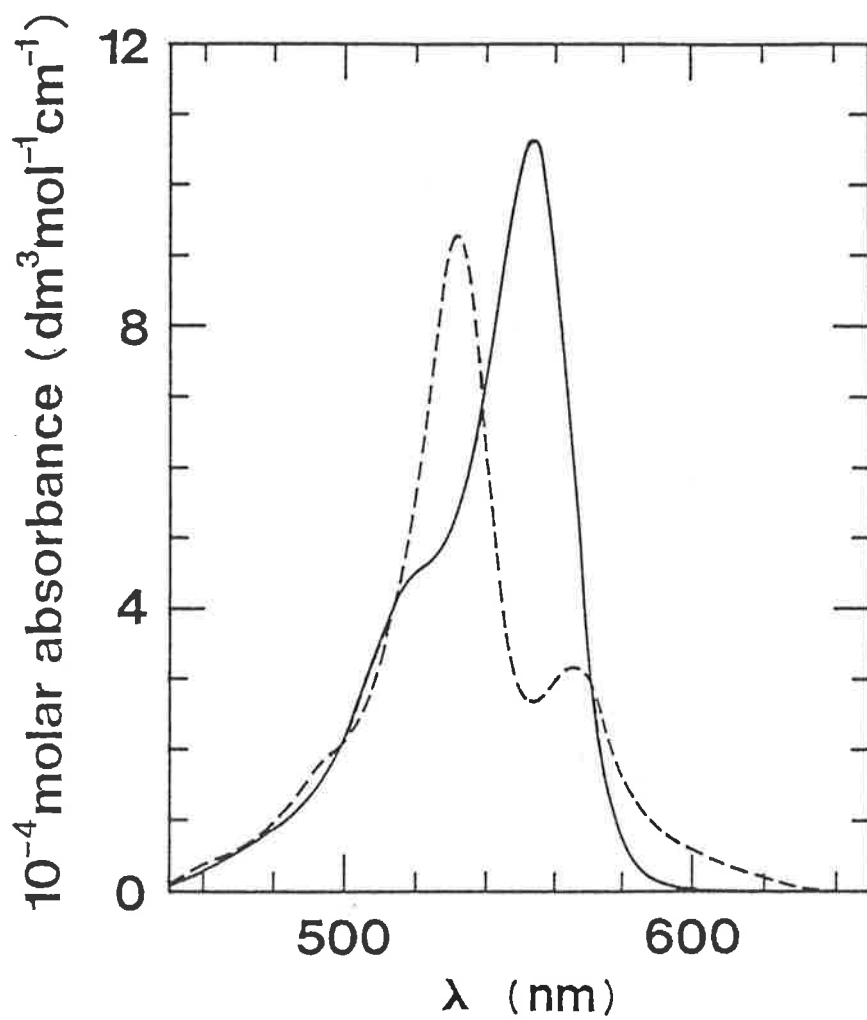
Figure 4.19: Calculated spectrum of (PB)$_2 \cdot \gamma CD$ (---) compared with the spectrum of PB alone (——)
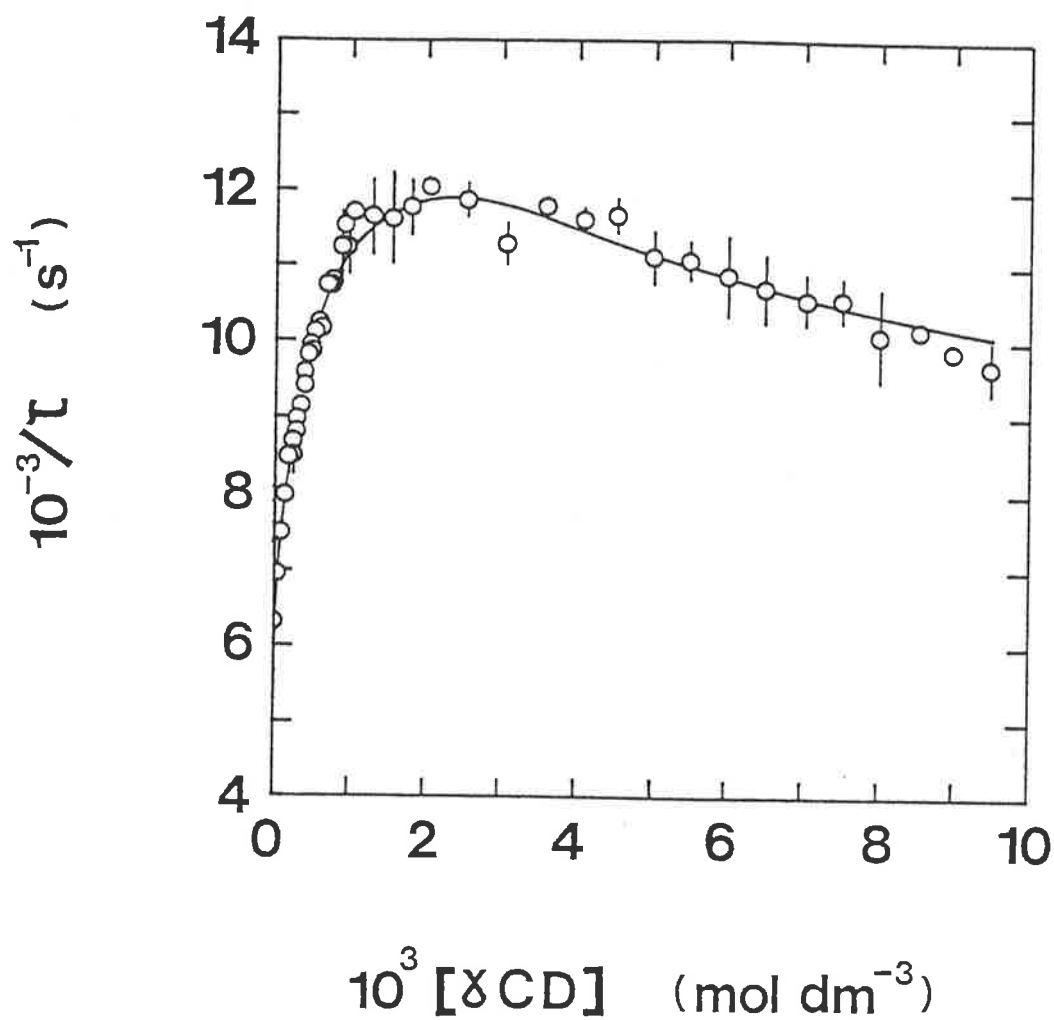
Figure 4.20: *The variation of 1/τ characterising the pyronine B-γCD system with total γCD concentration*

The circles represent the averaged experimental data points obtained at 533 and 553 nm, and the solid curve represents the best fit of these data to Equation 4.20. The error bars represent the mean errors of 1/τ obtained at 533 and 553 nm.

Experiments were performed at pH 5.70 in aqueous 1.00 mol dm⁻³ NaCl at 298.2 K.

$$K_2 = (1.28 \pm 0.04) \times 10^5 \text{ dm}^3 \text{ mol}^{-1}$$

The $1/\tau$ data were also fitted to a reaction scheme in which a fast third step (Reaction 4.21), analogous to that proposed for the inclusion of PY by γCD, was added to the processes given by Reactions 4.17 and 4.18:

$$(PB)_2 \cdot \gamma CD + \gamma CD \underset{k_{-3}}{\overset{k_3}{\rightleftharpoons}} (PB)_2 \cdot (\gamma CD)_2 \qquad (K_3) \qquad (4.21)$$
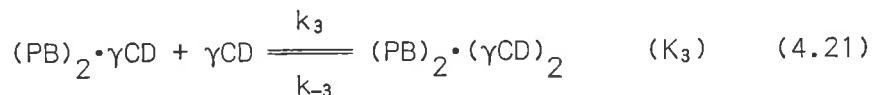
This treatment increased the standard deviation in K_1 and K_2, and the error in K_3 was greater than the magnitude of that constant. Thus, in the case of the PB/γCD system, the formation of the $(PB)_2 \cdot (\gamma CD)_2$ species appears unlikely.

The agreement between the K_1 and K_2 values derived from the equilibrium and temperature-jump spectrophotometric studies using the two-step equilibrium model is considered reasonable.

4.4.3 Rhodamine B

The variation of the visible spectrum of RB in the presence of γCD may be seen from Figure 4.21, and is consistent with the formation of the 1:1 inclusion complex RB·γCD according to the Equilibrium 4.22 (16 solutions were studied in which [γCD] was varied in the range 0–1.00 $\times 10^{-2}$ mol dm^{-3} and [RB] was constant at 9.2×10^{-6} mol dm^{-3}):

$$RB + \gamma CD \underset{k_{-1}}{\overset{k_1}{\rightleftharpoons}} RB \cdot \gamma CD \qquad (K_1) \qquad (4.22)$$

Fitting the absorbance data to this equilibrium in the range 550–565 nm at 1 nm intervals using program DATAFIT yields $K_1 = (7.1 \pm 1.8) \times 10^1$ dm^3 mol^{-1}. The very small absorbance changes observed in the equilibrium spectra prevented the fitting of the absorbance data over an extensive wavelength range. For this same reason, the spectrum of the RB·γCD complex
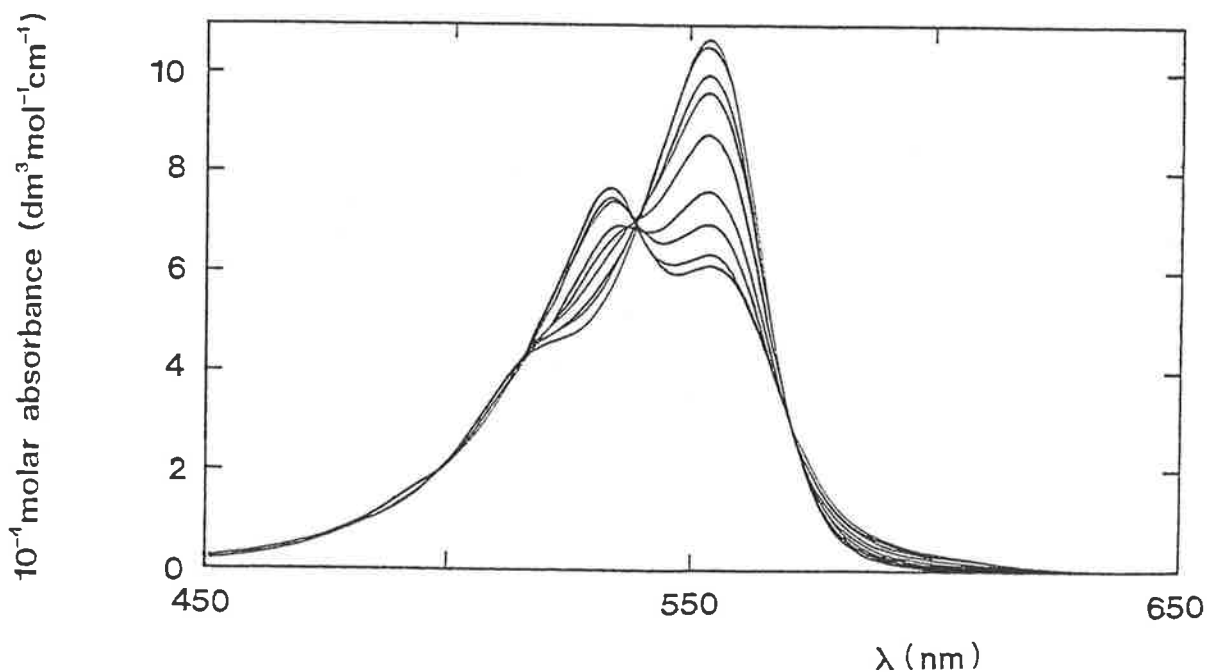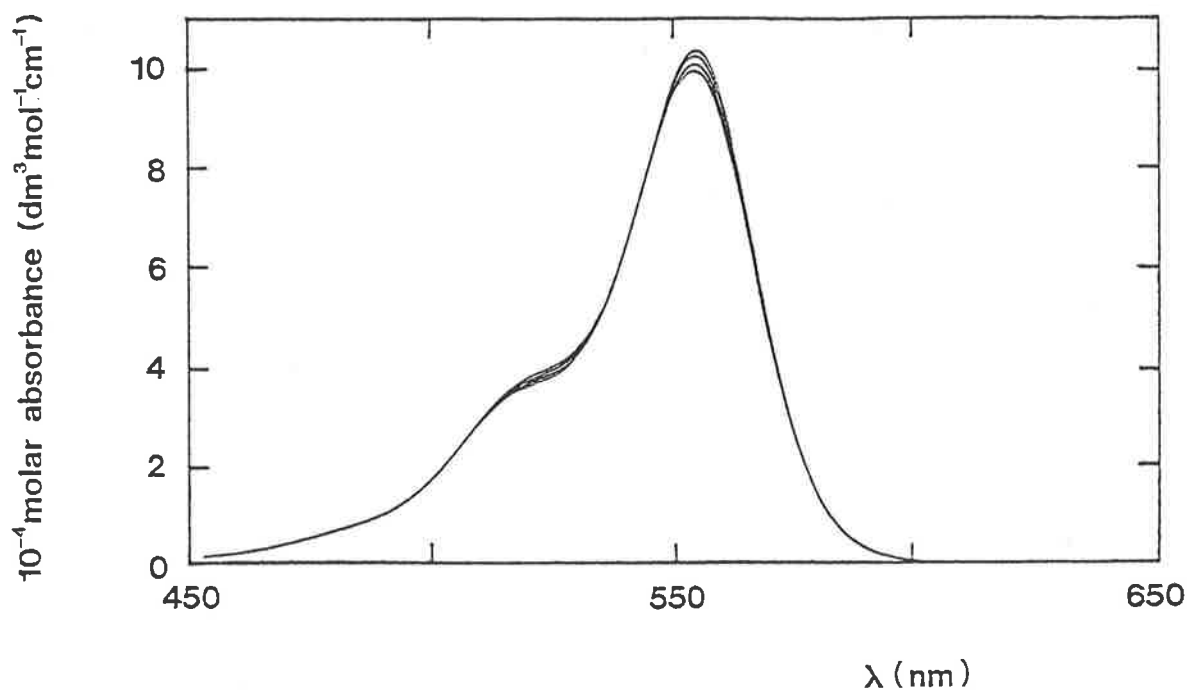
Figure 4.21:   The variation of the rhodamine B spectrum in the presence
of γCD, at pH 6.40 in aqueous 1.00 mol dm^{-3} at 298.2 K

The molar absorbance at 550 nm decreases systematically as
the total γCD concentration increases sequentially in the
range 0, 1.00 × 10^{-3}, 3.01 × 10^{-3} and 6.02 × 10^{-3} mol dm^{-3}
with the total rhodamine B concentration constant at
9.2 × 10^{-6} mol dm^{-3}.   These four spectra exemplify the
spectral variations for all sixteen solutions studied.

could not be derived.   However, it may be expected from Figure 4.21 that
the spectrum of the RB•γCD complex would be similar to that of the RB•βCD
complex (Figure 4.11), although in the former case the magnitude of the
perturbation of the RB spectrum would be weaker because of the 'looser'
fit of the dye in the γCD cavity and the consequent smaller environmental
change.

Temperature-jump spectrophotometric studies at 555 nm of RB and γCD
in aqueous 1.00 mol dm^{-3} NaCl, at pH 6.40 and 298.2 K, were unable to de-
tect the presence of any significant relaxations attributable to inclusion
processes.   It appears that a relaxation arising through Equilibrium 4.22
is characterised by small absorbance changes at the monitored wavelength,
and this would be anticipated in view of the spectra (Figure 4.21).
Temperature-jump studies of the PY/γCD and PB/γCD systems have shown
that the formation of the 1:1 inclusion complex is a rapid process
occurring within the instrumental heating time.   It may be assumed
that the process given by Reaction 4.22 is too fast to be studied by
the temperature-jump method, and it is not possible to determine values
of the kinetic parameters for the RB/γCD system.

Space-filling molecular models suggest that either a $-NEt_2$ group or
the ortho-carboxyphenyl moiety of RB may be included by γCD.   The induced
circular dichroic spectrum of RB in the presence of γCD is shown in
Figure 4.22.   The concentration of dye and γCD was chosen such that
RB exists predominantly as the RB•γCD complex.   As was the case with
βCD, the observed positive c.d. signal indicates that a $-NEt_2$ group of
RB is preferentially included by γCD.
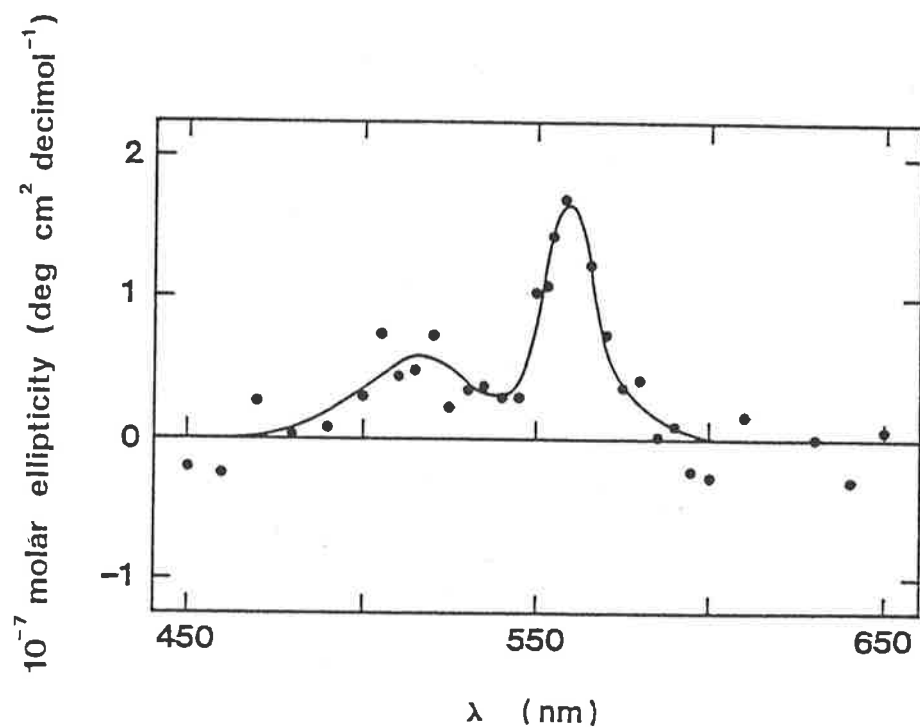
Figure 4.22: *The induced circular dichroic spectrum of rhodamine B in the presence of γCD, at pH 6.40 in aqueous 1.00 mol dm^{-3} NaCl at 298.2 K*

$$[R\bar{B}] = 1.50 \times 10^{-5} \, mol \, dm^{-3}$$
$$[\gamma C\bar{D}] = 5.02 \times 10^{-2} \, mol \, dm^{-3}$$

4.4.4 An interpretation of the derived spectra of cyclodextrin included dimers

The characteristic spectrum of $(dye)_2 \cdot \gamma CD$ (eg. Figure 4.15) arises from the existence of the $(dye)_2$ species in which exciton interactions [9] between the monomer units take place. The result of exciton effects is the splitting of excited states and the appearance of spectral shifts or splittings of the absorption band(s) of the monomer (eg. Figure 4.15). Gianneschi et al. [10] have applied exciton theory to interpret the spectra of the free $(PY)_2$ and $(PB)_2$ species, and have found that for both dyes there is an angle of ca. 0° between the monomer units of the dimer. Space-filling molecular models constructed on this basis show that both dye dimers are a sandwich structure of the two monomer units with parallel molecular axes and with the charged amino groups at opposite edges for a minimal Coulombic repulsion. It is of interest, then, also to deduce the dimer structure of these dyes when they are included by γCD and compare it with that of the unincluded dimer.

The method of Gianneschi et al. [10] and program EXCITON [11] were used to interpret the experimentally derived spectrum of the $(PY)_2 \cdot \gamma CD$ and $(PB)_2 \cdot \gamma CD$ species. Program EXCITON was used to calculate the theoretical dimer spectrum, and by varying the values of the exciton exchange parameter ϵ and the angle α between the transition moments of the monomer units the best theoretical spectrum for each case may be found. The theoretical spectrum may be calculated from the choice of two exciton interaction theories: either the crude adiabatic model of Fulton and Gouterman [12, 13], or the adiabatic model of Gianneschi and Kurucsev [14]. Both models were used to determine the best theoretical spectrum, but the adiabatic model [14] provided a more accurate description of exciton interactions in the dimers in that the theoretical spectrum fitted more closely the experimental spectrum, and the theoretical spectum calculated from this model only is shown in Figure 4.23. The
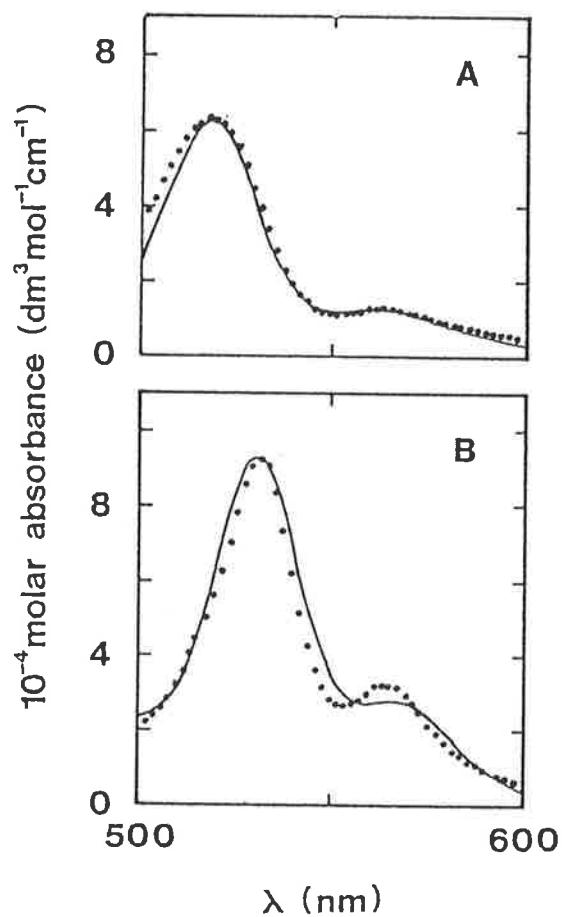
Figure 4.23: Comparison of experimental and theoretical dimer spectra

(A)   (PY)$_2$·γCD; ε = 0.85, α = 25°

(B)   (PB)$_2$·γCD; ε = 0.70, α = 20°

The circles represent the experimentally derived spectra, and the solid curves are the calculated adiabatic spectra. ε is the exciton exchange parameter and α is the angle between the transition moments of the monomers in the dimer. For the xanthene dyes the transition moment is oriented along the long axis of the xanthene moiety [7].

discrepancies observed between the theoretical and experimental spectra may be attributed to deficiencies in the adiabatic model in interpreting completely the spectrum of a dimer, and the derived nature of the experimental dimer spectrum. The best fit of the theoretical spectrum to the experimental spectrum was obtained only when the dye monomers were aligned at an angle of 20-25° to each other in $(dye)_2 \cdot \gamma CD$. Thus, it appears that the structures of $(PY)_2$ and $(PB)_2$ are slightly distorted when included by γCD to form $(PY)_2 \cdot \gamma CD$ and $(PB)_2 \cdot \gamma CD$ (α, ca. 20-25°), compared with the unincluded dimers (α, ca. 0°). This difference may arise from constraints imposed on the dimer by inclusion in the cyclodextrin cavity but could also be to some extent an artefact arising from the approximations used in deriving the $(PY)_2 \cdot \gamma CD$ and $(PB)_2 \cdot \gamma CD$ spectra.

4.5 Summary and Discussion

Table 4.1 summarises the interaction of the xanthene dyes with the cyclodextrins. The complexing ability of the cyclodextrins for a particular xanthene dye varies with the annular radius of the cyclodextrin in a manner similar to that observed for the crystal violet/ cyclodextrin system. These trends in cyclodextrin selectivity can be rationalised in terms of the relative sizes of the included species and the cyclodextrin annulus. The αCD annulus is too small to accommodate any of the xanthene dyes. The inclusion of $(PY)_2$ or $(PB)_2$ by γCD but not by βCD indicates that the annulus of the latter species is too small to accommodate $(PY)_2$ or $(PB)_2$, but the greater K_1 observed for $PY \cdot \beta CD$ and $PB \cdot \beta CD$ by comparison with that for $PY \cdot \gamma CD$ and $PB \cdot \gamma CD$ suggests that the annulus of βCD most closely approaches the optimal size for the inclusion of PY or PB. For the relatively larger RB, on the other

Dye	Alpha Cyclodextrin	Beta Cyclodextrin	Gamma Cyclodextrin
		$PY + \beta CD \underset{k_{-1}}{\overset{k_1}{\rightleftharpoons}} PY \cdot \beta CD \quad (K_1) \quad$ fast	$PY + \gamma CD \rightleftharpoons PY \cdot \gamma CD \quad (K_1) \quad$ fast
		$PY \cdot \beta CD + \beta CD \underset{k_{-2}}{\overset{k_2}{\rightleftharpoons}} PY \cdot (\beta CD)_2 \quad (K_2) \quad$ slow	$PY + PY \cdot \gamma CD \underset{k_{-2}}{\overset{k_2}{\rightleftharpoons}} (PY)_2 \cdot \gamma CD \quad (K_2) \quad$ slow
		$K_1^{equil} \ (5.2 \pm 1.2) \times 10^3 \ dm^3 \ mol^{-1}$	$(PY)_2 \cdot \gamma CD + \gamma CD \rightleftharpoons (PY)_2 \cdot (\gamma CD)_2 \quad (K_3) \quad$ fast
	No	$K_2^{equil} \ (1.7 \pm 0.4) \times 10^2 \ dm^3 \ mol^{-1}$	$K_1^{equil} \ (1.1 \pm 0.5) \times 10^2 \ dm^3 \ mol^{-1}$
	Inclusion	$K_1^{kin} \ (4.2 \pm 1.4) \times 10^3 \ dm^3 \ mol^{-1}$	$K_2^{equil} \ (5.3 \pm 2.5) \times 10^5 \ dm^3 \ mol^{-1}$
Pyronine Y	Complex	$K_2^{kin} \ (2.7 \pm 1.8) \times 10^2 \ dm^3 \ mol^{-1}$	$K_1^{kin} \ (1.0 \pm 0.1) \times 10^3 \ dm^3 \ mol^{-1}$
	Formed	$k_1 \ (1.1 \pm 0.2) \times 10^8 \ dm^3 \ mol^{-1} \ s^{-1}$	$K_2^{kin} \ (1.2 \pm 1.1) \times 10^5 \ dm^3 \ mol^{-1}$
		$k_{-1} \ (2.6 \pm 0.4) \times 10^4 \ s^{-1}$	$K_3^{kin} \ (5.2 \pm 2.2) \times 10^1 \ dm^3 \ mol^{-1}$
		$k_2 \ (5.4 \pm 1.2) \times 10^6 \ dm^3 \ mol^{-1} \ s^{-1}$	$k_2 \ (1.7 \pm 1.0) \times 10^9 \ dm^3 \ mol^{-1} \ s^{-1}$
		$k_{-2} \ (2.0 \pm 0.9) \times 10^4 \ s^{-1}$	$k_{-2} \ (1.4 \pm 0.5) \times 10^4 \ s^{-1}$
		$PB + \beta CD \underset{k_{-1}}{\overset{k_1}{\rightleftharpoons}} PB \cdot \beta CD \quad (K_1)$	$PB + \gamma CD \rightleftharpoons PB \cdot \gamma CD \quad (K_1) \quad$ fast
		$K_1^{equil} \ (4.0 \pm 2.4) \times 10^3 \ dm^3 \ mol^{-1}$	$PB + PB \cdot \gamma CD \underset{k_{-2}}{\overset{k_2}{\rightleftharpoons}} (PB)_2 \cdot \gamma CD \quad (K_2) \quad$ slow
	No	$K_1^{kin} \ (7.3 \pm 3.1) \times 10^3 \ dm^3 \ mol^{-1}$	$K_1^{equil} \ (2.6 \pm 0.7) \times 10^2 \ dm^3 \ mol^{-1}$
	Inclusion	$k_1 \ (1.1 \pm 0.1) \times 10^8 \ dm^3 \ mol^{-1} \ s^{-1}$	$K_2^{equil} \ (2.5 \pm 1.4) \times 10^5 \ dm^3 \ mol^{-1}$
Pyronine B	Complex	$k_{-1} \ (1.5 \pm 0.5) \times 10^4 \ s^{-1}$	$K_1^{kin} \ (4.3 \pm 0.1) \times 10^2 \ dm^3 \ mol^{-1}$
	Formed		$K_2^{kin} \ (1.28 \pm 0.04) \times 10^5 \ dm^3 \ mol^{-1}$
			$k_2 \ (8.2 \pm 0.2) \times 10^8 \ dm^3 \ mol^{-1} \ s^{-1}$
			$k_{-2} \ (6.40 \pm 0.05) \times 10^3 \ s^{-1}$

Rhodamine B

No

Inclusion

Complex

Formed

$$RB + \beta CD \underset{k_{-1}}{\overset{k_1}{\rightleftharpoons}} RB \cdot \beta CD \quad (K_1)$$

$K_1^{equil} \quad (6.9 \pm 0.7) \times 10^3 \; dm^3 \; mol^{-1}$

$K_1^{kin} \quad (5.9 \pm 2.3) \times 10^3 \; dm^3 \; mol^{-1}$

$k_1 \quad (1.3 \pm 0.2) \times 10^8 \; dm^3 \; mol^{-1} \; s^{-1}$

$k_{-1} \quad (2.2 \pm 0.5) \times 10^4 \; s^{-1}$

$$RB + \gamma CD \rightleftharpoons RB \cdot \gamma CD \quad (K_1)$$

$K_1^{equil} \quad (7.1 \pm 1.8) \times 10^1 \; dm^3 \; mol^{-1}$

Table 4.1: *Summary of the interaction of pyronine Y, pyronine B and rhodamine B with the cyclodextrins*

hand, $(RB)_2$ is too large to be accommodated by either the β- or γCD annulus, but RB still achieves a better fit into the βCD annulus than is the case with the larger γCD annulus.

The selectivity of the cyclodextrins for substrates in the formation of inclusion complexes can be quite subtle, as demonstrated by the ability of PY to form complexes of the type $PY \cdot (\beta CD)_2$ and possibly $(PY)_2 \cdot (\gamma CD)_2$ whereas PB apparently does not. It has been proposed from constructing space-filling molecular models of these inclusion complexes that the orientations of the respectively included species in the cyclo-dextrin cavity are slightly different for PY and PB, as a consequence of the included species striving for an optimum fit in the cavity. Although the relative sizes of the guest and the cyclodextrin annulus appear to be of primary importance, other factors may also contribute to the selectiv-ity of the cyclodextrins. For example, steric considerations suggest that either the ortho-carboxyphenyl moiety or a $-NEt_2$ group of RB may be included by β- and γCD. However, it has been shown that, for the 1:1 complexes formed, the $-NEt_2$ group was preferentially included. The dif-ference in the polarity of these two moieties may be responsible for determining the observed selectivity.

The kinetic data displayed in Table 4.1 may be used to deduce some mechanistic details of the inclusion reaction. The formation of the 1:1 complex dye·βCD is characterised by a forward rate constant k_1 that is of the order 10^8 dm^3 mol^{-1} s^{-1}. The magnitude of k_1 approaches that of the diffusion-controlled limit, and assumably the inclusion of a dye by βCD is initiated by a diffusion-controlled encounter between these two species, which then form dye·βCD at a slower rate as the dye enters the βCD annulus (Reaction 4.23):

$$D + \beta CD \rightleftharpoons (D---\beta CD) \rightleftharpoons D \cdot \beta CD \qquad (4.23)$$

The second step of Reaction 4.23 involves solvation changes, steric interactions and possibly conformational change of cyclodextrin and/or dye, as discussed in Section 1.4. The values of k_1 characterising the dye·βCD complexes of the xanthene dyes studied herein, and also for the CV·βCD complex (Table 3.1), are independent of the dye structure. This suggests that steric interactions do not make a major contribution to k_1 but rather it is the desolvation processes which are the dominant rate-determining factors in the inclusion of the dyes by βCD. The desolvation processes would involve the breakdown of the water structure around that part of the guest which is going to be included by cyclodextrin, and the release of hydrating water molecules from the cyclodextrin cavity. The role of desolvation in the kinetics of complex formation has also been discussed by others [15, 16].

The ca. 20-fold difference between the equilibrium constants K_1 and K_2 characterising the inclusion of PY in PY·βCD and PY·$(βCD)_2$, respectively, arises solely from $k_1 \simeq 20k_2$. Statistical considerations suggest that $k_1 \simeq 2k_2$ because the number of $-NMe_2$ groups that can be included by βCD to form PY·$(βCD)_2$ is halved by the formation of PY·βCD. Since k_2 is observed to be smaller than k_1 than was anticipated, and the extent of the contribution of desolvation processes to k_2 would be expected to be almost the same as for k_1, this would imply that there are other requirements more important in the formation of PY·$(βCD)_2$ compared with the formation of PY·βCD. The disposition of the dye in the βCD cavity may cause the sterically orienting interactions involved in the inclusion reaction to be slightly more critical in the association of PY·βCD and βCD than is the case for the formation of PY·βCD.

Equilibrium and temperature-jump spectrophotometric studies have shown that the enhanced dimerisation of PY and PB in the presence of γCD

arises from the formation of the $(dye)_2 \cdot \gamma CD$ species through the stepwise inclusion of two dye monomers by γCD (Reactions 4.24 and 4.25):

$$D + \gamma CD \rightleftharpoons (D\text{---}\gamma CD) \rightleftharpoons D \cdot \gamma CD \qquad \text{fast} \qquad (4.24)$$

$$D + D \cdot \gamma CD \rightleftharpoons (D\text{---}D \cdot \gamma CD) \rightleftharpoons D_2 \cdot \gamma CD \qquad \text{slow} \qquad (4.25)$$
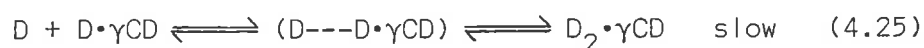
The inclusion of the each monomer by γCD may be considered to occur in two stages. The formation of the ordered and tightly assembled $(dye)_2 \cdot \gamma CD$ is slower than the formation of the loosely assembled $dye \cdot \gamma CD$ complex because the entrance of the second dye monomer into the γCD annulus of $dye \cdot \gamma CD$ is relatively hindered. The analysis of the derived spectrum of $(dye)_2 \cdot \gamma CD$ has suggested that the structures of $(PY)_2$ and $(PB)_2$ are slightly distorted when included by γCD compared with their structures in water alone. Interestingly, the inclusion of pyrene and acridine orange as dimers by γCD also gives rise to an asymmetrically twisted dimer configuration [17, 18]. Apparently, the sterically restricted environment of the cyclodextrin cavity may not allow the formation of a symmetric sandwich dimer.

This study of the interaction of some xanthene dyes with the cyclodextrins has reinforced and developed further those concepts deduced from the crystal violet/cyclodextrin system. The annular radii of the cyclodextrins and the relative size of the guest dictate the selectivity of the cyclodextrins for substrates in the formation of inclusion complexes. A range of cyclodextrin inclusion mechanisms has been shown to exist, and the kinetic data obtained has been discussed in terms of the mechanistic steps involved in the inclusion process. The enhanced dimerisation of dyes in the presence of cyclodextrin appears to proceed through a common inclusion mechanism. However, greater insight into this phenomenon requires an understanding of the dye dimerisation reaction, and this is the subject of the next chapter.

Bibliography

1. DEGANI, Y. and WILLNER, I. Chem. Phys. Letts. 104, 496 (1984).

2. BRITTAIN, H. G. Chem. Phys. Letts. 83, 161 (1981).

3. RAMETTE, R. W. and SANDELL, E. B. J. Am. Chem. Soc. 78, 4872 (1956).

4. FUJIKI, K., IWANAGA, C. and KOIZUMI, M. Bull. Chem. Soc. Jpn. 35, 185 (1962).

5. HARATA, K. Bull. Chem. Soc. Jpn. 51, 2737 (1978).

6. KAJTAR, M., HORVATH-TORO, Cs., KUTHI, E. and SZEJTLI, J. Acta Chim. Acad. Sci. Hung. 110, 327 (1982).

7. GAL, M. E., KELLY, G. R. and KURUCSEV, T. J. Chem. Soc. Faraday Trans. II 69, 395 (1973).

8. GIANNESCHI, L. P. and KURUCSEV, T. J. Chem. Soc. Faraday Trans. II 70, 1334 (1974).

9. KASHA, M., RAWLS, H. R. and ASHRAF EL-BAYOUMI, M. Pure Appl. Chem. 11, 371 (1965).

10. GIANNESCHI, L. P., CANT, A. and KURUCSEV, T. J. Chem. Soc. Faraday Trans. II 73, 664 (1977).

11. KURUCSEV, T. University of Adelaide, private communication.

12. FULTON, R. L. and GOUTERMAN, M. J. Chem. Phys. 35, 1059 (1961).

13. FULTON, R. L. and GOUTERMAN, M. J. Chem. Phys. 41, 2280 (1964).

14. GIANNESCHI, L. P. and KURUCSEV, T. J. Chem. Soc. Faraday Trans. II 72, 2095 (1976).

15. CRAMER, F., SAENGER, W. and SPATZ, H.-Ch. J. Am. Chem. Soc. 89, 14 (1967).

16. TURRO, N. J., OKUBO, T. and CHUNG, C.-J. J. Am. Chem. Soc. 104, 1789 (1982).

17. KANO, K., MATSUMOTO, H., HASHIMOTO, S. SISIDO, M. and IMANISHI, Y. J. Am. Chem. Soc. 107, 6117 (1985).

18. KOBAYASHI, N., HINO, Y., UENO, A. and OSA, T. Bull. Chem. Soc. Jpn. 56, 1849 (1983).

CHAPTER V

Kinetic Aspects Of The

Dimerisation Of Dyes

KINETIC ASPECTS OF THE DIMERISATION OF DYES

5.1 Introduction

Molecular aggregation via stacking is very important in many areas of dye chemistry and of biochemistry, for example, in stabilising the helical conformation of nucleic acids [1]. Dyes have been suggested [2] as simple models for investigating the stacking process and, while there have been numerous equilibrium studies of dye aggregation, kinetic studies have been limited in number. One reason for this is that the aggregation process is very rapid and kinetic studies require techniques that are specialised for studying fast reactions, for example, the temperature-jump method.

The aim of this study is to determine the kinetic parameters for the dimerisation reaction of those dyes used in the cyclodextrin studies described in this work (i.e. crystal violet (CV), pyronine Y (PY), pyronine B (PB), and rhodamine B (RB)):

$$2D \underset{k_{-d}}{\overset{k_d}{\rightleftharpoons}} D_2 \qquad (K_d) \qquad\qquad (5.1)$$
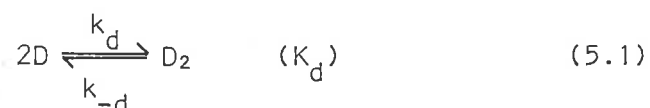
The results obtained may be considered in conjunction with the kinetic data from other dye systems, and discussed in terms of the general mechanism of the dimerisation reaction. Furthermore, it would be possible to compare the rate constants for the dimerisation of the dyes in the absence of cyclodextrin with those in the presence of cyclodextrin, and hence propose an explanation for cyclodextrin enhanced dimerisation of dyes.

5.2 Temperature-Jump Spectrophotometric Studies of the Dimerisation of Dyes

Initial temperature-jump spectrophotometric studies of CV, PY, PB and RB solutions were inconclusive in showing the existence of a relaxation arising through the dimerisation equilibrium of the dye (Reaction 5.1). The high molar absorbance of dye solutions obtained through using a temperature-jump cell of optical pathlength 1.00 cm (the same cell used for the dye/cyclodextrin studies) was found to limit the dye concentration range (typically < 3.00×10^{-5} mol dm^{-3} [dye]) over which reliable relaxation studies were possible. Relaxations that could be detected at the dye concentrations studied were characterised by very small amplitudes. Given the narrow dye concentration range studied and the very small amplitudes of the observed relaxations, it was not possible to be totally certain of the origin of the relaxation. It may be presumed that over the dye concentration range studied the proportion of dimeric species would be very small, and so relaxations arising through Equilibrium 5.1 would have very small amplitudes. However, the temperature-jump studies could not provide clear evidence that the observed relaxation arose from a chemical process (i.e. the dimerisation of the dye) and was not an artefact produced through detecting very small changes in absorbance. If higher dye concentrations could be studied at which a greater proportion of the dimer species would exist, the amplitude of a relaxation arising from the dimerisation reaction would be of greater magnitude, and temperature-jump studies would be more definitive.

A new temperature-jump cell of optical pathlength 0.23 cm was constructed, thus permitting studies at higher dye concentrations than was possible with the other cell of optical pathlength 1.00 cm. Temperature-jump spectrophotometric studies of dye solutions were performed using the same experimental conditions and monitoring wavelengths that were used for the dye/γCD studies. There was a slight exception for the CV studies as the

dye was found to be insoluble in aqueous 1.00 mol dm^{-3} NaCl at concentrations $> 5.00 \times 10^{-5}$ mol dm^{-3}, and so CV solutions in aqueous 0.50 mol dm^{-3} NaCl were used. Generally, for each dye studied, at dye concentrations $> 5.00 \times 10^{-5}$ mol dm^{-3} a relaxation producing a decrease in absorbance at the lower monitoring wavelength and an increase in absorbance at the higher monitoring wavelength was observed. The larger amplitude change always occurred at the higher monitoring wavelength. Relaxation times were determined by fitting the averaged relaxation traces to a single exponential curve, and for each dye over the concentration range studied the relaxation always occurred within the instrumental heating time. Thus, it was not possible to show that this relaxation arose through Equilibrium 5.1 by studying the variation of $1/\tau$ with dye concentration as expressed through Equation 5.2 derived in Section 2.1.1:

$$1/\tau^2 = 8k_d k_{-d}[D]_0 + k^2_{-d} \tag{5.2}$$

where $[D]_0$ is the total dye concentration. However, the measurement and analysis of the concentration dependence of the amplitude of the observed relaxation provides a way of showing that this relaxation does arise from the dimerisation of the dye.

The variation of amplitude for a relaxation arising through the monomer-dimer equilibrium (Reaction 5.1) may be expressed through Equation 5.3 [3] (see Section 2.1.1):

$$\Delta I/I_0 = \Delta T \left(\frac{\Delta\varepsilon \, l \, \Delta H^o}{RT^2}\right) \left[\frac{4}{[D]} + \frac{1}{[D_2]}\right]^{-1} \tag{5.3}$$

where ΔI is the relaxation amplitude, I_0 is the detected light intensity prior to the temperature jump, $\Delta\varepsilon = \varepsilon_{D_2} - 2\varepsilon_D$ where ε is a molar absorbance, l is the temperature-jump cell optical pathlength, ΔT is the temperature rise obtained from the temperature jump, and ΔH^o is the enthalpy change for the dimerisation process. Equation 5.3 may be simplified to:

$$\Delta I/I_0 = C\left[\frac{4}{[D]} + \frac{1}{[D_2]}\right]^{-1} \tag{5.4}$$

where C is a constant characterising the dimerisation equilibrium. The experimental quantities $\Delta I/I_0$ measured from the averaged relaxation traces and the total dye concentration $[D]_0$ were fitted to Equation 5.4 using the non-linear least-squares fitting program DATAFIT. The equilibrium concentrations $[D]$ and $[D_2]$ are related to the quantity $[D]_0$ through the equilibrium constant K_d, and thus this method provides a way of estimating K_d. The variation of $\Delta I/I_0$ with the total dye concentration for each dye studied is shown in Figure 5.1, as is the best fit curve of these data to Equation 5.4, obtained using program DATAFIT. The values of K_d and C obtained from the fitting for each dye studied are shown in Table 5.1. A comparison with literature K_d values, for example RB [15], K_d = 1.4×10^3 dm^3 mol^{-1}, and CV [19], K_d = 6.0×10^2 dm^3 mol^{-1}, indicates that the values of K_d derived are acceptable. The concentration dependence of the relaxation amplitude is consistent with that expected for the dye dimerisation equilibrium.

The amplitude concentration dependence of a relaxation arising through the monomer-dimer equilibrium is given by Equation 5.4, which predicts that $\Delta I/I_0$ will increase with the total dye concentration, as shown in Figure 5.1. At low dye concentrations (e.g. < 3.00×10^{-5} mol dm^{-3} [dye]), the amplitude is generally very small, but at higher dye concentrations the amplitude increases in magnitude quite markedly. The initial attempts at studying the dimerisation reaction were inconclusive, as the observed relaxation could not be confidently interpreted as arising through the dimerisation reaction in view of the very small amplitudes that characterised the relaxation. However, when it was possible to study higher dye concentrations, which was permitted by using a temperature-jump cell of sufficiently small optical pathlength, it was established that a relaxation was present, and its origin was
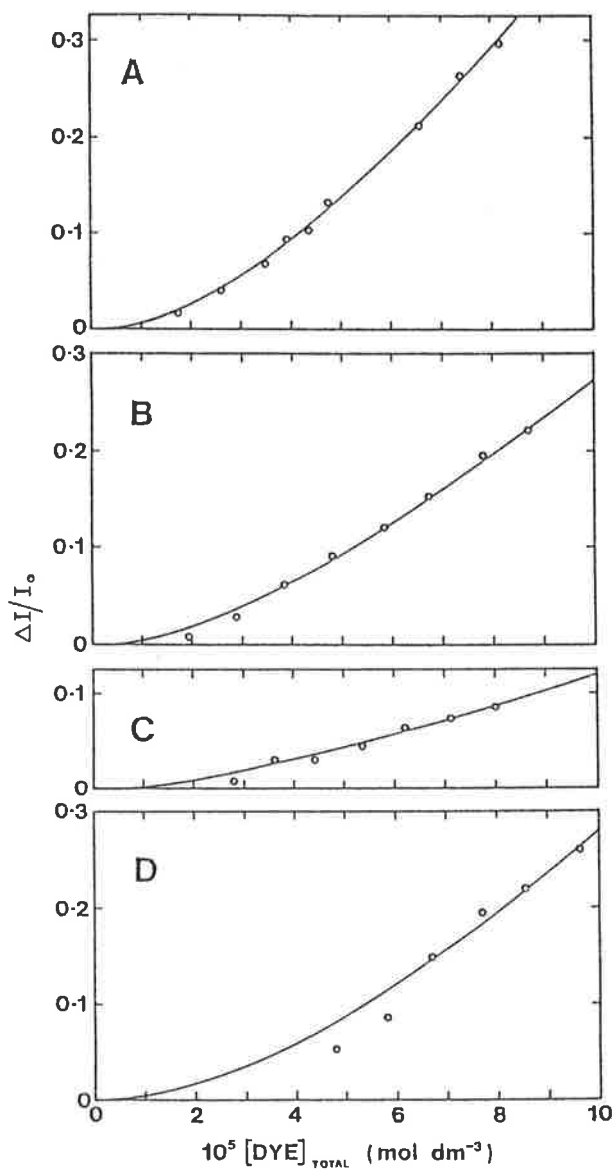
Figure 5.1: The variation of $\Delta I/I_0$ with total dye concentration

(A) Pyronine Y

(B) Pyronine B

(C) Rhodamine B

(D) Crystal violet

The circles represent the experimental points and the solid curve represents the best fit of the data to Equation 5.4. The standard error in each $\Delta I/I_0$ measurement is ca. ±2%.

Experimental data points refer to observations at: pyronine Y (547 nm), pyronine B (553 nm), rhodamine B (555 nm), and crystal violet (595 nm).

Dye*	K_d† $dm^3 \, mol^{-1}$	C† $dm^3 \, mol^{-1}$
Pyronine Y	$(1.1 \pm 0.2) \times 10^3$	$(7.3 \pm 0.9) \times 10^4$
Pyronine B	$(1.3 \pm 0.5) \times 10^3$	$(4.5 \pm 0.9) \times 10^4$
Rhodamine B	$(1.8 \pm 1.0) \times 10^3$	$(1.7 \pm 0.5) \times 10^4$
Crystal Violet	$(9.1 \pm 3.3) \times 10^2$	$(5.4 \pm 1.2) \times 10^4$

* Dye solutions were prepared in aqueous 1.00 mol dm^{-3} NaCl, except crystal violet which was in aqueous 0.50 mol dm^{-3} NaCl. All studies were at 298.2 K.

† The values of K_d and C were derived from the fitting of the amplitude data to Equation 5.4 using program DATAFIT to give the best fit curves shown in Figure 5.1.

Table 5.1: *Summary of the values of K_d and C obtained from the amplitude concentration dependence studies*

ascertained.* Temperature-jump studies were restricted to dye concentrations $< 1.00 \times 10^{-4}$ mol dm^{-3} to avoid any effects from relaxations arising from aggregation of the dye beyond the dimeric state. In the absence of contributions due to further aggregation of the dye, Equation 5.4 predicts that the amplitude will continue to increase with dye concentration until at very high dye concentrations (ca. 10^{-2} mol dm^{-3} [dye]) $\Delta I/I_0$ begins to plateau.
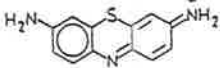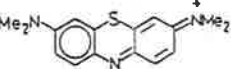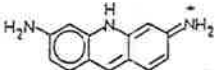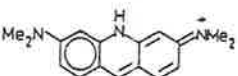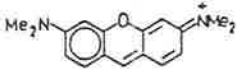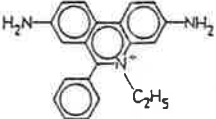
For studies of CV, PB and RB at dye concentrations similar to those used in the cyclodextrin studies (ca. 10^{-5} mol dm^{-3} [dye]), no relaxation due to the dimerisation reaction was observed. This has been previously mentioned from the dye/cyclodextrin temperature-jump studies, and shows that there is no significant concentration of free dimer present at the dye concentrations used. On the other hand, for PY, a relaxation of small amplitude was observed at dye concentrations similar to those used in the cyclodextrin studies. The fast relaxation that was reported from the PY/cyclodextrin temperature-jump studies can be attributed to the dimerisation of PY, and shows that there exists a small concentration of free dimer at the dye concentrations used. Since the equilibrium spectroscopic and kinetic data relating to the PY studies could be interpreted adequately without considering any contribution from the free dimer, the presence of this species can be neglected.

---

* In a temperature-jump study involving CV, it was reported that the detected relaxations were substantially slower than the instrumental heating time, and were thought to arise from the dimerisation of the dye [20]. In view of the results of the present study, the dimerisation of CV occurs much more rapidly, and the conclusions from the earlier study now appear no longer tenable.

5.3 A Survey of the Kinetic Aspects of the Dimerisation of Dyes

Table 5.2 summarises those kinetic studies of the dimerisation of dyes that have been reported.* Although these studies are few in number, they do embrace a variety of dimerising species, for example, cationic dyes (e.g. acridine orange), anionic dyes (e.g. Biebrich scarlet), and a nucleic acid base (N^6, N^9-dimethyladenine). It is evident from the rate constants listed in Table 5.2 that the dimerisation reaction is fast; generally the forward rate constants k_d are found to be within an order of magnitude of the diffusion-controlled limit. The very rapid nature of the dimerisation process has meant that kinetic studies have required techniques specialised for studying fast reactions, and Table 5.2 lists those experimental methods that have been used. The dimerisation of CV, PY, PB and RB were all found to be too fast to be quantitatively studied by the capacitor discharge temperature-jump. However, if the more rapid methods of heating that are used in the Raman-laser or Cable temperature-jump methods were utilised, then it may have been possible to measure the rate constants for the dimerisation reaction of these dyes. The Raman-laser temperature-jump method can extend kinetic studies into the nano-second timescale, and this technique appears very suitable for studying the dimerisation of dyes. It has been only in the more fortunate circum-stances that the Joule-heating temperature-jump method has been successful in studying the dimerisation process. A further advantage of the Raman-laser temperature-jump method is that dye solutions do not require the presence of added salts which may lead to experimental difficulties, for example, limited dye solubility due to 'salting-out' as experienced in the study of CV.

---

* The values of the rate constants for the various dimerisation studies listed in Table 5.2 have not been measured in identical experimental conditions. The temperature of kinetic measurements was in the range 293.2-298.2 K. The rate constants have been measured at different ionic strengths, but the rate of dimerisation has been shown to be rather insensitive to this parameter [9, 14, 18].

Dye	Experimental Technique	k_d dm^3 mol^{-1} s^{-1}	k_{-d} s^{-1}	K_d dm^3 mol^{-1}	Reference
Thionine	Raman-laser temperature-jump	2.4×10^9	9×10^5	2.66×10^3	4
	Raman-laser temperature-jump	7.1×10^8	9.4×10^5	7.50×10^2	5
Methylene Blue	Joule-heating temperature-jump	5.09×10^8	1.33×10^5	3.84×10^3	6
Proflavin	Raman-laser temperature-jump	1.1×10^9	3.0×10^6	3.66×10^2	7
	Raman-laser temperature-jump	7.9×10^8	2.0×10^6	3.95×10^2	8
Acridine Orange	Joule-heating temperature-jump	1.15×10^9	5.0×10^4	2.3×10^4	9
	Joule-heating temperature-jump	2.7×10^8	1.8×10^4	1.5×10^4	10
	Joule-heating temperature-jump	1.0×10^9	5.6×10^4	1.8×10^4	11
Pyronine Y	Coaxial-cable temperature-jump	2.3×10^9	1.7×10^5	1.4×10^4	12
Ethidium Bromide	Raman-laser temperature-jump	4.6×10^8	6.7×10^6	6.9×10^1	13

132
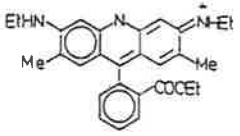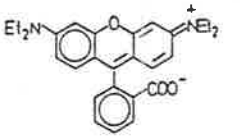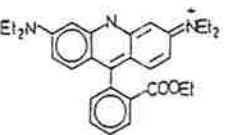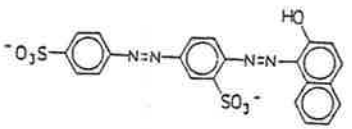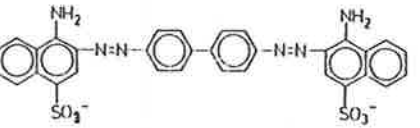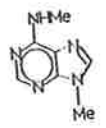
		k_d	k_{-d}	K_d	
Rhodamine 6G	Raman–laser temperature–jump	1.1×10^9	7.0×10^5	1.6×10^3	14
Rhodamine B	stopped–flow	4.5×10^5	3.2×10^2	1.4×10^3	15
Rhodamine 3B	stopped–flow	1.3×10^6	3.8×10^2	3.4×10^3	15
Biebrich Scarlet	Joule–heating temperature–jump	1.5×10^9	1.3×10^4	1.2×10^5	16
Congo Red	Joule–heating temperature–jump	6.7×10^6	1.2×10^2	1.7×10^2	17
N^6,N^9-Dimethyladenine	ultrasonic absorption	9.3×10^8	5.0×10^7	1.8×10^1	18

Table 5.2: Summary of kinetic data for dimerisation reactions

$$2D \underset{k_{-d}}{\overset{k_d}{\rightleftharpoons}} D_2 \qquad (K_d)$$
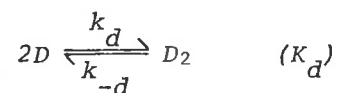
The data shown in Table 5.2 may be presented in a graphical form that conveniently allows the rate constants for the dimerisation reaction from different dye studies to be compared. In Figure 5.2, the kinetic data have been plotted as $\log k_d$ and $\log k_{-d}$ against $\log K_d$. From a kinetic viewpoint, the dyes can be divided into two distinct groups. The majority of the dyes belong to group I. The values of k_d for these dyes fall in the same order of magnitude, ca. 10^9 dm^3 mol^{-1} s^{-1}. This is close to, but significantly less than, the diffusion-controlled limit [21, 22], and suggests that the dimerisation reaction is essentially diffusion-controlled. A line of best fit through the $\log k_d$ versus $\log K_d$ data gives a slope of 0.06 ± 0.07 and an intercept of 8.8 ± 0.3, and shows that k_d may be considered independent of K_d. Furthermore, the group I dyes show a linear relationship between $\log k_{-d}$ and $\log K_d$; a line of best fit gives a slope of -0.94 ± 0.07 and an intercept of 8.8 ± 0.3, and indicates that differences in the stability of the dimers are reflected primarily in their dissociation rates. On the other hand, there are a small number of dyes (congo red, rhodamine 3B and rhodamine B) which belong to group II. The values of k_d and k_{-d} for these dyes are a few orders of magnitude smaller than the corresponding values in group I.

The observed kinetic results (i.e. Table 5.2 and Figure 5.2) may be discussed by dividing the dimerisation reaction (Reaction 5.1) into the following two processes:

$$D_{aq} + D_{aq} \underset{k_{21}}{\overset{k_{12}}{\rightleftharpoons}} (D - - - D)_{aq} \underset{k_{32}}{\overset{k_{23}}{\rightleftharpoons}} D_{2aq} + H_2O \qquad (5.5)$$

$$\text{encounter or} \qquad \text{dimer} \quad \text{bulk}$$
$$\text{outer sphere} \qquad \qquad \text{solvent}$$
$$\text{complex}$$
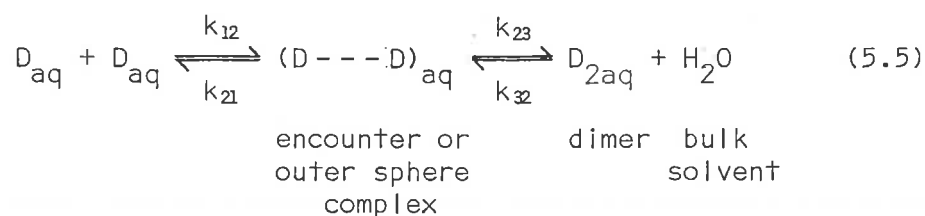
The general mechanism involves the diffusion-controlled formation of an encounter (or outer sphere) complex in which the two monomers are separated by one or more solvent molecules, followed by the activation-

Figure 5.2: Plots of $\log k_d$ and $\log k_{-d}$ against K_d for various dimerisation reactions in the absence of cyclodextrin (circles):

1:   N^6,N^9-dimethyladenine [18]
2:   ethidium bromide [13]
3:   proflavin [7]
4:   proflavin [8]
5:   thionine [5]
6:   rhodamine 6G [14]
7:   thionine [4]
8:   methylene blue [6]
9:   pyronine Y [12]
10: acridine orange [10]
11: acridine orange [11]
12: acridine orange [9]
13: Biebrich scarlet [16]
14: congo red [17]
15: rhodamine B [15]
16: rhodamine 3B [15]

Solid lines are the best fit lines through the $\log k_d$ and $\log k_{-d}$ against $\log K_d$ data (see text).

Plots of $\log k_2$ and $\log k_{-2}$ against $\log K_2$ for various dimerisation reactions in the presence of cyclodextrin (squares):

17: pyronine Y/γCD
18: pyronine B/γCD
19: crystal violet/γCD
20: methyl orange/γCD [26]
21: tropaeolin/γCD [27]
22: tropaeolin/βCD [27]

The number in brackets refers to the reference.
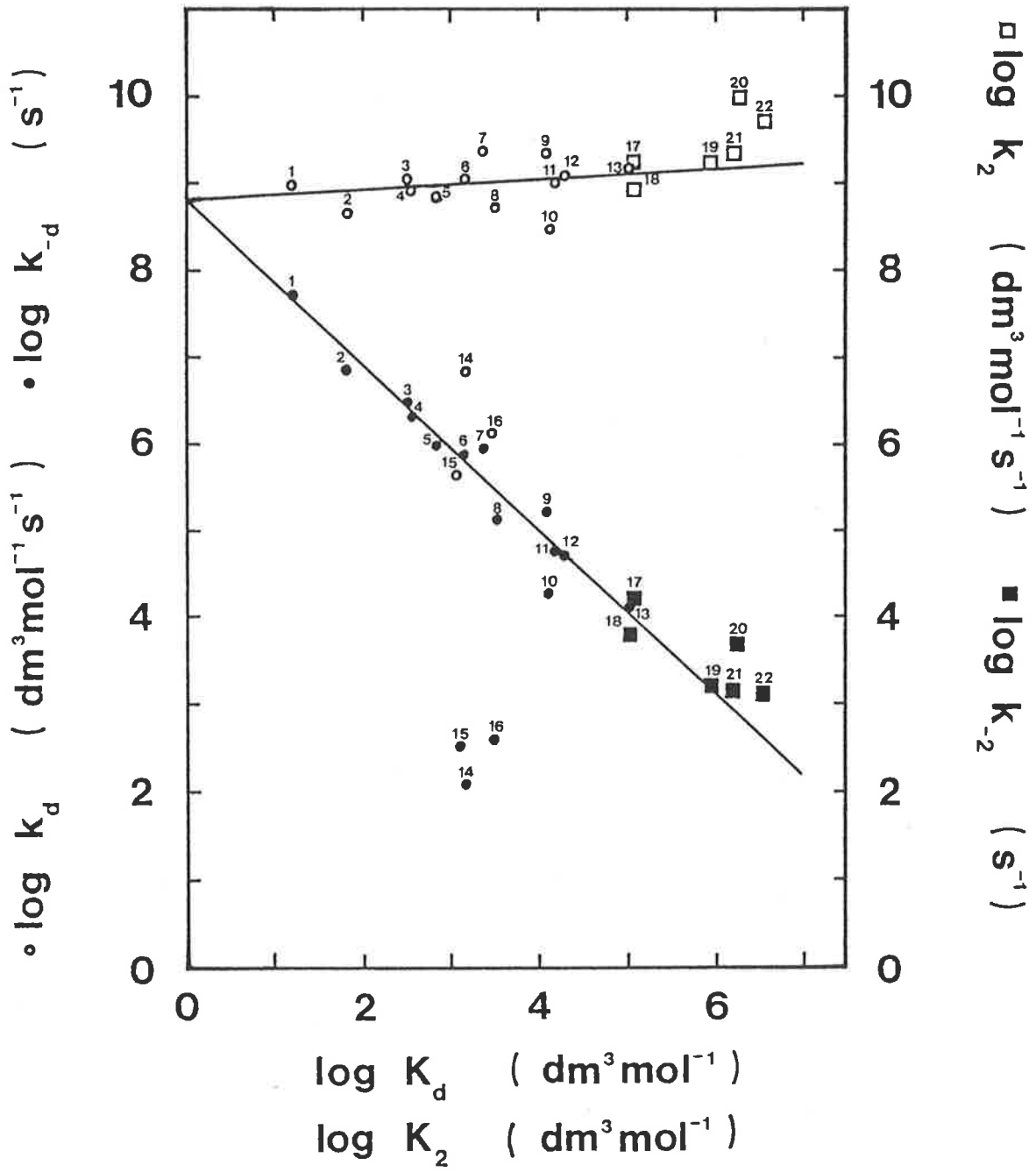
controlled collapse of the complex to form the dimer. This latter step involves two kinetically indistinguishable processes: the ejection of solvent molecules by the complex and the geometrical rearrangement of the complex to the most stable dimer configuration.

Applying the steady-state hypothesis to the encounter complex allows the experimental rate constants to be expressed as follows:

$$k_d = \frac{k_{12}k_{23}}{k_{21} + k_{23}} \tag{5.6}$$

$$k_{-d} = \frac{k_{21}k_{32}}{k_{21} + k_{23}} \tag{5.7}$$

By assuming that the first step of Reaction 5.5 is diffusion-controlled, the rate constants k_{12} and k_{21} may be calculated by means of the equations of Debye [21] and Eigen [22], respectively:

$$k_{12} = \frac{4\pi N_A D_A a}{1000} \left(\frac{\theta}{e^\theta - 1} \right) \quad dm^3 \ mol^{-1} \ s^{-1} \tag{5.8}$$

$$k_{21} = \frac{6D_A}{a^2} \left(\frac{\theta e^\theta}{e^\theta - 1} \right) \ s^{-1} \tag{5.9}$$

with

$$\theta = \frac{Z^2 e_0^2}{\varepsilon a k_B T}$$

where N_A is Avogadro's constant, a is the distance of closest approach of the monomers in the encounter complex (usually a value corresponding to two water molecules separating the monomers), D_A is the diffusion coefficient of the monomer, Z is the charge of a monomer, e_0 is the electrostatic charge, ε is the dielectric constant, k_B is Boltzmann's constant, and T is the absolute temperature.

Consider the dyes belonging to group I. Calculated values of k_{12} and k_{21} for the dyes [4, 6, 7, 11-14] fall in the same order of magnitude, ca. 10^9-10^{10} dm^3 mol^{-1} s^{-1}/s^{-1}, and this would not be unexpected, given the similarity in molecular dimensions and degree of charge of the group I dyes. The difference in the dimerisation of the dyes is not reflected in the first step of Reaction 5.5. The rate constant k_{23} may be determined from Equation 5.6 and, since the values of k_{12}, k_{21} and k_d are of similar magnitude and show little variation with the dye, then this is reflected in the value of k_{23} (ca. 10^9-10^{10} s^{-1}). The rate constant k_{23} corresponds to the first order rate constant for the loss of solvent from the solvation sphere and/or the rearrangement of dye monomers to the most stable dimer configuration. The rate constant k_{23} may be compared with the rate constant for solvent exchange on large metal ions (e.g. caesium ion [23], 5×10^9 s^{-1}), and suggests that k_{23} is a measure of the solvent exchange rate. The solvation sphere around the monomers may be considered as both labile and structured. The rate constant k_{32} may be calculated from Equation 5.7 and, given that the values of k_{21} and k_{23} are of similar magnitude and show little dependence on the dye, it follows that, since the value of k_{-d} varies considerably with dye, this is then reflected in the value of k_{32}. Thus, for the dyes in group I the backward reaction represented by k_{-d} in Equilibrium 5.1 is governed entirely by k_{32}. The rate constant k_{32} relates to the stability of the dimer and is a measure of the forces responsible for the stacking interaction. For example, for the homologous dyes acridine orange and proflavin, and similarly methylene blue and thionine, it is found that for the latter dye in each case the absence of methyl groups leads to a reduced stability of the dimer (K_d decreases, k_{-d} (k_{32}) increases), implicating the importance of such groups in the stacking interaction. This effect may be attributed to either hydrophobic interactions [18] or dispersion forces [11]. The nature of the attractive force(s) responsible for the stability

of aggregates is a subject of contention and may vary from one dye system to another, but the hydrophobic interaction and dispersion (or van der Waals) forces are intimately involved. The balance of evidence, however, is in favour of the importance of dispersion forces arising from dye-dye interactions [11, 24].

The group II dyes show anomalously slow rates of dimerisation. In view of their structures (e.g. rhodamine 3B and rhodamine B compared with rhodamine 6G), the slower rates of dimerisation compared with the group I dyes may be considered not to arise from the first step in Reaction 5.5. Assumably, the group II dyes possess particular features that lead to a higher activation energy for the formation of the dimer in the second step of Reaction 5.5. For instance, RB has been classed as a group II dye on the basis of the rate constants shown in Table 5.2, yet the observations from the studies described in Section 5.2 would have it belong to group I. Wong et al. [25] have found that the rate constants for the dimeri-sation of RB vary enormously with ionic strength. Given that the values in Table 5.2 refer to studies in the natural ionic strength of RB solu-tions and that the observations from Section 5.2 refer to studies in aqueous 1.00 mol dm^{-3} NaCl, this fact would appear to be supported. The rates of dimerisation of the dyes belonging to group I, in contrast, show very little dependence on ionic strength [14, 18], which suggests that RB dimerises through a different reaction pathway compared with the dyes in group I.

Ohling [12] has studied the effect of pressure on the dimerisation of pyronine Y. The pressure dependence of the forward rate constant k_d was found to be small (volume of activation, $\Delta V_d^{\#}$, ca. zero), while the backward rate constant k_{-d} was found to decrease with increasing pressure (volume of activation, $\Delta V_{-d}^{\#}$, positive). The decrease in k_{-d} was respons-

ible for the higher stability of the dimer under pressure. A volume profile of the dimerisation of pyronine Y was constructed and discussed in view of the specific role of water as solvent. The second step of Reaction 5.5 was characterised by a volume change that was large and negative, consistent with the loss of one or more solvent molecules from the solvation sphere of the encounter complex into the bulk water.

The dimerisation of some dyes (e.g. acridine orange, thionine, proflavin and pyronine Y) have been studied in aqueous alcohol solutions [4, 7, 11, 12]. It was found that, as the concentration of the alcohol component in the aqueous mixtures was increased, the tendency for the dye to undergo dimerisation decreased, which was expected because in the pure organic solvent no dimerisation takes place. This effect of decreasing the equilibrium constant K_d was found to arise from the combination of decreasing the forward rate constant k_d and increasing the backward rate constant k_{-d}. The studies of thionine and proflavin by Dewey et al. [4, 7] have interpreted these observations in terms of specific dye-alcohol interactions. The alcohols decrease the dimerisation of these dyes by forming relatively strong solvational complexes, and this solvational process competes with the dimerisation reaction. Furthermore, the alcohol attack on the dimer is more effective than that of water, and this is the cause of the increase in k_{-d} with increasing alcohol concentration. Dewey et al. [7] have concluded that solvent effects on dye stacking are determined by specific dye-solvent interactions involving dispersion forces, and that solvent-solvent contributions are relatively unimportant.

5.4 Cyclodextrin Enhanced Dimerisation of Dyes

The formation of the $(dye)_2 \cdot CD$ species by CV, PY and PB, respectively, with γCD described herein, and also by methyl orange (MO) with γCD [26] and tropaeolin (TR) with $\beta-$ and γCD [27], arises through the scheme given by Reactions 5.10 and 5.11:

$$D + CD \rightleftharpoons D \cdot CD \qquad\qquad \text{fast} \qquad (5.10)$$

$$D + D \cdot CD \underset{k_{-2}}{\overset{k_2}{\rightleftharpoons}} D_2 \cdot CD \quad (K_2) \quad \text{slow} \qquad (5.11)$$
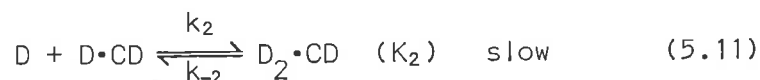
The dyes MO, TR and possibly PY also form the 2:2 complex with γCD. The kinetic studies of enhanced dimerisation of dyes by cyclodextrin are summarised in Table 5.3. The equilibrium data for the inclusion of the roccellin (ROC) dimer by γCD [28] is also shown in Table 5.3 for further comparison.

The enhanced dimerisation of a dye in the presence of cyclodextrin can be attributed to the increased stability of $(dye)_2$ in $(dye)_2 \cdot CD$, compared with its stability in water alone. For example, the formation of the dimer $(CV)_2$ in water alone is characterised by a dimerisation constant, $K_d = 9.1 \times 10^2$ dm^3 mol^{-1} (Table 5.1), whereas the effective dimerisation constant of CV in the presence of γCD, as defined as $K_1 \cdot K_2 \cdot [\gamma CD]$, equals 2.4×10^5 dm^3 mol^{-1} approximately (data from Table 5.3) at a $[\gamma CD] = 5.0 \times 10^{-4}$ mol dm^{-3}.

The kinetic parameters characterising Equilibrium 5.11 may be compared with those characterising Equilibrium 5.1. It has not been possible to determine the rate constants k_d and k_{-d} for the dimerisation of CV, PY and PB from temperature-jump spectrophotometric studies. However, Ohling [12] has obtained $k_d = 2.3 \times 10^9$ dm^3 mol^{-1} s^{-1} and $k_{-d} = 1.7 \times 10^5$ s^{-1} for the dimerisation of PY in aqueous 1.00 mol dm^{-3} NaCl at 5 MPa. A comparison of these values with $k_2 = 1.7 \times 10^9$ dm^3 mol^{-1} s^{-1}

System	K_1 $dm^3\ mol^{-1}$	K_2 $dm^3\ mol^{-1}$	K_3 $dm^3\ mol^{-1}$	k_2 $dm^3\ mol^{-1}\ s^{-1}$	k_{-2} s^{-1}
Crystal Violet/γCD	$(4.63 \pm 0.07) \times 10^2$	$(1.03 \pm 0.09) \times 10^6$	–	$(1.73 \pm 0.08) \times 10^9$	$(1.68 \pm 0.07) \times 10^3$
Pyronine Y/γCD	$(1.0 \pm 0.1) \times 10^3$	$(1.2 \pm 1.1) \times 10^5$	$(5.2 \pm 2.2) \times 10^1$	$(1.7 \pm 0.1) \times 10^9$	$(1.4 \pm 0.5) \times 10^4$
Pyronine B/γCD	$(4.3 \pm 0.1) \times 10^2$	$(1.28 \pm 0.04) \times 10^5$	–	$(8.2 \pm 0.2) \times 10^8$	$(6.40 \pm 0.05) \times 10^3$
Methyl Orange/γCD*	$(4.5 \pm 0.7) \times 10^1$	$(2.0 \pm 1.1) \times 10^6$	$(6.1 \pm 2.5) \times 10^3$	$(9.4 \pm 5.1) \times 10^9$	$(4.8 \pm 0.8) \times 10^3$

^-O_3S—⟨C$_6$H$_4$⟩—N=N—⟨C$_6$H$_4$⟩—NMe_2
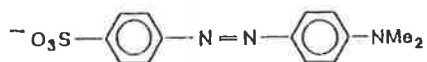
System	K_1	K_2	K_3	k_2	k_{-2}
Tropaeolin/βCD†	$(7.1 \pm 0.7) \times 10^2$	$(4 \pm 7) \times 10^6$	–	$(5 \pm 6) \times 10^9$	$(1.3 \pm 1.5) \times 10^3$
Tropaeolin/γCD†	$(4.18 \pm 1.47) \times 10^2$	$(1.68 \pm 0.54) \times 10^6$	$(1.77 \pm 1.54) \times 10^2$	$(2.27 \pm 0.61) \times 10^9$	$(1.35 \pm 0.23) \times 10^3$

^-O_3S—⟨C$_6$H$_4$⟩—N=N—⟨naphthalene, HO⟩
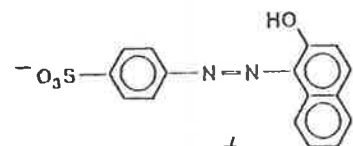
System					
Roccellin/γCD≠	$K_1 \cdot K_2 = (9.0 \pm 1.8) \times 10^{10}\ dm^6\ mol^{-2}$		–	–	–

^-O_3S—⟨naphthalene⟩—N=N—⟨naphthalene, HO⟩
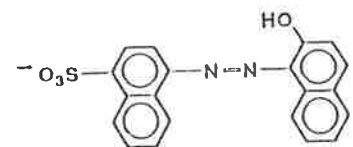
* Reference 26   † Reference 27   ≠ Reference 28   Note: equilibrium study only.

Table 5.3: *Summary of kinetic data for the enhanced dimerisation of dyes by cyclodextrin*

and $k_{-2} = 1.4 \times 10^4$ s^{-1} characterising the formation of $(PY)_2 \cdot \gamma CD$, suggests that the greater stability of $(PY)_2$ afforded by inclusion by γCD arises from a slower rate of dissociation of the dimer. It may be anticipated that for the other dyes the increased stability of $(dye)_2$ included in $(dye)_2 \cdot CD$ is also a result of a decreased dimer dissociation rate.

The parameters k_2, k_{-2} and K_2 shown in Table 5.3 have been included in Figure 5.2. For the small number of kinetic studies, the plots of log k_2 and log k_{-2} against log K_2 show behaviour similar to that observed for the kinetic data characterising the dimerisation of those dyes belonging to group I defined earlier. The values of k_2 for the dye systems studied are of the same order of magnitude, so that k_2 may be considered independent of K_2. The values of k_2, within the errors quoted in Table 5.3, are also very similar in magnitude to those of k_d, indicating that cyclodextrin has little or no apparent effect on the forward rate of dimerisation. The steric constraints placed on the formation of $(dye)_2$ in $(dye)_2 \cdot CD$ would be expected to be dependent on the structure of the dye and substantially greater than those placed on the formation of $(dye)_2$ in water alone, and yet the values of k_2 and k_d are apparently similar. This suggests that the rates of steric orientation do not make a major contribution to k_2 and k_d but rather it is the desolvation process, involving the ejection of solvent molecules by the dimerising molecules, which is the dominant rate-determining factor. There appears to be a linear relationship between log k_{-2} and log K_2, and the log k_{-2} versus log K_2 data is also quite close to the line of best fit through the log k_{-d} versus log K_d data. The differences in the stability of dimers, either $(dye)_2$ or $(dye)_2 \cdot CD$, are reflected primarily in their dissociation rates, k_{-d} or k_{-2}, respectively. Furthermore, the comparison of the log k_{-d} versus log K_d data with the log k_{-2} versus log K_2 data

reinforces the idea that the increased stability of $(dye)_2$ in $(dye)_2 \cdot CD$ is a consequence of a decreased dimer dissociation rate.

Equilibrium 5.11 may be divided into a two-step process analogous to Reaction 5.5. The decreased dimer dissociation rate arises through the step k_{32}. The dissociation of a dye monomer from $(dye)_2 \cdot CD$ must overcome a greater energy barrier than its dissociation from $(dye)_2$, owing to the disruption of dispersion forces existing between $(dye)_2$ and the interior of the cyclodextrin cavity. The decreased interaction of $(dye)_2$ in $(dye)_2 \cdot CD$ with solvent water would also contribute to a decrease in k_{32}. Not surprisingly, whereas the formation of dye-alcohol complexes through dye(monomer)-solvent interactions leads to a decreased stability of the dimer, the formation of $(dye)_2 \cdot CD$ gives rise to dye(dimer)-cyclodextrin interactions and an increased stability of the dimer. The extent of the increased stability of $(dye)_2$ included in $(dye)_2 \cdot CD$ may be correlated with the fit of $(dye)_2$ in the cyclodextrin cavity, and hence the strength of the dispersion force interaction between $(dye)_2$ and the cyclodextrin. The tropaeolin dimer, in which there is a superimposition of the phenyl sulphonate and naphthyl moieties, is of sufficient size to be accommodated in the βCD cavity, whereas the other dye dimers are too large, due to either the size of the aromatic rings as in roccellin, or the steric hindrance to inclusion imposed by the dialkylamino groups as in CV, PY and PB. The possibility of the inclusion of $(MO)_2$ by βCD is uncertain [28, 29]. The $(ROC)_2 \cdot \gamma CD$ species exhibits the largest stability of the $(dye)_2 \cdot \gamma CD$ complexes by virtue of the closeness of fit between the large dimer and the large γCD cavity. Both $(PY)_2 \cdot \gamma CD$ and $(PB)_2 \cdot \gamma CD$ show the smallest stabilities. Space-filling molecular models of $(PY)_2$ and $(PB)_2$ suggest that in each case the dialkylamino groups of the monomers project out from the plane of the super-imposed xanthene moieties, and prevent a close fit of the dimer in the γCD

cavity. In contrast, space-filling molecular models indicate that in $(CV)_2$ the dimethylamino groups of the monomers lie in the plane of the superimposed CV phenyl rings and provide less hindrance to the inclusion of the dimer by γCD, and so the $(CV)_2 \cdot \gamma CD$ complex has a greater stability.

Bibliography

1.   PULLMAN, B. Molecular Associations in Biology, Academic Press Inc., New York, 1968.

2.   HAMMES, G. G. Adv. Protein Chem. 23, 1 (1968).

3.   THUSIUS, D. J. Am. Chem. Soc. 94, 356 (1972).

4.   DEWEY, T. G., WILSON, P. S. and TURNER, D. H. J. Am. Chem. Soc. 100, 4550 (1978).

5.   INAOKA, W., HARADA, S. and YASUNAGA, T. Bull. Chem. Soc. Jpn. 51, 1701 (1978).

6.   SPENCER, W. and SUTTER, J. R. J. Phys. Chem. 83, 1573 (1979).

7.   DEWEY, T. G., RAYMOND, D. A. and TURNER, D. H. J. Am. Chem. Soc. 101, 5822 (1979).

8.   TURNER, D. H., FLYNN, G. W., LUNDBERG, S. K., FALLER, L. D. and SUTIN, N. Nature 239, 215 (1972).

9.   SCHWARZ, G. and BALTHASAR, W. Eur. J. Biochem. 12, 461 (1970).

10.   HAMMES, G. G. and HUBBARD, C. D. J. Phys. Chem. 70, 1615 (1966).

11.   ROBINSON, B. H., SEELIG-LOFFLER, A. and SCHWARZ, G. J. Chem. Soc. Faraday Trans. I 71, 815 (1975).

12.   OHLING, W. Ber. Bunsenges. Phys. Chem. 88, 109 (1984).

13.   TURNER, D. H., YUAN, R., FLYNN, G. W. and SUTIN, N. Biophys. Chem. 2, 385 (1974).

14.   INAOKA, W., HARADA, S. and YASUNAGA, T. Bull. Chem. Soc. Jpn. 53, 2120 (1980).

15.   WONG, M. M. and SCHELLY, Z. A. J. Phys. Chem. 78, 1891 (1974).

16.   HAGUE, D. N., HENSHAW, J. S., JOHN, V. A., POOLEY, M. J. and CHOOK, P. B. Nature 229, 190 (1971).

17.   YASUNAGA, T. and NISHIKAWA, S. Bull. Chem. Soc. Jpn. 45, 1262 (1972).

18.   PORSCHKE, D. and EGGERS, F. Eur. J. Biochem. 26, 490 (1972).

19.   STORK, W. H. J., LIPPITS, G. J. M. and MANDEL, M. J. Phys. Chem. 76, 1772 (1972).

20.   SCHILLER, R. L., COATES, J. H. and LINCOLN, S. F. J. Chem. Soc. Faraday Trans. I 80, 1257 (1984).

21.   DEBYE, P. Trans. Electrochem. Soc. 82, 265 (1942).

22.   EIGEN, M. Z. Phys. Chem. (Frankfurt) 1, 179 (1954).

23.   EIGEN, M. Plenary Lecture Proc. 7th Int. Conf. Coordination Chemistry, Stockholm, 1962 (Butterworth, London, 1963) p. 67.

24. DUFF, D. G. and GILES, C. H.   in **Water a Comprehensive Treatise** (F. Franks, ed.) Vol IV, Plenum Press, New York, 1975.

25. WONG, M. M., HECKMAN, R. A. and SCHELLY, Z. A.   J. Phys. Chem. **77**, 1317 (1973).

26. CLARKE, R. J., COATES, J. H. and LINCOLN, S. F.   Carbohydr. Res. **127**, 181 (1984).

27. CLARKE, R. J., COATES, J. H. and LINCOLN, S. F.   J. Chem. Soc. Faraday Trans. I **80**, 3119 (1984).

28. CLARKE, R. J., COATES, J. H. and LINCOLN, S. F.   J. Chem. Soc. Faraday Trans. I, in press.

29. CLARKE, R. J., Ph.D. Thesis, University of Adelaide (1985).

CHAPTER VI

Summary And General Discussion

SUMMARY AND GENERAL DISCUSSION

The annular radii of the cyclodextrins and the relative sizes of
potential guests are important factors influencing the selectivity
of the cyclodextrins in the formation of inclusion complexes. The
equilibrium and kinetic studies described herein, and summarised in
Tables 3.1 and 4.1, have demonstrated that:

(1) The annular radii of the cyclodextrins exert a substantial degree
     of selectivity for a given included species. For example, the
     stabilities of the 1:1 inclusion complexes formed between the dyes
     studied and the cyclodextrins decrease in the order βCD > γCD > αCD.
     The importance of the annular radii of the cyclodextrins in the
     specificity of inclusion complex formation has also been highlight-
     ed in several other studies [1-4].

(2) A cyclodextrin of given annular radius exerts a substantial degree
     of selectivity for different included species. This is indicated,
     for example, by the large difference between the equilibrium con-
     stants K_1 and K_2 characterising the inclusion of dye and $(dye)_2$,
     respectively, by γCD.

Cyclodextrin selectivity may be related to the degree of structural
complementarity between a guest and host cyclodextrin cavity. Space-
filling molecular models of possible inclusion complexes show that an
optimum match between the size of the included species and the size of
the cyclodextrin cavity leads to an optimum binding. A guest should not
be so large that it will not fit in the cyclodextrin cavity and therefore
not bind to the cyclodextrin, nor should it be too small so that it will
easily pass in and out of the cavity with little binding. There is a
preferential affinity of the included species for a cyclodextrin cavity
large enough to allow maximum penetration, yet small enough to allow for
effective cyclodextrin-substrate interaction. The concept that higher

stability constants characterise inclusion complexes in which the guest

fits closely the cyclodextrin cavity is consistent with the participation

of dispersion forces in complex formation.

The cavity of γCD appears to be too large to form 1:1 complexes of

relatively high stability, but is of appropriate size to include two guest

molecules relatively strongly. Two guest-one host complexation, particu-

larly by γCD, again emphasises the importance of an included species

achieving an optimal fit in the host cyclodextrin cavity. In the case

of a two guest-one host complex, it may be considered that one guest

molecule acts as a space-regulator, which narrows the cyclodextrin

cavity to allow the inclusion of the other guest molecule more strong-

ly than if it were included alone. Ueno et al. [5] have shown that α-

naphthyloxyacetic acid is included relatively weakly by γCD, but the

binding is enhanced by the addition of cyclohexanol. A ternary complex

is formed in which cyclohexanol and α-naphthyloxyacetic acid both occupy

the γCD cavity, cyclohexanol acting as a space-regulator. In a sub-

sequent study [6], in which a naphthalene moiety was covalently attach-

ed to γCD, they showed the role of the appended naphthalene moiety in

narrowing the large γCD cavity to allow the inclusion of various kinds

of molecules in themselves too small to form stable complexes with native

γCD. Furthermore, in comparison with native γCD this modified γCD pro-

duced larger overall ester hydrolysis rates in water [7]. A 12-fold

increase was observed for para-nitrophenylacetate, arising from both an

increased rate of intracomplex hydrolysis and stronger binding, and an

11-fold increase for meta-nitrophenylacetate, arising primarily from

stronger binding.

Temperature-jump spectrophotometric studies have shown the formation

of the 1:1 inclusion complex, dye·CD, to be a fast bimolecular reaction:

$$D + CD \xrightleftharpoons[k_{-1}]{k_1} D \cdot CD \qquad (K_1) \qquad\qquad (6.1)$$
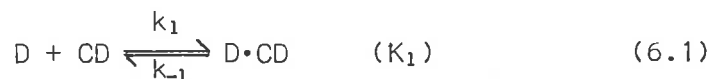
In this work, the formation of dye•CD complexes could be studied directly only in the case of the dye•βCD complexes. Hersey and Robinson [8] have suggested that the mechanism for 1:1 complex formation may be more complex than the process given by Reaction 6.1. They studied the interaction of a variety of azo dyes with αCD by temperature-jump and stopped-flow methods, and observed that at relatively high [αCD] the variation of $1/\tau$ and k_{obs} with total αCD concentration deviated slightly from the linear behaviour expected for a reaction described by Equilibrium 6.1. Furthermore, they found that the equilibrium constant derived kinetically (assuming a reaction of the form given by Reaction 6.1) was significantly less than the equilibrium constant derived spectrophotometrically. Hersey and Robinson proposed a mechanism for 1:1 complex formation that involves a fast pre-equilibrium step to form a binary intermediate, which then undergoes a slower isomerisation to the final stable product. Temperature-jump studies of the formation of dye•βCD complexes are unable to distinguish between the mechanism given by Reaction 6.1 and that proposed by Hersey and Robinson, since at relatively high [βCD], where the variation of $1/\tau$ with total βCD concentration may be anticipated to be non-linear, measured relaxation times are comparable to the instrumental heating time. However, as the values of K_1 derived kinetically for the dye•βCD complexes are identical within experimental error to those derived spectrophotometrically, Reaction 6.1 appears to explain adequately the formation of the 1:1 inclusion complexes studied in this work. Since a conformational change of cyclodextrin upon the binding of a guest has been firmly established only in the case of αCD [9], perhaps the mechanism of Hersey and Robinson is applicable only to the formation of 1:1 inclusion complexes involving αCD.

Reaction 6.1 may be considered to occur in two stages:

$$D + CD \rightleftharpoons (D\text{---}CD) \rightleftharpoons D\cdot CD \qquad k_1, k_{-1} \qquad (K_1)$$

$$(6.2)$$
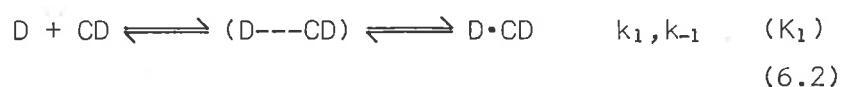
The first stage is the diffusion-controlled formation of a collisional complex characterised by a rate of formation of the order 10^9-10^{10} dm^3 mol^{-1} s^{-1} in which the solvation of the two interacting species is not greatly altered. The second stage is the slower formation of the inclusion complex itself, and involves solvation changes, steric interactions and possibly conformational change of cyclodextrin and/or guest (see Section 1.4). The ClO_4^- ion forms a complex with βCD in which the ion does not bind in the cavity of βCD but rather straddles an open end of the cyclodextrin [10], and to some degree this complex may be considered to resemble the collisional species (D---CD). Consistent with the Scheme 6.2, the formation of the $ClO_4^-\cdot$βCD complex is found to be diffusion-controlled ($k_1 = 2.0 \times 10^9$ dm^3 mol^{-1} s^{-1}) [10]. In contrast, inorganic anions such as I^-, Br^- and NO_3^-, which can be bound in the cavity of βCD, exhibit rates of complexation that are considerably less than diffusion-controlled ($k_1 = 4.4 - 6.5 \times 10^7$ dm^3 mol^{-1} s^{-1}) [10]. Rohrbach et al. [10] have proposed that a conformational change of βCD is responsible for the rate-determining behaviour, since anion desolvation could not explain the kinetic data and the anions are too small for steric interactions to be significant in the formation of the complexes. However, there is no evidence from X-ray structural data to support a conformational change of βCD upon the binding of guests [11]. Temperature-jump studies by Sano et al. [12] have detected a relaxation arising from a conformational change of cyclodextrin in the binding of I^- to αCD, but not in the case of βCD. A conformational change of cyclodextrin as a rate-determining factor in the inclusion of guests is clearly substantiated only for the formation of αCD complexes [8, 12]. Therefore, an alternative explanation to the proposal of Rohrbach et al. may be that the

release of hydrating water molecules from the βCD cavity is rate-determining in the complexation of the anions by βCD. Recent ultrasonic relaxation studies of aqueous cyclodextrin solutions have detected relaxations in a similar timescale to that of the inclusion of anions by βCD, and though their interpretation is a subject of debate, they may arise from a change in solvation of the cyclodextrin cavity [13, 14]. It may be proposed that the release of hydrating water molecules from the cyclodextrin cavity has an important role in controlling the maximal formation rates of inclusion complexes. The values of the rate constant k_1 characterising the dye·βCD complexes studied herein were found to be of the order 10^8 dm^3 mol^{-1} s^{-1} and independent of the dye structure. In consequence of this, it was concluded that steric interactions do not make a major contribution to k_1, and it is the desolvation processes which are the dominant rate-determining factors. In the formation of the dye·βCD complexes, it is not possible to distinguish between the breakdown of water structure around the dye, or the breakdown of water structure within the cyclodextrin cavity, as the rate-determining step. Nevertheless, the crucial role of desolvation in the inclusion process is apparent.

Steric interactions were a minor determinant of the formation rates for the dye·βCD complexes studied. Nonetheless, steric effects arising from interactions between the guest and groups on the rim and on the inside of the cyclodextrin cavity can affect the rate of complex formation. For example, when the entering group is an aromatic species, the meta- and ortho-substituted derivatives show a slower formation rate than the para-substituted derivative [15, 16]. It was not possible to determine from temperature-jump spectrophotometric studies the rate constants characterising the formation of the dye·γCD complexes, but it may be anticipated that the rate constant k_1 for the dye·γCD species would

be larger than that for dye•βCD, as the larger γCD annulus provides less steric hindrance for the inclusion of the dye. Kinetic studies reported in the literature, however, show that k_1 can decrease with an increase in cyclodextrin annulus [15], or be invariant of the size of the cyclodextrin annulus [2]. Although the concept of an increase in k_1 with an increase in the size of cyclodextrin annulus appears plausible, this effect may be mitigated through the increasing size of the cyclodextrin annulus allowing a greater penetration of the guest into the cavity and thereby giving rise possibly to further steric interactions.

Temperature-jump spectrophotometric studies have shown that the formation of dye•(CD)$_2$ complexes arises through the following equilibria:

$$D + CD \rightleftharpoons (D\text{---}CD) \rightleftharpoons D\cdot CD \qquad k_1, k_{-1} \ (K_1) \quad \text{fast}$$

$$\text{(6.3)}$$

$$D\cdot CD + CD \rightleftharpoons (CD\text{---}D\cdot CD) \rightleftharpoons D\cdot CD_2 \quad k_2, k_{-2} \ (K_2) \quad \text{slow}$$

$$\text{(6.4)}$$
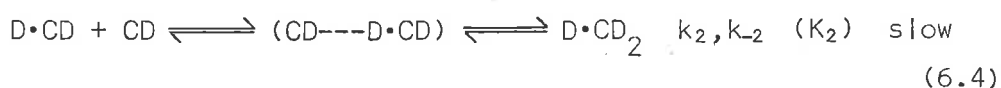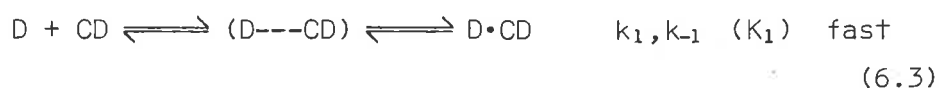
The formation of the D•(CD)$_2$ species could be studied only in the case of pyronine Y. The slower formation of pyronine Y•(βCD)$_2$ may be attributed to the increased steric hindrance the second βCD experiences in its complexation of pyronine Y•βCD. Moreover, the replacement of the methyl groups of pyronine Y by ethyl groups in pyronine B sufficiently increases steric hindrance so that the pyronine B•(βCD)$_2$ complex is not observed to form.

A feature of the inclusion of dyes by cyclodextrin is that any tendency which they may have to form dimers in solution is enhanced by the possibility of inclusion in a suitably large cavity. At concentrations of dye in which the dimer concentration is negligible, there may be observed in the presence of cyclodextrin increased concentrations of the dimer due to the formation of the complex (dye)$_2$•CD. The enhanced

dimerisation of a dye by cyclodextrin can be attributed to the increased stability of $(dye)_2$ in $(dye)_2 \cdot CD$, compared with its stability in water alone. Temperature-jump spectrophotometric studies have deduced the mechanism of two guest-one host complexation:

$$D + CD \rightleftharpoons (D\text{---}CD) \rightleftharpoons D \cdot CD \qquad k_1, k_{-1} \ (K_1) \ \text{fast} \qquad (6.5)$$

$$D + D \cdot CD \rightleftharpoons (D\text{---}D \cdot CD) \rightleftharpoons D_2 \cdot CD \qquad k_2, k_{-2} \ (K_2) \ \text{slow} \qquad (6.6)$$
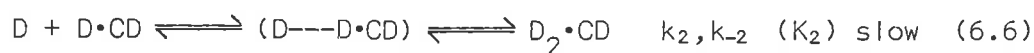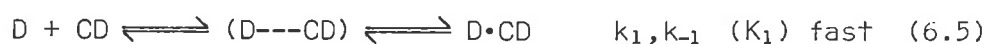
This scheme has been found to explain the inclusion of methyl orange by γCD [17] and tropaeolin by β- and γCD [18], in addition to the formation of $(dye)_2 \cdot CD$ complexes by crystal violet, pyronine Y and pyronine B, respectively, with γCD studied herein. Thus, this mechanism of two guest-one host complexation appears to be widely applicable. The inclusion of methyl orange, tropaeolin and possibly pyronine Y by γCD also gives rise to the 2:2 species, $(dye)_2 \cdot (CD)_2$, in which the reaction shown in Equilibrium 6.7 is incorporated into the scheme given by Reactions 6.5 and 6.6:

$$D_2 \cdot CD + CD \rightleftharpoons (CD\text{---}D_2 \cdot CD) \rightleftharpoons D_2 \cdot CD_2 \qquad k_3, k_{-3} \ (K_3) \ \text{fast}$$
$$(6.7)$$
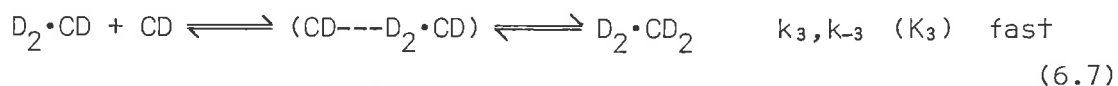
Equilibrium fluorescence measurements of the inclusion of pyrene by γCD are also consistent with the equilibria given by Reactions 6.5, 6.6 and 6.7 [19]. Interestingly, an equilibrium fluorescence study [20] has suggested that the formation of the 2:2 complex between pyrenyl butyrate and γCD arises through the association of two 1:1 inclusion complexes:

$$D + CD \rightleftharpoons D \cdot CD \qquad (6.8)$$

$$2D \cdot CD \rightleftharpoons D_2 \cdot CD_2 \qquad (6.9)$$

This mechanism, however, has yet to be verified by kinetic studies.

Reaction 6.6 may be compared with the dye dimerisation reaction:

$$D + D \rightleftharpoons (D\text{---}D) \rightleftharpoons D_2 \qquad k_d, k_{-d} \ (K_d) \qquad (6.10)$$

The kinetic aspects of the dimerisation process have been discussed in Chapter 5. The steric constraints placed on the formation of $(dye)_2$ in $(dye)_2 \cdot CD$ would be expected to be dependent on the structure of the dye and to be substantially greater than those placed on the formation of $(dye)_2$ in water alone, and yet the values of the rate constants k_d and k_2 are very similar (see Figure 5.2). The rates of steric orientation do not make a major contribution to k_d and k_2, and it is the desolvation process, involving the ejection of solvent molecules from the outer sphere complex, which is the dominant rate-determining factor. The increased stability of $(dye)_2$ included in $(dye)_2 \cdot CD$ is a consequence of a decreased dimer dissociation rate (k_{-d}) arising from the dispersion force interactions between $(dye)_2$ and the interior of the cyclodextrin annulus, and the decreased interaction of included $(dye)_2$ with solvent water. The extent of enhancement of dye dimerisation promoted by cyclo-dextrin is related to the ability of the dimer to achieve an optimal fit in the cyclodextrin cavity.

Two guest-one host complexation by cyclodextrin may have some use in the facilitation of chemical reactions. The increased ester hydroly-sis rates produced by a modified γCD have already been mentioned, al-though in this case one guest did not participate directly in the cata-lysis. If two molecules are able to undergo a chemical reaction together, it may be anticipated that the mutual binding of the two molecules in a cyclodextrin cavity would lead to an increased stability of the binary complex formed between the two molecules, and hence an increase in the efficiency of the reaction between them compared with that in the absence of cyclodextrin. The cyclodextrin cavity may be viewed as a reaction medium in which two molecules can be brought together effectively. The two molecules must fit the cavity correctly, both in terms of the com-patibility of the size of the binary complex with the cavity and the

orientation of the two molecules with respect to each other. Planar molecules would be expected to fulfill these requisites best. Breslow and Rideout [21] have found that βCD accelerates the Diels-Alder reaction of cyclopentadiene and acrylonitrile by several orders of magnitude compared with the rate in ordinary organic solvents. Tamaki [22] has shown that 2-anthracenesulphonate forms a 2:1 inclusion complex with γCD in aqueous solution, and this complex formation greatly enhanced the photo-dimerisation of the anthracene. The quantum yield for photodimerisation in the presence of γCD was an order of magnitude greater than that in the absence of cyclodextrin. In a subsequent study, Tamaki [23] showed that the photodimerisation of 2-anthracenesulphonate was also acceler-ated in the presence of βCD in which a 2:2 complex is formed. Whereas the four configurational isomers of the photodimer were obtained in the presence of γCD with similar ratio of yields to that in the absence of cyclodextrin, only one of the isomers was obtained in the presence of βCD. Cyclodextrin can impose its own geometrical control in catalysis. These few examples provide an adequate demonstration of the potential of two guest-one host complexation in chemical synthesis.

This work has implicated the annular radii of the cyclodextrins and the relative size of the guest as significant factors in determining the selectivity of the cyclodextrins for substrates in the formation of in-clusion complexes. The ability of the cyclodextrins to include two guest molecules simultaneously has been highlighted. The kinetic studies des-cribed herein have established the existence of a range of inclusion mechanisms which increase in complexity as the size of the cyclodextrin annulus increases. The kinetic data has been discussed in terms of the mechanistic steps involved in the inclusion reaction. The kinetic studies have also emphasised the importance of desolvation processes in complex formation.

Bibliography

1. CROMWELL, W. C., BYSTROM, K. and EFTINK, M. R. J. Phys. Chem. 89, 326 (1985).

2. TURRO, N. J., OKUBO, T. and CHUNG, C.-J. J. Am. Chem. Soc. 104, 1789 (1982).

3. CLARKE, R. J., COATES, J. H. and LINCOLN, S. F. J. Chem. Soc. Faraday Trans I, in press.

4. CLARKE, R. J., Ph.D. Thesis, University of Adelaide (1985),

5. UENO, A., TAKAHASHI, K., HINO, Y. and OSA, T. J. Chem. Soc. Chem. Commun. 1981, 194.

6. UENO, A., TOMITA, Y. and OSA, T. J. Chem. Soc. Chem. Commun. 1983, 976.

7. UENO, A., MORIWAKI, F., HINO, Y. and OSA, T. J. Chem. Soc. Perkin Trans. II 1985, 921.

8. HERSEY, A. and ROBINSON, B. H. J. Chem. Soc. Faraday Trans. I 80, 2039 (1984).

9. MANOR, P. C. and SAENGER, W. J. Am. Chem. Soc. 96, 3630 (1974).

10. ROHRBACH, R. P., RODRIGUEZ, L. P., EYRING, E. M. and WOJCIK, J. F. J. Phys. Chem. 81, 944 (1977).

11. LINDNER, K. and SAENGER, W. Angew. Chem. Int. Ed. Engl. 17, 694 (1978).

12. SANO, T., YAMAMOTO, M., HORI, H. and YASUNAGA, T. Bull. Chem. Soc. Jpn. 57, 678 (1984).

13. KATO, S., NOMURA, H. and MIYAHARA, Y. J. Phys. Chem. 89, 5417 (1985).
    Ultrasonic absorption measurements of aqueous α-, β- and γCD solutions have been interpreted in terms of two fast processes attributed to a simultaneous solvational and conformational change of cyclodextrin (k_{c1}, k_{-c1}), followed by a further solvational change (k_{c2}, k_{-c2}):

$$CD \underset{k_{-c1}}{\overset{k_{c1}}{\rightleftharpoons}} CD' \underset{k_{-c2}}{\overset{k_{c2}}{\rightleftharpoons}} CD''$$
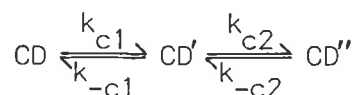
14. RAUH, S. and KNOCHE, W. J. Chem. Soc. Faraday Trans. I 81, 255 (1985).
    In this relaxation study of aqueous cyclodextrin solutions the relaxation time of ca. 5×10^{-8} s is interpreted in terms of a narrow distribution of relaxation times attributed to solvational changes in the cyclodextrin cavity. A second faster relaxation observed for αCD is attributed to the rotation of a glucose unit. These authors dispute the claim [13] that a conformational change of γCD contributes to the observed relaxations.

15. YOSHIDA, N. and FUJIMOTO, M. Bull. Chem. Soc. Jpn. 55, 1039 (1982).

16. CRAMER, F., SAENGER, W. and SPATZ, H.-Ch. J. Am. Chem. Soc. 89, 14 (1967).

17. CLARKE, R. J., COATES, J. H. and LINCOLN, S. F. Carbohydr. Res. 127, 181 (1984).

18. CLARKE, R. J., COATES, J. H. and LINCOLN, S. F. J. Chem. Soc. Faraday Trans. I 80, 3119 (1984).

19. KOBAYASHI, N., SAITO, R., HINO, H., HINO, Y., UENO, A. and OSA, T. J. Chem. Soc. Perkin Trans. II 1983, 1031.

20. HERSKSTROETER, W. G., MARTIC, P. A. and FARID, S. J. Chem. Soc. Perkin Trans. II 1984, 1453.

21. BRESLOW, R. and RIDEOUT, D. J. Am. Chem. Soc. 102, 7816 (1980).

22. TAMAKI, T. Chem. Letts. 1984, 53.

23. TAMAKI, T. and KOKUBO, T. J. Inclusion Phenom. 2, 815 (1984).

APPENDICES

A Materials And Methods

B Computational Methods

C Reciprocal Relaxation Time Data

D Derivation Of Reciprocal Relaxation

   Time Expressions

A. MATERIALS AND METHODS

The α-, β- and γ-cyclodextrins (Sigma) were used without further purification, and were stored as the anhydrous material over phosphorous pentoxide in a vacuum desiccator. Analytical-reagent-grade NaCl (B.D.H.) was used as the supporting electrolyte in all solutions investigated. Sodium chloride has been shown [1] not to form complexes with the cyclodextrins. Buffer solutions used in the studies of the pH-dependence of the pyronine Y and pyronine B spectrum in the absence of cyclodextrin were prepared using the A.R. grade salts, sodium acetate (B.D.H.), Na_2HPO_4 (B.D.H.), Tris (Sigma) and sodium carbonate (Univar). Aqueous HCl and NaOH solutions were prepared by the dilution of the contents of a B.D.H. concentrated volumetric solutions ampoule.

Crystal violet (George T. Gurr Ltd.) was recrystallised from doubly distilled water and elemental analysis showed the recrystallised product to be the bihydrate. Calculated for $C_{25}H_{30}N_3Cl \cdot 2H_2O$: C, 67.6%; H, 7.66%; N, 9.46%; Cl, 7.98%. Found (Canadian Microanalytical Service): C, 67.6%; H, 7.61%; N, 9.46%; Cl, 8.06%. Pyronine B was obtained from Sigma as the metal salt [2] $PB_2Fe_2Cl_8$ and was purified by extraction with ethyl acetate, rotary evaporation of the extract to dryness, and recrystallisation of the residue from ethyl acetate. Calculated for $C_{42}H_{54}N_4O_2Fe_2Cl_8$: C, 48.40%; H, 5.22%; N, 5.38%; Cl, 27.21%. Found (Canadian Microanalytical Service): C, 48.25%; H, 5.29; N, 5.32%; Cl, 26.95%. Rhodamine B (Sigma) was purified using the chromatographic method of Gal et al. [3]. The percentages found from the elemental analysis did not entirely agree with those calculated for $C_{28}H_{31}N_2O_3Cl$. While the C/N ratio determined from the elemental analysis agreed with the calculated value, there was a slightly higher percentage of Cl present than calculated. This suggested that the rhodamine B sample contained a small amount of an impurity, which was probably

a salt. Pyronine Y was obtained from Sigma as a sample of approximately 60% purity. Aqueous solutions of the crude dye contained an insoluble material which was probably the primary source of the impurity. Several different methods of purifying the dye were attempted but they were all unsuccessful. The extractive procedure of Gianneschi and Kurucsev [4] was ineffective, and chromatographic methods were impractical because the dye decomposed on the absorbent. Attempts to remove the impurity by recrystallisation of the dye from various organic solvents was also unsuccessful. Consequently, the crude pyronine Y was used without further purification, except that stock solutions of the dye were filtered through a Millipore filter (GS 0.22 μm) prior to use. UV/visible spectra of filtered pyronine Y solutions were similar, e.g. in both shape and position of the absorbance maximum, to those of identical concentrations of dye obtained by Gianneschi and Kurucsev [4]. Filtering appeared to be a crude but sufficient method of removing the impurity in the dye. Pyronine Y, pyronine B, and rhodamine B were stored over phosphorous pentoxide in a vacuum desiccator.

Crystal violet, pyronine Y, pyronine B, and rhodamine B were all found to adsorb slightly to glass surfaces, but only crystal violet was found to adsorb significantly to silica surfaces. It was found that the transfer of a dye solution (the visible spectrum of which had been determined) from a silica spectrophotometer cell to a dry glass volumetric flask for five minutes and the subsequent redetermination of the spectrum in the same silica cell resulted in a 5-6% decrease in molar absorbance of the visible absorbance maximum of the dye. This adsorption process is completed well within five minutes. Accordingly, precautions were necessary to ensure that the effect of adsorption in the spectrophotometric studies was essentially eliminated. All volumetric flasks used in the preparation of solutions were simultaneously thoroughly cleaned

with detergent (Decon-90) and subsequently rinsed with doubly distilled water to ensure a similar surface history. Solutions of cyclodextrins and/or dye in aqueous 1.00 mol dm^{-3} NaCl were prepared by weight in the dried volumetric flasks. The silica spectrophotometer cell was thoroughly rinsed with each solution whose spectrum was required prior to the determination of that spectrum. For the solutions studied the degree of surface adsorption of the dye should be constant throughout the spectrophotometric study. Inevitably, the impure state of some of the dyes and the effect of adsorption causes some concern about the precise molar absorbances of the dyes in the solutions studied. An examination of the literature indicated that a molar absorbance of 9.8×10^4 dm^3 mol^{-1} cm^{-1} at 592 nm for crystal violet [5], 1.03×10^5 dm^3 mol^{-1} cm^{-1} at 553 nm for rhodamine B [3], and 8.1×10^4 dm^3 mol^{-1} cm^{-1} at 545 nm for pyronine Y [4] were appropriate standards to adopt for the spectrum of the dyes under the conditions of the spectrophotometric studies. There was no available literature value for pyronine B, and so a molar absorbance of 1.07×10^5 dm^3 mol^{-1} cm^{-1} at 553 nm was determined. With the spectral data pertaining to a series of solutions containing a range of cyclodextrin concentrations, the molar absorbance of the solution containing no cyclodextrin was set at the appropriate value and all other molar absorbances for the series were suitably adjusted. A knowledge of the absolute value of molar absorbance of free dye is not essential to the equilibrium and kinetic calculations which form the major part of this work; however, the values of molar absorbances for a set of dye solutions are internally consistent. All solutions were prepared immediately prior to spectrophotometric study, and exposure to light was kept to a minimum.

B. COMPUTATIONAL METHODS

B.1 Program DATAFIT

The program **DATAFIT** is a non-linear least-squares curve fitting procedure
developed by Kurucsev [3, 6]. The object of program **DATAFIT** is to fit an
arbitrary function (that represents the mathematical relationship which
characterises the experimental system and is otherwise referred to as
the model) of not more than 20 parameters (the values of which are deter-
mined by the fitting procedure) and four variables (dependent plus in-
dependent) to a data set (experimental data) containing not more than 99
points.

This program seeks out a minimum in the sum of the squares of the
residuals by using an iterative search procedure. The program minimises
the function

$$\phi = \sum_{i=1}^{n} \omega_i F_i^2 \qquad (B.1)$$

in which n is the number of points, F_i is a residual defined in such a
way that it would approach zero for all i as the parameters approached
their 'best' value if the data were completely free of errors. The
statistical weight ω_i can either be set to unity for all points or be
calculated by the program. By using statistical weights, the fit obtain-
ed is independent of the choice of independent and dependent variables,
since for each variable the minimisation assumes variances in the amount
specified.

The user specifies the control constants (e.g. the number of data
points, variables, etc. and the initial estimates of the values of the
parameters), the data set (including estimates of relative variance),
and a subroutine in standard form which gives the equation(s) to be used

for the particular model. The program allows the user to select from three optimisation methods to satisfy Equation B.1 (methods 3 and 5 of Pitha and Jones [7] and the B search method of Flanagan et al. [8]), whether and how statistical weights are to be used, whether auxiliary constants are to be read, the maximum number of iterations to be allowed and the convergence criterion. The indicators of the 'goodness of fit' from program DATAFIT are presented in several forms. Each iteration of the attempted minimisation of Equation B.1 is listed showing the reduction in the sum of squares of residuals and the convergence of the parameters to a 'best' value, and a table summarises the 'best' value of each parameter and its variability. Two plots are displayed, one comparing the experimental and calculated (DATAFIT) points plotted against one of the variables (called the function plot), and in the other the values of the residuals are plotted against one of the variables (residuals plot).

In this work, the program DATAFIT was used to analyse the equilibrium and temperature-jump spectrophotometric data in terms of an appropriate cyclodextrin inclusion mechanism. The absorbance data were fitted to models which considered the total absorbance of the chemical system (at a given wavelength) as the sum of the terms $\varepsilon_i[a_i]$, where ε_i is a molar absorbance and $[a_i]$ is an equilibrium concentration for the ith species, using the variables of absorbance at a given wavelength and initial concentrations of dye and cyclodextrin, and parameters consisting of equilibrium constants and the molar absorbances of the respective species in the chemical system. The temperature-jump data were fitted to models involving reciprocal relaxation time expressions, using the variables of a reciprocal relaxation time and initial concentrations of dye and cyclodextrin, and parameters consisting of the equilibrium constants and rate constants. The equilibrium concentra-

ions of species were calculated from initial concentrations of dye and cyclodextrin using the Newton-Raphson Approximation method [9].

From the primary experimental observations (i.e. the equilibrium spectra or the variation of $1/\tau$ with total cyclodextrin concentration) the variety of models considered most likely to interpret these observations were fitted to the experimental data using program DATAFIT, and the choice of the 'best' model decided on the basis of the following criteria:

(1) The function plot was used to access the 'goodness of the fit' of the particular models by examining the agreement between the experimental and calculated points. The 'best' model was considered to be the one which showed the greatest degree of coincidence of calculated and experimental points. This conclusion was supported by examining the residuals plot where the 'best' model should show randomly distributed residuals. Any model which exhibited a systematic variation in the residuals was completely rejected.

(2) The standard deviation of the parameters and the sum of squares of residuals were compared between the different models, and the 'best' model was considered to be the one which minimised the values. In some cases, especially with the fitting of the absorbance data, it was not possible to discern clearly the 'best' model from condition (1), and the choice had to be decided by condition (2) only.

(3) The fitting of the absorbance data allows the evaluation of the values of the equilibrium constants within a wavelength range. The values derived should be relatively consistent within this range, and thus this provides another test of the suitability of a model. If any systematic variation or deviation in the values was observed then this implied a deficiency in the model.

B.2 Prediction Analysis

The physical law which characterises an experiment can be written in the general form:

$$\eta_i = f(\epsilon_{1i}, \ldots \epsilon_{ji}, \ldots \epsilon_{mi}; \alpha_1, \ldots \alpha_k, \ldots \alpha_p)$$

$$(B.2)$$

where the dependent variable, η_i of the ith measurement is a function of the m independent variables, ϵ_{ji}, and of the p unknown parameters, α_k. The purpose of the experiment is to find the values of the parameters α_k. The object of prediction analysis is to make an estimate of the precision of the parameters α_k, and to find how the precision of the results depends on variations in the experimental conditions (e.g. number of data points taken, distribution of these data points, and the precision and accuracy of the instrumentation used). Prediction analysis is an aid in designing experiments, in choosing the experimental conditions such that sufficient accuracy is achieved, and in ensuring a meaningful interpretation of the results. The basic theory of prediction analysis has been described by Wolberg [10], and Gianneschi and Kurucsev [4] have applied this method to the derivation of the spectra of aggregates.

Prediction analysis was performed using the program **PREDAN** developed by Kurucsev [6], and several conditions must be fulfilled in order to apply this program to a given set of experimental circumstances. These include the knowledge of the mathematical relationship (of the general form given by Equation B.2) which is assumed to apply to the experimental data, and that estimates of the values of the parameters are available, either in the form of results on a closely related system or based on preliminary measurements on the actual system to be studied. The aim of using prediction analytical techniques was to determine the optimum experimental conditions necessary for the characterisation of two guest-one host inclusion complex formation by equilibrium spectrophotometric methods. The reaction scheme given by Equations 3.4 and 3.5, and ex-

pressed through Equation 3.6, was assumed to apply to the absorbance data. This assumption was supported by the results of the temperature-jump spectro-photometric study, and the conclusions deduced from the fitting of absorbance data obtained from a preliminary study of the crystal violet/γCD system. The values of the molar absorbances required in Equation 3.6 were estimated from the spectra (e.g. Figure 3.6), and the values of the equilibrium constants used were those derived from the temperature-jump study. Thus, it was possible to use program PREDAN to determine how the precision of the equilibrium constants that could be derived from the absorbance data depended on the variation of the experimental conditions.

C. RECIPROCAL RELAXATION TIME DATA

$[CV]$[*] $(mol\ dm^{-3} \times 10^5)$	$[\beta CD]$[*] $(mol\ dm^{-3})$	$(1/\tau)$[†] $(s^{-1} \times 10^{-4})$
1.48 ± 0.03	$(3.01 \pm 0.02) \times 10^{-4}$	7.19 ± 1.43
1.48 ± 0.03	$(5.98 \pm 0.03) \times 10^{-4}$	12.12 ± 1.82
1.48 ± 0.03	$(7.52 \pm 0.04) \times 10^{-4}$	12.48 ± 1.87
1.49 ± 0.03	$(9.14 \pm 0.08) \times 10^{-4}$	16.23 ± 2.43
1.48 ± 0.03	$(1.055 \pm 0.008) \times 10^{-3}$	15.94 ± 1.59
1.50 ± 0.03	$(1.21 \pm 0.01) \times 10^{-3}$	18.41 ± 1.84
1.50 ± 0.03	$(1.36 \pm 0.01) \times 10^{-3}$	19.51 ± 1.95

* The errors in initial concentrations were estimated from the known uncertainties in weighing.

† The standard errors in $1/\tau$ were estimated from non-linear regression of voltage against time data.

Table C.1:   *Initial concentrations and observed reciprocal relaxation times for the inclusion of crystal violet by βCD at pH 6.50 in aqueous 1.00 mol dm^{-3} NaCl at 298.2 K*

Table C.2: *Initial concentrations and observed reciprocal relaxation times for the inclusion of crystal violet by γCD at pH 6.50 in aqueous 1.00 mol dm^{-3} NaCl at 298.2 K*

$[CV]^*$ (mol dm$^{-3} \times 10^5$)	$[\gamma CD]^*$ (mol dm^{-3})	$(1/\tau)^\dagger$ (s$^{-1} \times 10^{-3}$)
1.64 ± 0.03	$(8.0 \pm 0.2) \times 10^{-6}$	2.39 ± 0.07
1.34 ± 0.03	$(1.57 \pm 0.06) \times 10^{-5}$	2.24 ± 0.05
1.62 ± 0.03	$(4.79 \pm 0.03) \times 10^{-5}$	3.53 ± 0.10
1.35 ± 0.03	$(6.29 \pm 0.07) \times 10^{-5}$	3.32 ± 0.04
1.63 ± 0.03	$(9.56 \pm 0.05) \times 10^{-5}$	4.32 ± 0.05
1.35 ± 0.03	$(1.279 \pm 0.009) \times 10^{-4}$	4.21 ± 0.18
1.63 ± 0.03	$(1.594 \pm 0.008) \times 10^{-4}$	5.30 ± 0.09
1.35 ± 0.03	$(1.91 \pm 0.01) \times 10^{-4}$	5.12 ± 0.12
1.34 ± 0.03	$(2.56 \pm 0.01) \times 10^{-4}$	5.70 ± 0.16
1.34 ± 0.03	$(3.18 \pm 0.01) \times 10^{-4}$	6.03 ± 0.04
1.34 ± 0.03	$(3.86 \pm 0.01) \times 10^{-4}$	6.57 ± 0.15
1.34 ± 0.03	$(4.46 \pm 0.02) \times 10^{-4}$	6.77 ± 0.30
1.34 ± 0.03	$(5.10 \pm 0.02) \times 10^{-4}$	7.05 ± 0.16
1.46 ± 0.03	$(5.73 \pm 0.02) \times 10^{-4}$	7.29 ± 0.31
1.46 ± 0.03	$(6.39 \pm 0.02) \times 10^{-4}$	8.04 ± 0.29
1.47 ± 0.03	$(7.01 \pm 0.02) \times 10^{-4}$	8.22 ± 0.20
1.46 ± 0.03	$(7.65 \pm 0.02) \times 10^{-4}$	8.16 ± 0.33
1.46 ± 0.03	$(8.29 \pm 0.03) \times 10^{-4}$	8.53 ± 0.18
1.47 ± 0.03	$(8.92 \pm 0.03) \times 10^{-4}$	8.57 ± 0.09
1.46 ± 0.03	$(9.56 \pm 0.03) \times 10^{-4}$	8.50 ± 0.03
1.46 ± 0.03	$(1.021 \pm 0.003) \times 10^{-3}$	8.67 ± 0.09
1.46 ± 0.03	$(1.083 \pm 0.003) \times 10^{-3}$	8.88 ± 0.09
1.47 ± 0.03	$(1.146 \pm 0.003) \times 10^{-3}$	8.80 ± 0.15
1.46 ± 0.03	$(1.211 \pm 0.003) \times 10^{-3}$	9.32 ± 0.14
1.52 ± 0.03	$(1.274 \pm 0.004) \times 10^{-3}$	9.42 ± 0.35
1.51 ± 0.03	$(1.345 \pm 0.004) \times 10^{-3}$	9.37 ± 0.34
1.51 ± 0.03	$(1.402 \pm 0.004) \times 10^{-3}$	9.45 ± 0.39
1.52 ± 0.03	$(1.465 \pm 0.004) \times 10^{-3}$	9.61 ± 0.51

$[CV]^*$ (mol dm^{-3} × 10^5)	$[\gamma CD]^*$ (mol dm^{-3})	$(1/\tau)^\dagger$ (s^{-1} × 10^{-3})
1.52 ± 0.03	(1.529 ± 0.004) × 10^{-3}	10.14 ± 0.39
1.51 ± 0.03	(1.593 ± 0.004) × 10^{-3}	9.71 ± 0.18
1.52 ± 0.03	(1.991 ± 0.005) × 10^{-3}	9.89 ± 0.15
1.52 ± 0.03	(2.389 ± 0.006) × 10^{-3}	9.64 ± 0.20
1.44 ± 0.03	(2.43 ± 0.02) × 10^{-3}	10.25 ± 0.32
1.51 ± 0.03	(2.791 ± 0.007) × 10^{-3}	9.57 ± 0.19
1.53 ± 0.03	(3.187 ± 0.008) × 10^{-3}	9.45 ± 0.51
1.51 ± 0.03	(3.99 ± 0.01) × 10^{-3}	9.33 ± 0.15
1.44 ± 0.03	(4.01 ± 0.02) × 10^{-3}	9.34 ± 0.29
1.65 ± 0.03	(4.78 ± 0.03) × 10^{-3}	9.48 ± 0.27
1.44 ± 0.03	(5.63 ± 0.03) × 10^{-3}	8.08 ± 0.19
1.66 ± 0.03	(6.43 ± 0.03) × 10^{-3}	9.35 ± 0.49
1.45 ± 0.03	(6.44 ± 0.03) × 10^{-3}	8.236 ± 0.001
1.43 ± 0.03	(7.23 ± 0.03) × 10^{-3}	7.70 ± 0.63
1.67 ± 0.03	(7.96 ± 0.04) × 10^{-3}	8.57 ± 0.48
1.44 ± 0.03	(8.86 ± 0.04) × 10^{-3}	7.13 ± 0.64
1.65 ± 0.03	(9.62 ± 0.04) × 10^{-3}	7.86 ± 0.36
1.43 ± 0.03	(1.043 ± 0.005) × 10^{-2}	7.106 ± 0.008
1.65 ± 0.03	(1.117 ± 0.005) × 10^{-2}	7.50 ± 0.12
1.44 ± 0.03	(1.210 ± 0.005) × 10^{-2}	7.04 ± 0.19
1.65 ± 0.03	(1.271 ± 0.005) × 10^{-2}	7.06 ± 0.24
1.45 ± 0.03	(1.368 ± 0.006) × 10^{-2}	6.34 ± 0.08
1.65 ± 0.03	(1.444 ± 0.006) × 10^{-2}	7.02 ± 0.11
1.43 ± 0.03	(1.526 ± 0.006) × 10^{-2}	6.28 ± 0.09
1.67 ± 0.03	(1.598 ± 0.006) × 10^{-2}	6.76 ± 0.19

* The errors in initial concentrations were estimated from the known uncertainties in weighing.

† The standard errors in 1/τ were estimated from non-linear regression of voltage against time data. The 1/τ values above are the average of the values obtained at 530 nm and and 595 nm. The quoted error in 1/τ is the mean of those obtained at 530 nm and 595 nm.

$[PY]^{*}$ $(mol\ dm^{-3} \times 10^{5})$	$[\beta CD]^{*}$ $(mol\ dm^{-3})$	$(1/\tau)^{\dagger}$ $(s^{-1} \times 10^{-4})$
1.28 ± 0.03	$(4.7 \pm 0.1) \times 10^{-5}$	3.33 ± 0.33
1.28 ± 0.03	$(9.8 \pm 0.1) \times 10^{-5}$	4.33 ± 0.43
1.28 ± 0.03	$(1.50 \pm 0.01) \times 10^{-4}$	3.71 ± 0.37
1.28 ± 0.03	$(1.98 \pm 0.02) \times 10^{-4}$	4.48 ± 0.45
1.28 ± 0.03	$(3.20 \pm 0.02) \times 10^{-4}$	6.42 ± 0.64
1.28 ± 0.03	$(4.17 \pm 0.02) \times 10^{-4}$	7.35 ± 0.73
1.35 ± 0.03	$(5.51 \pm 0.01) \times 10^{-3}$	5.37 ± 0.54
1.36 ± 0.03	$(6.01 \pm 0.02) \times 10^{-3}$	5.19 ± 0.52
1.36 ± 0.03	$(6.52 \pm 0.02) \times 10^{-3}$	4.98 ± 0.50
1.35 ± 0.03	$(7.01 \pm 0.02) \times 10^{-3}$	5.85 ± 0.59
1.36 ± 0.03	$(7.51 \pm 0.02) \times 10^{-3}$	6.20 ± 0.62
1.35 ± 0.03	$(8.01 \pm 0.02) \times 10^{-3}$	6.09 ± 0.61
1.35 ± 0.03	$(8.51 \pm 0.02) \times 10^{-3}$	7.21 ± 0.72
1.35 ± 0.03	$(9.02 \pm 0.02) \times 10^{-3}$	6.78 ± 0.68

* The errors in initial concentrations were estimated from the known uncertainties in weighing.

† The standard errors in $1/\tau$ were estimated from non-linear regression of voltage against time data.

Table C.3: Initial concentrations and observed reciprocal relaxation times for the inclusion of pyronine Y by βCD at pH 6.10 in aqueous 1.00 mol dm^{-3} NaCl at 298.2 K

$[PB]^*$ (mol dm$^{-3} \times 10^5$)	$[\beta CD]^*$ (mol dm^{-3})	$(1/\tau)^\dagger$ (s$^{-1} \times 10^{-4}$)
1.02 ± 0.02	$(1.01 \pm 0.02) \times 10^{-4}$	2.37 ± 0.23
1.01 ± 0.02	$(2.05 \pm 0.02) \times 10^{-4}$	5.49 ± 0.55
1.02 ± 0.02	$(4.00 \pm 0.03) \times 10^{-4}$	5.49 ± 0.55
1.02 ± 0.02	$(4.98 \pm 0.03) \times 10^{-4}$	6.26 ± 0.63
1.01 ± 0.02	$(7.99 \pm 0.04) \times 10^{-4}$	10.41 ± 1.04
1.00 ± 0.02	$(9.03 \pm 0.04) \times 10^{-4}$	12.48 ± 1.25
1.01 ± 0.02	$(9.98 \pm 0.05) \times 10^{-4}$	13.36 ± 1.34

* The errors in initial concentrations were estimated from the known uncertainties in weighing.

† The standard errors in $1/\tau$ were estimated from non-linear regression of voltage against time data.

Table C.4: Initial concentrations and observed reciprocal relaxation times for the inclusion of pyronine B by βCD at pH 5.70 in aqueous 1.00 mol dm^{-3} NaCl at 298.2 K

$[RB]^*$ (mol dm^{-3} × 10^6)	$[\beta CD]^*$ (mol dm^{-3})	$(1/\tau)^\dagger$ (s^{-1} × 10^{-4})
9.1 ± 0.2	(9.9 ± 0.2) × 10^{-5}	4.28 ± 0.64
9.1 ± 0.2	(1.51 ± 0.02) × 10^{-4}	3.41 ± 0.51
9.1 ± 0.2	(1.98 ± 0.03) × 10^{-4}	5.86 ± 0.88
9.1 ± 0.2	(2.52 ± 0.03) × 10^{-4}	5.11 ± 0.77
9.1 ± 0.2	(3.00 ± 0.03) × 10^{-4}	6.48 ± 0.97
9.1 ± 0.2	(4.04 ± 0.04) × 10^{-4}	7.70 ± 0.77
9.1 ± 0.2	(5.00 ± 0.05) × 10^{-4}	8.73 ± 0.87
9.1 ± 0.2	(6.00 ± 0.06) × 10^{-4}	10.25 ± 1.02

* The errors in initial concentrations were estimated from the known uncertainties in weighing.

† The standard errors in 1/τ were estimated from non-linear regression of voltage against time data.

Table C.5: *Initial concentrations and observed reciprocal relaxation times for the inclusion of rhodamine B by βCD at pH 6.40 in aqueous 1.00 mol dm^{-3} NaCl at 298.2 K*

$[PY]^*$ (mol dm^{-3} × 10^6)	$[\gamma CD]^*$ (mol dm^{-3})	$(1/\tau)^\dagger$ (s^{-1} × 10^{-4})
8.5 ± 0.2	(1.57 ± 0.01) × 10^{-4}	1.87 ± 0.14
8.5 ± 0.2	(2.52 ± 0.01) × 10^{-4}	2.05 ± 0.15
8.5 ± 0.2	(3.51 ± 0.01) × 10^{-4}	2.28 ± 0.17
8.5 ± 0.2	(4.53 ± 0.02) × 10^{-4}	2.34 ± 0.18
8.5 ± 0.2	(5.50 ± 0.02) × 10^{-4}	2.47 ± 0.18
8.6 ± 0.2	(6.57 ± 0.02) × 10^{-4}	2.48 ± 0.19
8.5 ± 0.2	(7.50 ± 0.02) × 10^{-4}	2.46 ± 0.18
8.5 ± 0.2	(8.52 ± 0.03) × 10^{-4}	2.48 ± 0.19
8.5 ± 0.2	(9.52 ± 0.03) × 10^{-4}	2.44 ± 0.02
8.8 ± 0.2	(7.02 ± 0.02) × 10^{-4}	2.44 ± 0.03
8.7 ± 0.2	(8.04 ± 0.02) × 10^{-4}	2.45 ± 0.03
8.7 ± 0.2	(9.06 ± 0.02) × 10^{-4}	2.49 ± 0.04
8.7 ± 0.2	(1.002 ± 0.003) × 10^{-3}	2.395 ± 0.005
8.8 ± 0.2	(1.255 ± 0.004) × 10^{-3}	2.41 ± 0.18
8.7 ± 0.2	(1.504 ± 0.004) × 10^{-3}	2.34 ± 0.18
8.7 ± 0.2	(1.762 ± 0.005) × 10^{-3}	2.38 ± 0.05
8.7 ± 0.2	(2.005 ± 0.006) × 10^{-3}	2.32 ± 0.17
8.7 ± 0.2	(2.505 ± 0.007) × 10^{-3}	2.20 ± 0.17
8.7 ± 0.2	(3.008 ± 0.008) × 10^{-3}	2.11 ± 0.16
8.7 ± 0.2	(3.501 ± 0.009) × 10^{-3}	1.97 ± 0.03
8.7 ± 0.2	(4.01 ± 0.01) × 10^{-3}	1.85 ± 0.09
8.4 ± 0.2	(4.51 ± 0.02) × 10^{-3}	1.85 ± 0.04
8.4 ± 0.2	(5.02 ± 0.03) × 10^{-3}	1.68 ± 0.08
8.4 ± 0.2	(5.51 ± 0.03) × 10^{-3}	1.68 ± 0.03
8.4 ± 0.2	(6.01 ± 0.03) × 10^{-3}	1.67 ± 0.08
8.4 ± 0.2	(6.51 ± 0.03) × 10^{-3}	1.60 ± 0.06
8.4 ± 0.2	(7.00 ± 0.04) × 10^{-3}	1.57 ± 0.04

$[PY]^*$ (mol dm^{-3} × 10^6)	$[\gamma CD]^*$ (mol dm^{-3})	$(1/\tau)^\dagger$ (s^{-1} × 10^{-4})
8.4 ± 0.2	(7.51 ± 0.04) × 10^{-3}	1.44 ± 0.02
8.4 ± 0.2	(8.03 ± 0.04) × 10^{-3}	1.589 ± 0.009
8.4 ± 0.2	(8.51 ± 0.04) × 10^{-3}	1.45 ± 0.03
8.4 ± 0.2	(9.02 ± 0.04) × 10^{-3}	1.393 ± 0.005
8.4 ± 0.2	(9.52 ± 0.05) × 10^{-3}	1.37 ± 0.01
8.4 ± 0.2	(1.004 ± 0.005) × 10^{-2}	1.294 ± 0.001
10.7 ± 0.03	(2.01 ± 0.01) × 10^{-4}	2.19 ± 0.02
10.8 ± 0.03	(3.00 ± 0.01) × 10^{-4}	2.42 ± 0.24
10.8 ± 0.03	(4.01 ± 0.02) × 10^{-4}	2.62 ± 0.26
10.7 ± 0.03	(5.01 ± 0.02) × 10^{-4}	2.58 ± 0.26
10.8 ± 0.03	(6.02 ± 0.02) × 10^{-4}	2.82 ± 0.28
10.3 ± 0.03	(2.00 ± 0.01) × 10^{-4}	1.90 ± 0.19
10.4 ± 0.03	(3.01 ± 0.01) × 10^{-4}	2.07 ± 0.21
10.4 ± 0.03	(4.02 ± 0.02) × 10^{-4}	2.50 ± 0.25
10.4 ± 0.03	(5.02 ± 0.02) × 10^{-4}	2.65 ± 0.26
10.3 ± 0.03	(6.06 ± 0.02) × 10^{-4}	2.54 ± 0.25

* The errors in initial concentrations were estimated from the known uncertainties in weighing.

† The standard errors in 1/τ were estimated from non-linear regression of voltage against time data. The 1/τ values above are the average of the values obtained at 517 nm and 547 nm. The quoted error in 1/τ is the mean error of those obtained at 517 nm and 547 nm.

Table C.6: Initial concentrations and observed reciprocal relaxation times for the inclusion of pyronine Y by γCD at pH 6.10 in aqueous 1.00 mol dm^{-3} NaCl at 298.2 K

[PB]* (mol dm^{-3} × 10^6)	[γCD]* (mol dm^{-3})	(1/τ)† (s^{-1} × 10^{-3})
9.8 ± 0.2	(1.03 ± 0.01) × 10^{-5}	7.16 ± 1.19
9.8 ± 0.2	(2.03 ± 0.02) × 10^{-5}	6.33 ± 0.34
9.8 ± 0.2	(3.06 ± 0.03) × 10^{-5}	6.59 ± 0.35
9.8 ± 0.2	(4.08 ± 0.03) × 10^{-5}	6.64 ± 0.23
9.8 ± 0.2	(6.12 ± 0.04) × 10^{-5}	6.94 ± 0.20
9.8 ± 0.2	(8.15 ± 0.06) × 10^{-5}	7.465 ± 0.005
9.8 ± 0.2	(1.01 ± 0.01) × 10^{-4}	7.49 ± 0.09
9.8 ± 0.2	(1.26 ± 0.01) × 10^{-4}	7.73 ± 0.01
9.7 ± 0.2	(1.51 ± 0.01) × 10^{-4}	7.98 ± 0.05
9.8 ± 0.2	(2.04 ± 0.01) × 10^{-4}	8.51 ± 0.18
9.5 ± 0.2	(2.47 ± 0.01) × 10^{-4}	8.53 ± 0.27
9.5 ± 0.2	(3.06 ± 0.01) × 10^{-4}	8.82 ± 0.18
9.5 ± 0.2	(3.57 ± 0.01) × 10^{-4}	9.15 ± 0.25
9.5 ± 0.2	(4.08 ± 0.02) × 10^{-4}	9.40 ± 0.26
9.5 ± 0.2	(4.61 ± 0.02) × 10^{-4}	9.83 ± 0.09
9.5 ± 0.2	(5.12 ± 0.02) × 10^{-4}	9.92 ± 0.09
9.5 ± 0.2	(5.62 ± 0.02) × 10^{-4}	10.13 ± 0.16
9.4 ± 0.2	(6.13 ± 0.02) × 10^{-4}	10.30 ± 0.02
9.5 ± 0.2	(6.67 ± 0.02) × 10^{-4}	10.18 ± 0.01
9.5 ± 0.2	(7.16 ± 0.02) × 10^{-4}	10.74 ± 0.05
9.5 ± 0.2	(7.66 ± 0.02) × 10^{-4}	10.70 ± 0.10
9.4 ± 0.2	(8.24 ± 0.03) × 10^{-4}	10.80 ± 0.03
9.6 ± 0.2	(8.71 ± 0.03) × 10^{-4}	11.24 ± 0.61
9.6 ± 0.2	(9.22 ± 0.03) × 10^{-4}	11.53 ± 0.14
9.6 ± 0.2	(9.74 ± 0.03) × 10^{-4}	11.26 ± 0.42
9.5 ± 0.2	(1.025 ± 0.003) × 10^{-3}	11.70 ± 0.07
9.6 ± 0.2	(1.278 ± 0.003) × 10^{-3}	11.65 ± 0.50
9.6 ± 0.2	(1.537 ± 0.004) × 10^{-3}	11.64 ± 0.79
9.5 ± 0.2	(1.800 ± 0.005) × 10^{-3}	11.77 ± 0.33

$[\text{PB}]^*$ $(\text{mol dm}^{-3} \times 10^6)$	$[\gamma\text{CD}]^*$ (mol dm^{-3})	$(1/\tau)^\dagger$ $(\text{s}^{-1} \times 10^{-3})$
9.6 ± 0.2	$(2.042 \pm 0.005) \times 10^{-3}$	12.04 ± 0.15
9.6 ± 0.2	$(2.559 \pm 0.007) \times 10^{-3}$	11.86 ± 0.22
9.6 ± 0.2	$(3.075 \pm 0.008) \times 10^{-3}$	11.37 ± 0.34
9.5 ± 0.2	$(3.584 \pm 0.009) \times 10^{-3}$	11.80 ± 0.03
9.5 ± 0.2	$(4.093 \pm 0.009) \times 10^{-3}$	11.63 ± 0.13
9.2 ± 0.2	$(4.49 \pm 0.02) \times 10^{-3}$	11.67 ± 0.23
9.1 ± 0.2	$(5.00 \pm 0.03) \times 10^{-3}$	11.15 ± 0.40
9.2 ± 0.2	$(5.50 \pm 0.03) \times 10^{-3}$	11.10 ± 0.23
9.2 ± 0.2	$(6.00 \pm 0.03) \times 10^{-3}$	10.90 ± 0.55
9.2 ± 0.2	$(6.49 \pm 0.03) \times 10^{-3}$	10.72 ± 0.46
9.1 ± 0.2	$(7.02 \pm 0.04) \times 10^{-3}$	10.56 ± 0.34
9.2 ± 0.2	$(7.49 \pm 0.04) \times 10^{-3}$	10.57 ± 0.31
9.2 ± 0.2	$(8.00 \pm 0.04) \times 10^{-3}$	10.09 ± 0.63
9.2 ± 0.2	$(8.52 \pm 0.04) \times 10^{-3}$	10.17 ± 0.11
9.2 ± 0.2	$(8.98 \pm 0.04) \times 10^{-3}$	9.88 ± 0.13
9.2 ± 0.2	$(9.48 \pm 0.05) \times 10^{-3}$	9.67 ± 0.33
9.2 ± 0.2	$(1.002 \pm 0.005) \times 10^{-2}$	9.80 ± 0.08

* The errors in initial concentrations were estimated from the known uncertainties in weighing.

† The standard errors in $1/\tau$ were estimated from non-linear regression of voltage against time data. The $1/\tau$ values above are the average of the values obtained at 533 nm and 553 nm. The quoted error in $1/\tau$ is the mean error of those obtained at 533 nm and 553 nm.

Table C.7: *Initial concentrations and observed reciprocal relaxation times for the inclusion of pyronine B by γCD at pH 5.70 in aqueous 1.00 mol dm*$^{-3}$ *NaCl at 298.2 K*

D. DERIVATION OF RECIPROCAL RELAXATION TIME EXPRESSIONS

The dimerisation of a dye, D, in the cavity of a cyclodextrin, CD, may be considered to arise through the following mechanism:

$$D + CD \underset{}{\overset{K_1}{\rightleftharpoons}} DCD \qquad \text{fast} \qquad (D.1)$$

$$D + DCD \underset{k_{-2}}{\overset{k_2}{\rightleftharpoons}} D_2CD \qquad \text{slow} \qquad (D.2)$$

If, after perturbation of the Equilibria D.1 and D.2, the first reaction step relaxes much more rapidly than the second, then the first reaction step can be considered to be decoupled from the second. The following differential rate equation may be used to derive an expression describing the relaxation of the second step:

$$\frac{dC_{D_2CD}}{dt} = k_2 C_{DCD} C_D - k_{-2} C_{D_2CD} \qquad (D.3)$$

For a small perturbation of Equilibrium D.2,

$$\frac{d\Delta C_{D_2CD}}{dt} = k_2 \bar{C}_{DCD} \Delta C_D + k_2 \bar{C}_D \Delta C_{DCD} - k_{-2} \Delta C_{D_2CD} \qquad (D.4)$$

where $\bar{C}$ corresponds to the concentration of a species once the new equilibrium position has been reached.

In order to find an expression for the relaxation time, the right hand side of this equation must be expressed in terms of ΔC_{D_2CD} alone. Using the principle of mass conservation,

$$\Delta C_{CD} + \Delta C_{DCD} + \Delta C_{D_2CD} = 0 \qquad (D.5)$$

and

$$\Delta C_D + \Delta C_{DCD} + 2\Delta C_{D_2CD} = 0 \qquad (D.6)$$

From which,

$$\Delta C_{DCD} = -\Delta C_{CD} - \Delta C_{D_2CD} \qquad (D.7)$$

and

$$\Delta C_D = \Delta C_{CD} - \Delta C_{D_2CD} \qquad (D.8)$$

Since the first step can be considered to be at equilibrium throughout the relaxation of the second:

$$K_1 = \frac{\bar{C}_{DCD}}{\bar{C}_D \cdot \bar{C}_{CD}} \qquad (D.9)$$

Differentiation of Equation D.9 with respect to $\bar{C}_{CD}$, and a change of differentials to differences leads, on rearrangement, to:

$$\Delta C_{DCD} = K_1\bar{C}_D\Delta C_{CD} + K_1\bar{C}_{CD}\Delta C_D \qquad (D.10)$$

Substituting for ΔC_{DCD} and ΔC_D from Equations D.7 and D.8, respectively:

$$\Delta C_{CD} = \frac{K_1\bar{C}_{CD} - 1}{K_1(\bar{C}_D+\bar{C}_{CD}) + 1} \cdot \Delta C_{D_2CD} \qquad (D.11)$$

Substituting for ΔC_{CD} back into Equation D.7 and D.8, ΔC_{DCD} and ΔC_D can be expressed totally in terms of ΔC_{D_2CD}:

$$\Delta C_{DCD} = -\frac{K_1(\bar{C}_D+2\bar{C}_{CD})}{K_1(\bar{C}_D+\bar{C}_{CD}) + 1} \cdot \Delta C_{D_2CD} \qquad (D.12)$$

$$\Delta C_D = -\frac{(K_1\bar{C}_D+2)}{K_1(\bar{C}_D+\bar{C}_{CD}) + 1} \cdot \Delta C_{D_2CD} \qquad (D.13)$$

Now substituting for ΔC_{DCD} and ΔC_D back in Equation D.4:
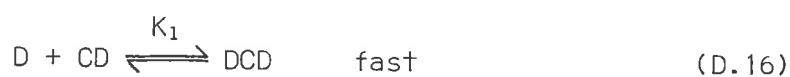
$$\frac{d\Delta C_{D_2CD}}{dt} = -\left[k_2 \cdot \frac{\bar{C}_D(\bar{C}_D+\bar{C}_{DCD}+4\bar{C}_{CD})}{\bar{C}_D + \bar{C}_{CD} + 1/K_1} + k_{-2}\right]\Delta C_{D_2CD} \qquad (D.14)$$

Thus, by definition, the relaxation time of the second step (Equation D.2) is given by the expression:

$$\frac{1}{\tau_2} = k_2 \cdot \frac{\bar{C}_D(\bar{C}_D + \bar{C}_{DCD} + 4\bar{C}_{CD})}{\bar{C}_D + \bar{C}_{CD} + 1/K_1} + k_{-2} \qquad (D.15)$$

The method of derivation presented here is that described by Czerlinski [11]; however, an alternative method [12], utilising matrix algebra, gives the same result.

The mechanism describing the formation of the 1:2 dye-cyclodextrin complex, DCD_2 is as follows:

$$D + CD \underset{}{\overset{K_1}{\rightleftharpoons}} DCD \qquad \text{fast} \qquad (D.16)$$

$$DCD + CD \rightleftharpoons DCD_2 \qquad \text{slow} \qquad (D.17)$$

This mechanism is analogous to Reactions D.1 and D.2, such that Equation D.15 may be written as

$$\frac{1}{\tau_2} = k_2 \cdot \frac{\bar{C}_{CD}(\bar{C}_{CD} + \bar{C}_{DCD} + 4\bar{C}_D)}{\bar{C}_{CD} + \bar{C}_D + 1/K_1} + k_{-2} \qquad (D.18)$$

Consider the mechanism describing the formation of a 2:2 dye-cyclodextrin complex, D_2CD_2:

$$D + CD \underset{}{\overset{K_1}{\rightleftharpoons}} DCD \qquad \text{fast} \qquad (D.19)$$

$$D + DCD \underset{k_{-2}}{\overset{k_2}{\rightleftharpoons}} D_2CD \qquad \text{slow} \qquad (D.20)$$

$$D_2CD + CD \underset{}{\overset{K_3}{\rightleftharpoons}} D_2CD_2 \qquad \text{fast} \qquad (D.21)$$

In this case, an expression describing the relaxation of the second step may be derived by using the 'substitution method' of Czerlinski [11]. This involves considering the mechanism in two parts. An equation for $1/\tau_2$ is first derived by considering the first two reaction steps alone, and then another equation for $1/\tau_2$ is derived by considering the last two reaction steps. The overall equation for $1/\tau_2$ is then obtained by a combination of these two equations. The equilibrium factor associated

with k_2 is taken to be that derived from the consideration of the first two reaction steps, whereas that associated with k_{-2} is taken to be that derived from the consideration of the last two reaction steps.

The first two reaction steps have already been considered above, and these resulted in Equation D.15. For the last two steps, the expression for the reciprocal relaxation time may be derived from the following differential rate equation:

$$\frac{-dC_{DCD}}{dt} = k_2 C_{DCD} C_D - k_{-2} C_{D_2CD} \tag{D.22}$$

For a small perturbation of Equilibrium D.20,

$$\frac{-d\Delta C_{DCD}}{dt} = k_2 \bar{C}_{DCD} \Delta C_D + k_2 \bar{C}_D \Delta C_{DCD} - k_{-2} \Delta C_{D_2CD} \tag{D.23}$$

In order to find an expression for the relaxation time, the right hand side of this equation must be expressed in terms of ΔC_{DCD} alone. From the principle of mass conservation,

$$\Delta C_D + \Delta C_{DCD} + 2\Delta C_{D_2CD} + 2\Delta C_{D_2CD_2} = 0 \tag{D.24}$$

and from Equations D.20 and D.21

$$\Delta C_D = \Delta C_{DCD} \tag{D.25}$$

and

$$\Delta C_{CD} = -\Delta C_{D_2CD_2} \tag{D.26}$$

Substituting for ΔC_D from Equation D.25 into Equation D.24 yields:

$$\Delta C_{D_2CD} = -\Delta C_{DCD} - \Delta C_{D_2CD_2} \tag{D.27}$$

Since the last step can be considered to be at equilibrium throughout the relaxation of Reaction D.20:

$$K_3 = \frac{\bar{C}_{D_2CD_2}}{\bar{C}_{D_2CD} \cdot \bar{C}_{CD}} \tag{D.28}$$

Differentiation of Equation D.28 with respect to $\bar{C}_{D_2CD}$, and a change of differentials to differences leads, on rearrangement, to:

$$\Delta C_{D_2CD_2} = K_3\bar{C}_{CD}\Delta C_{D_2CD} + K_3\bar{C}_{D_2CD}\Delta C_{CD} \qquad (D.29)$$

Substituting for ΔC_{D_2CD} and ΔC_{CD} from Equations D.27 and D.26, respectively, yields:

$$\Delta C_{D_2CD_2} = \frac{-K_3\bar{C}_{CD}}{K_3(\bar{C}_{CD}+\bar{C}_{D_2CD}) + 1} \cdot \Delta C_{DCD} \qquad (D.30)$$

Substituting for $\Delta C_{D_2CD_2}$ back into Equation D.27:

$$\Delta C_{D_2CD} = \frac{-(K_3\bar{C}_{D_2CD}+1)}{K_3(\bar{C}_{CD}+\bar{C}_{D_2CD}) + 1} \cdot \Delta C_{DCD} \qquad (D.31)$$

Now substituting for ΔC_{D_2CD} and ΔC_D from Equations D.31 and D.25, respectively, back into Equation D.23:

$$\frac{d\Delta C_{DCD}}{dt} = -\left[k_2(\bar{C}_D+\bar{C}_{DCD}) + k_{-2}\cdot\frac{K_3\bar{C}_{D_2CD}+1}{K_3(\bar{C}_{CD}+\bar{C}_{D_2CD})+1} \right]\Delta C_{DCD} \qquad (D.32)$$

Thus, by definition, the relaxation time of the second step, by consideration of the two steps D.20 and D.21, is given by the expression:

$$\frac{1}{\tau_2''} = k_2(\bar{C}_D + \bar{C}_{DCD}) + k_{-2}\cdot\frac{\bar{C}_{D_2CD} + 1/K_3}{\bar{C}_{CD} + \bar{C}_{D_2CD} + 1/K_3} \qquad (D.33)$$

Now, combining Equation D.15 and D.33 according to the substitution method, the overall reciprocal relaxation time of Reaction D.20 of the three step mechanism (Equations D.19, D.20 and D.21) is given by the expression:

$$\frac{1}{\tau_2} = k_2 \cdot \frac{\bar{C}_D(\bar{C}_D+\bar{C}_{DCD}+4C_{CD})}{\bar{C}_D + \bar{C}_{CD} + 1/K_1} + k_{-2} \cdot \frac{\bar{C}_{D_2CD} + 1/K_3}{\bar{C}_{CD} + \bar{C}_{D_2CD} + 1/K_3}$$

$$(D.34)$$

Bibliography

1. GELB, R. I., SCHWARTZ, L. M., RADEOS, M. and LAUFER, D. A. J. Phys. Chem. 87, 3349 (1983).

2. CHAMBERLAIN, E. M., POWELL, B. F., WILLIAMS, D. E. and CONN, J. J. Org. Chem. 27, 2263 (1962).

3. GAL, M. E., KELLY, G. R. and KURUCSEV, T. J. Chem. Soc. Faraday Trans. II 69, 395 (1973).

4. GIANNESCHI, L. P. and KURUCSEV, T. J. Chem. Soc. Faraday Trans. II 70, 1334 (1974).

5. STORK, W. H. J., LIPPITS, G. J. M. and MANDEL, M. J. Phys. Chem. 76, 1772 (1972).

6. KURUCSEV, T. University of Adelaide, private communication.

7. PITHA, J. and JONES, R. N. Can. J. Chem. 44, 3031 (1966).

8. FLANAGAN, P. D., VITALE, P. A. and MENDELSOHN, J. Technometrics 11, 265 (1969).

9. SCARBOROUGH, J. B. Numerical Mathematical Analysis, Johns Hopkins Press, Baltimore, U.S.A., 1955.

10. WOLBERG, J. R. Prediction Analysis, van Nostrand, Princeton, N.J., U.S.A., 1967.

11. CZERLINSKI, G. H. Chemical Relaxation, Dekker, New York, 1966.

12. BERNASCONI, C. F. Relaxation Kinetics, Academic Press Inc., New York, 1976.

Schiller, R. L., Coates, J. H., & Lincoln, S. F. (1984). Kinetic and equilibrium studies of crystal violet-cyclodextrin inclusion complexes. *Journal of the Chemical Society, Faraday Transactions 1: Physical Chemistry in Condensed Phases, 80*(5), 1257-1266.